Aus dem Physiologischen Institut
der Ludwig-Maximilians-Universität München
Vorstand: Prof. Dr. Magdalena Götz

Heterogeneity in astrocyte responses after acute injury *in vitro* and *in vivo*

Dissertation
zum Erwerb des Doktorgrades der Naturwissenschaften (Dr. rer. nat.)
an der Medizinischen Fakultät
der Ludwig-Maximilians-Universität München

vorgelegt von
Sophia Bardehle
aus Dresden
2013

Gedruckt mit Genehmigung der Medizinischen Fakultät der Ludwig-Maximilians-Universität München

Betreuerin: Prof. Dr. Magdalena Götz

Zweitgutachter: Prof. Dr. Rainer Glaß

Dekan: Prof. Dr. med. Dr. h.c. Maximilian Reiser, FACR, FRCR

Tag der mündlichen Prüfung: 20. September 2013

Eidesstattliche Versicherung

Ich erkläre hiermit an Eides statt, dass ich die vorliegende Dissertation selbständig verfasst, mich außer der angegebenen keiner weiteren Hilfsmittel bedient und alle Erkenntnisse, die aus dem Schrifttum ganz oder annähernd übernommen sind, als solche kenntlich gemacht und nach ihrer Herkunft unter Bezeichnung der Fundstelle einzeln nachgewiesen habe.

Ich erkläre des Weiteren, dass die hier vorgelegte Dissertation nicht in gleicher oder in ähnlicher Form bei einer anderen Stelle zur Erlangung eines akademischen Grades eingereicht wurde.

München,

X

Sophia Bardehle

Summary

Astrocytes present a major population of glial cells in the adult mammalian brain. The heterogeneity of astrocytes in different regions of the healthy central nervous system (CNS) and their physiological functions are well understood. In contrast, rather little is known about the diversity of astrocyte reactions under pathological conditions. After CNS injury the reaction of astrocytes, also termed 'reactive astrogliosis', is characterized by morphological and molecular changes such as hypertrophy, polarization, migration and up-regulation of intermediate filaments. So far, it was unknown whether all astrocytes undergo these changes, or whether only specific subpopulations of reactive astrocytes possess special plasticity. Since some quiescent, postmitotic astrocytes in the cortical gray matter apparently de-differentiate and re-enter the cell cycle upon injury, reactive astrocytes have the ability to acquire restrictive stem cell potential. However, the mechanisms leading to increased astrocyte numbers after acute injury, e.g. proliferation and migration, had not been investigated live *in vivo*. For the first time, recently established *in vivo* imaging using 2-photon laser scanning microscopy (2pLSM) allowed to follow single GFP-labeled astrocytes for days and weeks after cortical stab wound injury. Tracing morphological changes during the transition from a quiescent to reactive state, these live observations revealed a heterogeneous behavior of reactive astrocytes depending on the lesion size. Different subsets of astrocytes either became hypertrophic, polarized and/ or divided, but never migrated towards the injury. Intriguingly, the lack of astrocyte migration was not only contradictory to what had been predicted based on *in vitro* and *in situ* studies, but was also in stark contrast to the motility of other glial cells. Additionally, live imaging provided first evidence that only a small subset of reactive astrocytes in juxtavascular positions re-gains proliferative capacity after injury. While astrocyte proliferation was affected by conditional deletion of RhoGTPase Cdc42 – a key regulator of cell polarity –, the vascular niche was preserved, indicating that juxtavascular astrocytes are uniquely suited for proliferation after injury. Following the behavior of *cdc42*-deficient astrocytes by live imaging using an *in vitro* scratch wound assay, cell-autonomous effects including disturbed polarity and impaired directional migration confirmed a crucial role of Cdc42 signaling in reactive astrocytes after acute injury *in vitro* and *in vivo*.

These novel insights revise current concepts of reactive astrocytes involved in glial scar formation by assigning regenerative potential to a minor pool of proliferative, juxtavascular astrocytes, and suggesting specific functions of different astrocyte subsets after CNS trauma.

Zusammenfassung

Astrozyten bilden die größte Gruppe von Gliazellen im Gehirn erwachsener Säugetiere. Die Heterogenität von Astrozyten in verschiedenen Regionen des zentralen Nervensystems (ZNS), sowie deren physiologischen Funktionen sind relativ gut untersucht. Hingegen ist die Diversität der astrozytären Reaktion unter pathologischen Bedingungen bis jetzt wenig verstanden. In Folge einer Verletzung des ZNS reagieren Astrozyten mit bestimmten molekularen und morphologischen Veränderungen wie Hypertrophie, Polarisierung, Wanderung und Hochregulation bestimmter Intermediärfilamente. Diese Veränderungen werden insgesamt als „reaktive Gliose" zusammengefasst. Darüber hinaus scheinen nach akuten Gehirnverletzungen einige reife, postmitotische Astrozyten in der Großhirnrinde zu de-differenzieren, in den Zellzyklus einzutreten und begrenzt Stammzelleigenschaften zu erlangen. Es ist bisher nicht bekannt, ob alle Astrozyten auf Verletzungen reagieren, oder ob Teilpopulationen verschiedener Plastizität existieren. Weiterhin sind die Mechanismen, die zum Anstieg von Astrozyten nach akuter Verletzung führen, z.B. Proliferation und Wanderung, *in vivo* bislang nicht verstanden. Deshalb wurde hier erstmals das Verhalten von Fluoreszenz-markierten Astrozyten im Gehirn der Maus nach akuter kortikaler Verletzung live über einen längeren Zeitraum mittels 2-Photonenmikroskopie untersucht. Die Beobachtungen zeigten morphologische Veränderungen und heterogene Verhaltensmuster reaktiver Astrozyten, d.h. hypertrophe, polarisierende und sich teilende Astrozyten in Abhängigkeit von der Läsionsgröße. Im Gegensatz zu *in vitro* und *in situ* Studien, sowie bekannter Motilität anderer Typen von Gliazellen, wurde die Wanderung von Astrozyten zum Ort der Verletzung *in vivo* nicht beobachtet. Allerdings wurde entdeckt, dass sich nur eine kleine Teilpopulation von Astrozyten teilt, und diese vorrangig in direktem Kontakt mit Blutgefäßen (juxtavaskulär) liegt. Selbst nach Verlust der RhoGTPase Cdc42 – einem Schlüsselfaktor für Zellpolarität –, der zu einem Proliferationsdefekt der Astrozyten führte, blieb die vaskuläre Nische erhalten. In einem *in vitro* Verletzungsmodell zeigten *cdc42*-defizienten Astrozyten Polaritätsdefekte, verbunden mit desorientierter Wanderung und verminderter Zellteilung. Schlussfolgernd, spielen Cdc42-vermittelte Signalwege eine wichtige Rolle für die Reaktion von Astrozyten auf eine akute Verletzung *in vitro* und *in vivo.*

Die hier präsentierte Studie trägt bedeutend zum Verständnis reaktiver Astrozyten in Bezug auf deren Rolle in der Narbenbildung und Regeneration von geschädigtem Hirngewebe bei. Insbesondere wurden neue Erkenntnisse über verschiedene Teilpopulationen von Astrozyten mit vermutlich unterschiedlichen Funktionen gewonnen. Hierbei konnte vor allem den juxtavaskulär proliferierenden Astrozyten nach einer traumatischen Hirnverletzung hohe Plastizität zugesprochen werden.

Table of contents

1 Introduction

1.1 Glial cells in the central nervous system

The mammalian brain is composed of a complex neuronal network which is structurally and functionally supported by neuroglial cells (“nerve glue”) [1,2] that are subdivided into macroglia and microglia [1,3]. Microglia are resident macrophages of mesodermal origin [4-8], while macroglia derive from neuroectodermal tissue. Macroglia are further classified into astrocytes (“star-shaped” cell), ependymal glia and cells of the oligodendrocyte lineage [2]. The latter includes myelinating oligodendrocytes and oligodendrocyte precursors (OPCs), also referred to as NG2+ (neuroglial antigen 2) cells or polydendrocytes [9-12].

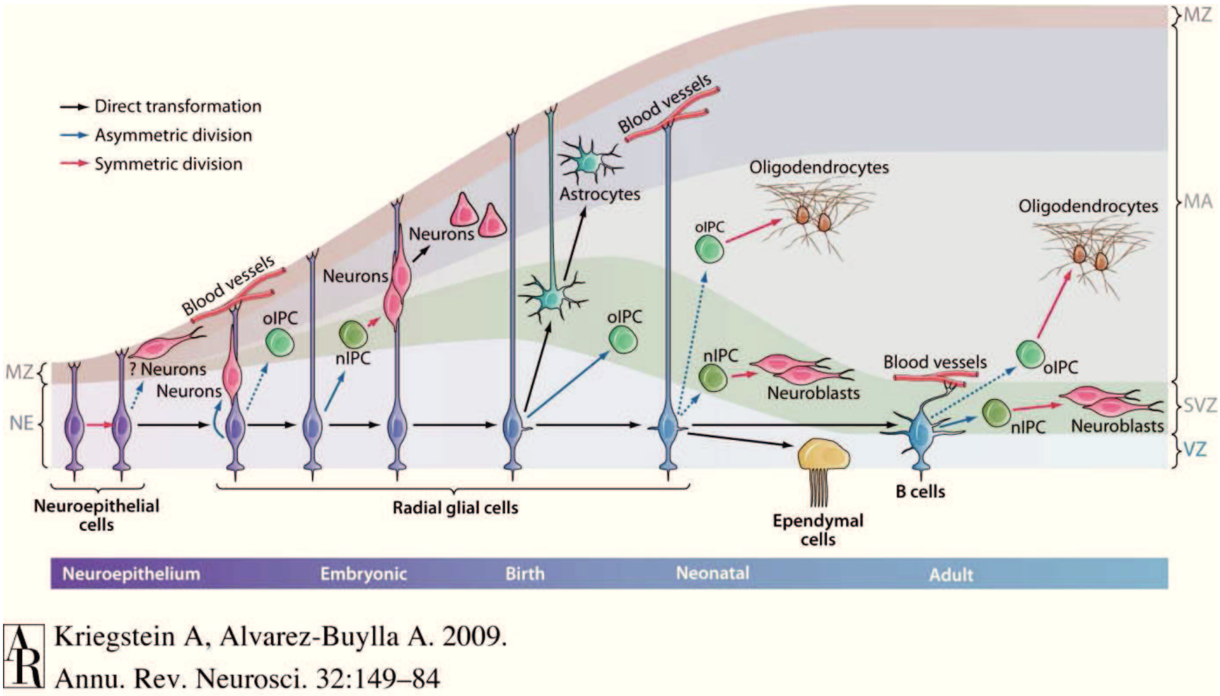

Figure 1.1 Gliogenesis follows neurogenesis in postnatal stages of the developing mouse brain. Astrocytes develop from radial glia or intermediate progenitor cells (IPC) during cortical maturation. MA, mantle; MZ, marginal zone; NE, neuroepithelium; nIPC, neurogenic progenitor cell; oIPC, oligodendrocytic progenitor cell; SVZ, subventricular zone; VZ, ventricular zone; adapted from Kriegstein and Alvarez-Buylla {Kriegstein, 2009 #31}.

Astrocytes are the most abundant glial cells in the mammalian brain with variable density (~1.5-3.5x10^4cells/mm^3) [13] in different brain regions, as well as diverging astrocyte-to-neuron-ratio in mouse (1:3) and human (1.4:1); [14,15]. Moreover, the morphological complexity of astrocytes is species-specific [16] and region-dependent [12]. In the cortex, astrocytes develop from radial glia in the ventricular zone (VZ) or from multipotent progenitors in the subventricular zone (SVZ) of the lateral ventricle (Figure 1.1) [17]. During the first postnatal weeks in mammals, glial precursors migrate to the cerebral cortex, expand locally by proliferation, and differentiate morphologically (from a bipolar to a ramified shape) and functionally into mature astrocytes [18-21].

In the adult CNS distinct astrocyte subtypes are defined by region-specific morphology (Figure 1.2) and functional diversity [1,12,22], e.g. astrocytes in the cerebral cortex [23], in the spinal cord [24], in the SVZ [25,26], or Bergmann glia in the cerebellum and Müller glia in the retina [12].

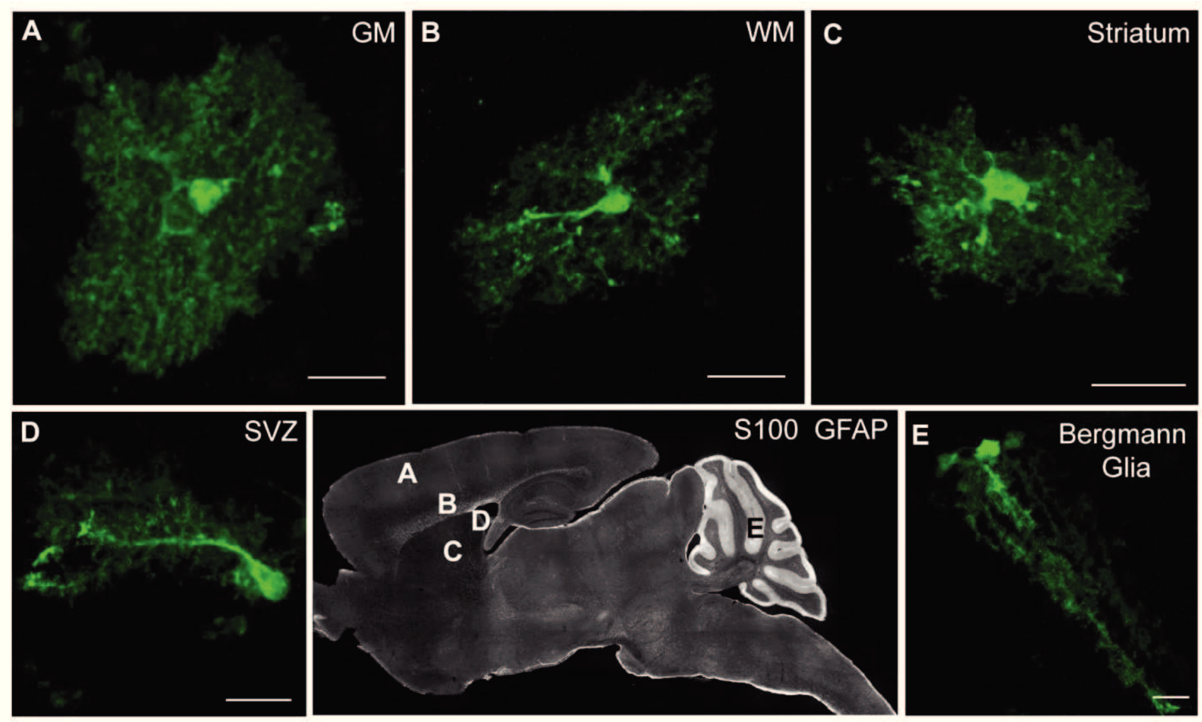

Figure 1.2 Morphological diversity of astrocytes in different brain regions of an adult mouse. Sagittal brain section (centered panel in the lower row) stained for the astroglial markers S100 and GFAP showing the localization of **(A)** a protoplasmic astrocyte in the cortical gray matter (GM), **(B)** a fibrous astrocyte in the white matter (WM), **(C)** a striatal astrocyte, **(D)** a bipolar astrocyte in the SVZ and **(E)** Bergmann glia in the cerebellum. **(A-E)** Confocal images of cytoplasmic GFP-labeled astrocytes in the brain of an adult GLAST^{CreERT2}/ CAG-eGFP reporter mouse.

One particular region, the cerebral cortex, is anatomically subdivided into the gray matter (GM) – location of neuronal cell somata – and the white matter (WM) comprising myelinated axon tracts. Both regions comprise two distinct astroglial populations: the protoplasmic astrocytes in the cerebral cortical GM and fibrous astrocytes in the WM. Protoplasmic astrocytes have many fine branched processes around the soma with at least one process forming a vascular endfoot (see part 1.2.1) [27]. The overall spheroid volume of protoplasmic astrocytes in the GM is organized in spatially restricted, non-overlapping domains [28].

In contrast, fibrous astrocytes in the cortical WM are oriented parallel to axonal tracts and have an elongated cell shape with ramified processes that interdigitate with neighboring astrocytes[16]. On a molecular level, astrocytes are characterized by the expression of a variety of astroglial-enriched antigens depending on the stage of differentiation, the CNS region, and the activation status. While mature, quiescent protoplasmic astrocytes in the GM express e.g. S100β and glutamate transporters, immature astrocytes in the developing cortex express proteins, which are up-regulated in a subset of reactive astrocytes (see Table 1-1), e.g. brain-lipid binding protein (BLBP) or intermediate filaments like glial fibrillary acidic protein (GFAP), nestin and vimentin. Common molecular markers of radial glia in the adult brain are re-expressed in reactive, cortical astrocytes after injury, reflecting some degree of de-differentiation and restricted, but lifelong stem cell potential of astrocytes [26,29-32] (see part 1.3.2). However, while more than 300 astrocyte-enriched genes have been identified analyzing different developmental stages and brain regions [29,33-35], a correlation of specific marker expression in distinct astrocyte subsets has not yet been discovered in the healthy brain (part 1.2), nor under pathological conditions (part 1.3).

Table 1-1 List of astroglial markers

Antigen	Function	Expression pattern	References
ALDH1L1	Aldehyde dehydrogenase 1, family member L1	Mature astrocytes in brain & spinal cord, up-regulation after injury	33,36,37
Aquaporin-4 (AQP4)	Water channel	Mature astrocytes in brain and spinal cord, localized in astrocytic endfeet/ glia limitans	38
Brain-lipid-binding protein (BLBP)	Lipid binding, transporter activity	Radial glia, developing brain & spinal cord, reactive astrocytes	39-41
Chondroitin sulfate proteo-glycans (CSPG)	ECM component, glial scar	Secretion by reactive astrocytes	42,43
Connexin 30, 43 (Cx30, Cx43)	Gap junctions; Astrocyte/ Oligodendrocyte junctions	Mature astrocytes, Cx30 later than p14, in WM & GM astrocytes; Cx30/43 perivascular co-localization	44-46
Glial fibrillary acidic protein (GFAP)	Intermediate filament	Reactive astrocytes, radial glia, immature astrocytes, SVZ astrocytes, ependymal cells in adult brain, aNSC	47-51
GLAST / EAAT1	Glutamate/ Aspartate transporter	Mature astrocytes in brain, radial glia, spinal cord, retina	52-57
GLT-1 / EAAT2	Glutamate transporter	Mature astrocytes in brain & spinal cord	53,54,58
Glutamine synthetase (GS)	Glutamate metabolism	Mature astrocytes in brain, spinal cord & retina	59-61
Nestin	Intermediate filament	Reactive astrocytes in adult brain, immature astrocytes	21
RC2	Cytoskeletal protein binding	Radial glial, immature astrocytes	40,62
S100β	Ca2+ binding protein	Mature astrocytes in brain, spinal cord & retina; ependymal cells	63-66
Vimentin	Intermediate filament	Reactive astrocytes in adult brain, immature astrocytes	21

1.2 Astrocyte functions in brain physiology

Astrocytes are involved in various pivotal regulatory processes such as brain energy metabolism [67], pH control, ion and fluid homeostasis [68,69], guidance of synaptogenesis [70] as well as modulation of synaptic plasticity and transmission in the adult brain [71-73] (overview depicted in Figure 1.3 A).

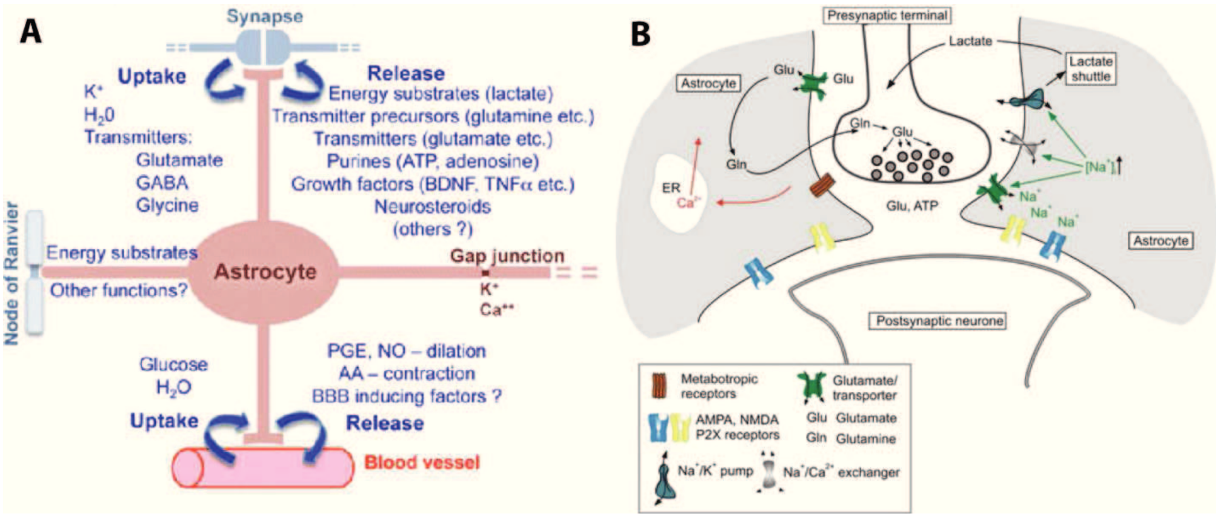

Figure 1.3 (A) Illustration of astroglial functions in the healthy brain; adapted from Sofroniew and Vinters [74]. **(B)** The tripartite synapse forms a functional unit composed of a presynaptic synapse and postsynaptic neuron, as well as astrocytic endfeet (depicted in grey) that modulate synaptic transmission; adapted from Papura et al. [75].

The concept of a "tripartite synapses" (Figure 1.3 B) includes pre- and postsynaptic synaptic terminals ensheathed by astrocytic endfeet, which reciprocally control neuronal activity propagated by release of neurotransmitters [14,76,77]. Astrocyte-specific expression of glutamate transporters (e.g. GLAST, GLT-1) and glutamine synthetase (GS) mediate uptake and intracellular enzymatic conversion of the excitatory amino acid glutamate [61]. This implies important functions of astrocytes in balancing neurotransmitter concentrations, as well as ion levels [54,78,79]. Extracellular sodium (Na+), calcium (Ca2+) and potassium (K+) levels are regulated via ion channels expressed in astrocytic endfeet membranes e.g. the inwardly rectifying channel Kir4.1 [80]. Notably, astrocytic endfeet forming an essential glio-vascular unit (part 1.2.1; Figure 1.4) for bi-directional neurovascular coupling and maintenance of the blood-brain barrier (BBB) integrity [3,74,81,82], as astrocyte dysfunctions are associated with epileptogenesis [83,84].

1.2.1 Gliovascular unit and the blood-brain barrier

The gliovascular unit (depicted in Figure 1.4.) is composed of vascular endothelial cells lining the blood vessel lumen, which are partially covered with smooth muscle cells and pericytes. Perivascular cells in perivascular 'Virchow-Robin spaces' are separated by a vascular basal membrane (BM) from the juxtavascular parenchyma (neuropil) by the *glia limitans* [85-90].

The *glia limitans* forms a physical barrier between the brain parenchyma and the vasculature by ensheathing astrocyte endfeet that are anchored with dystroglycans and integrins to laminin isoforms at the BM [91-93]. Notably, dysfunctions of astrocyte-BM interactions, e.g. by astrocyte-specific deletion of β1-integrin, were associated with a partial astrogliosis [94] and impaired astrocyte polarity after injury [95,96].

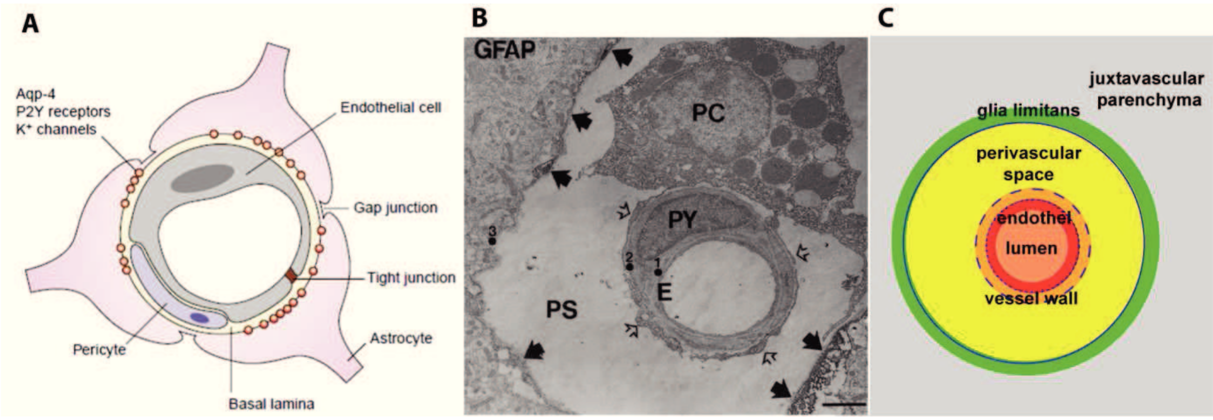

Figure 1.4 Gliovascular unit and blood-brain barrier. (A) Cross-section of the gliovascular unit building the blood-brain barrier; adapted from Nedergaard et al. [14]. **(B)** Ultrastructure of the gliovascular unit; PC: perivascular cell; PY: pericyte; PS: perivascular space; E: endothelial cell; adapted from Bechmann et al. [97]. **(C)** Simplified illustration of the compartments around cerebral blood vessels are subdivided by the inner basement membrane (BM; indicated as a dotted circle) adjacent to the endothelial cell layer, and the outer BM (dashed circle) defining the perivascular space (also termed Virchow-Robin space). The outermost gliovascular lamina (continuous black circle) and astrocytic endfeet forming the *glia limitans* (black filled arrows in B) as interface to the juxtavascular parenchyma (also referred to as neuropil); modified from Prodinger et al. [85].

Particularly with regard to the astrocyte-vascular interaction, on the one hand astrocytic endfeet are found at all types of cerebral blood vessels – diving arteries, ascending veins, and small capillaries [27] – and on the other hand astrocyte somata directly contact blood vessels in the cortex and retina (previously referred as 'perivascular astrocytes') [12,98].

However, those astrocytes directly apposed to a blood vessel have been addressed herein and might be a subpopulation with specific functions at the blood-brain interface. The blood-brain barrier (BBB) is important to control the penetration of molecules and fluids from the cerebral blood stream into the brain parenchyma in a size-restricted and polarity dependent manner[86,99]. While the first barrier is mediated by endothelial cells connected by tight junctions, astrocytic endfeet provide the outer barrier by expression of water channels including aquaporins (e.g. Aqp4; see Table 1-1) [100]. Moreover, astrocytes controls the cerebral blood flow by intracellular calcium signaling [101], as well as the release of nitric oxide (NO), lactate and adenosine [102-104]. Thus, the cross-talk between vascular endothelial cells, pericytes and astrocytes plays a crucial role for the development, as well as for the maintenance of the BBB [90,105,106], as many CNS pathologies are associated with BBB dysfunctions [107-112].

1.3 Astrocyte functions under pathological conditions

Astrocytes are involved in many CNS pathologies including traumatic brain injury [113-118], stroke [119-121], brain tumors [122-124], epilepsy [84,125-128], infections [129-131] as well as progressive neurodegenerative disorders like Alzheimer's disease [132-134], Parkinson's disease [135] or amyotrophic lateral sclerosis (ALS) [136,137]. After CNS trauma transient disruption of the BBB allows rapid infiltration of leukocytes initiating an inflammatory reaction with local activation of resident microglia followed by the reaction of OPCs and astrocytes termed 'reactive gliosis' [138-140]. Reactive astrogliosis has been earlier defined as molecular, morphological and functional changes that astrocytes undergo in response to CNS injuries (Figure 1.5) [74,139]. The role of reactive astrocytes in glial scar formation has been described as a "double-edged sword" with beneficial neuroprotective functions, e.g. reformation of the BBB to restrict inflammation, as well as detrimental effects counteracting axonal regeneration, e.g. secretion of ECM molecules such as chondroitin sulfate proteoglycans (CSPGs; see Table 1-1) [138,141-145].

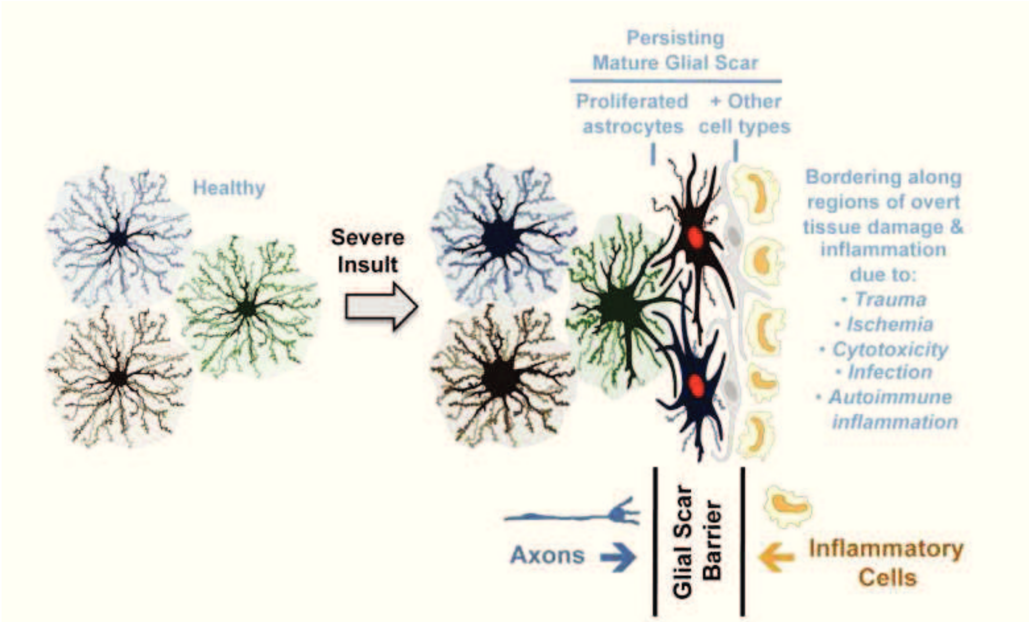

Figure 1.5 Hallmarks of astrogliosis after CNS injury: cellular hypertrophy, proliferation and glial scar formation; adapted from Sofroniew [139].

General cellular hallmarks of reactive astrocytes after acute cortical injury are (1) hypertrophy and polarization, (2) up-regulation of intermediate filaments, e.g. GFAP and (3) increasing astrocytes numbers at the lesion side due to re-gained proliferative capacity of some astrocytes (Figure 1.6) [113,114,116,117]. Morphologically, most reactive astrocytes become hypertrophic with swelling of their cell somata and primary processes. Nevertheless, reactive astrocytes retain an overall stable cell volume (~25 x 10^3 µm^3) and separated territories as shown by dye-filling studies [28].

On molecular level, the up-regulation of intermediate filaments, including GFAP, vimentin and nestin and secretion of extra cellular matrix (ECM) components like tenascins and CSPGs are widely found in reactive astrocytes (Figure 1.6; Table 1-1) [32,113,148,149].

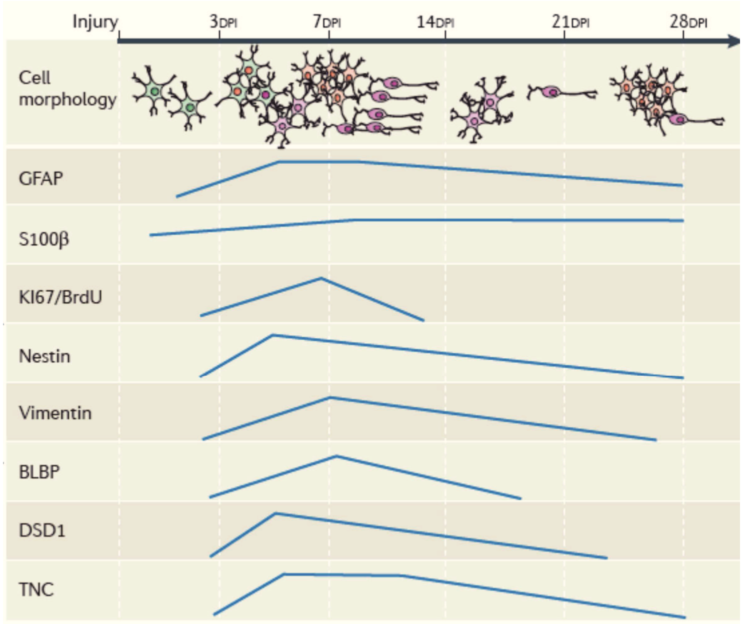

Figure 1.6 Illustration of molecular and morphological changes of reactive astrocytes after acute brain injury. Transient changes in their expression profile including the re-expression of early astroglial marker (nestin, vimentin, BLBP, TNC) and regained proliferative activity (Ki67/ BrdU+ cells); adapted from Robel et al. [32].

During reactive gliosis the importance of intermediate filaments regulating cytoskeletal stability and cell activation [150] became clear when CNS pathologies were identified with GFAP mutations (Rosenthal fibers in Alexander disease [151]) or with aberrant GFAP isoforms as found in Alzheimer's disease [48]. While GFAP-deficient astrocytes showed impaired BBB maintenance [152], the loss of both GFAP and vimentin (GFAP-/-Vim-/- mice) led to attenuated reactive gliosis and improved neuronal regeneration [153,154]. In comparison to the expression of intermediate filaments, Stat3 – a key transcriptional activator – has been also shown to influence glial scarring, wound healing and inflammation after spinal cord injury, e.g. by astrocyte-specific Stat3 deletion [155,156]. Taken these studies together with pharmacological ablation of astrocytes [157] and targeted ablation of proliferating astrocytes after traumatic brain injury [158] or spinal cord injury [159,160] supported crucial homeostatic functions of quiescent astrocytes in the healthy brain (part 1.2), and essential regulatory functions of proliferative astrocyte in inflammatory and regenerative processes after injury.

More recently, transcriptome studies compared quiescent astrocytes from healthy brains to reactive astrocytes isolated from ischemic, inflammatory conditions [161,162] or traumatic brain injury (Sirko, Götz, unpublished). The comparison of these results revealed some commonly up-regulated genes (e.g. GFAP, vimentin), while gene expression profiles differs largely between different CNS pathologies. According to the study conducted by Sirko et al., more than 500 genes (>2 fold change) were identified to be differentially regulated in reactive astrocytes five days after traumatic brain injury compared to astrocytes from intact brains. Amongst those, regulated genes were found to be enriched in cellular processes like proliferation, signal transduction, cell death, ECM remodeling, cytokine signaling, inflammation and CNS development. While those studies considered the entire population of reactive astrocytes, and thereby underestimated possible astroglial diversity, it is important to investigate the behavior of single cells by *in vivo* fate mapping using novel live imaging techniques (part 1.5). To unravel how and which astrocytes contribute to glial scar formation, it is important to investigate whether ALL astrocytes respond to an injury – and do so in a similar manner – or whether different subsets of astrocytes react by either hypertrophy, polarization, proliferation or migration. Whereas astrocyte polarization – the formation of elongated cellular processes – was associated with lesion-directed migration of astrocytes *in vitro* [146,147], and had been assumed from analysis of fixed spinal cord tissue {Okada, 2006 #208}, the migration of reactive astrocytes in the injured brain had not yet been shown live *in vivo*.

The reaction of astrocytes can be triggered by numerous extracellular factors including inflammatory cytokines [162], growth factors (e.g. FGF, TGF, EGF, VEGF) [164,165], reactive oxygen species (ROS), NO [102,166-169], sonic hedgehog (Shh) [170-172]. Those triggers are known to activate complex network of para- and autocrine signaling pathways in reactive astrocytes (Figure 1.7); see reviews [141,173].

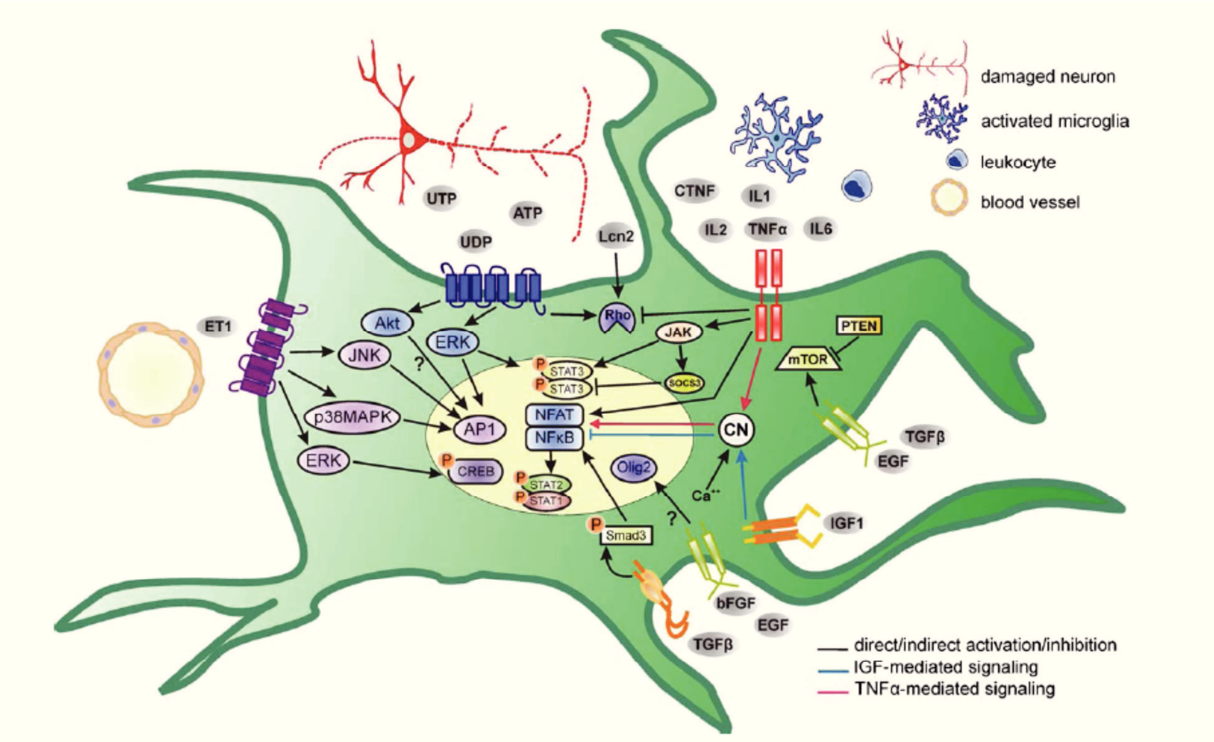

Figure 1.7 Signaling molecules and pathways triggering reactive astrocytes.; adapted from Buffo et al. [141].

However, although diverse intracellular pathways are described, such as JAK/STAT [155,156,174], Wnt/β-catenin [130], TGFβ/SMAD [162,175,176], mTOR [177,178], Notch [179] and ephrin-mediated signaling [180] via MAP/ERK and RhoGTPase activated cascades, a link of selected pathways to specific responses of reactive astrocytes is lacking.

Therefore, it remains open whether different molecular factors trigger different astrocytic responses, and which intracellular signaling cascades are specific for astrocyte polarization, migration or proliferation is still elusive. One key candidate regulating cell polarity and cytoskeleton stability is the RhoGTPase Cdc42, but still little is known about its influence on astrogliosis *in vivo*. Astrocyte-specific deletion of intrinsic regulators involved in cell polarity, migration and proliferation, such as the small RhoGTPase Cdc42 (part 1.3.1) would either affect all astrocytes, or only particular subsets in its reaction to injury, and thereby would provide more information about mechanisms regulating astrogliosis.

1.3.1 RhoGTPase Cdc42: key regulator of cell polarity

The RhoGTPase Cdc42 is a key regulator of cell polarity [181-183] including cytoskeletal dynamics [184], proliferation [185-187] and directional migration [188] of different cell types such as neutrophils, macrophages [189,190], Langerhans cells of the skin [191], fibroblasts and astrocytes [146,147,192,193]. The regulation of these cellular processes (Figure 1.8) is mediated by the activation of Cdc42 that couples different downstream targets, e.g. WASP/Arp2/3 complex, Par6/aPKC, JNK/MAPK and mTOR pathway [184,186,194,195].

In reactive astrocytes intrinsic functions of Cdc42 signaling have been addressed using an *in vitro* scratch assay. Thereby, the influence of Cdc42 on cell polarity including cytoskeletal re-arrangement was studied with regard to re-orientation of the Golgi apparatus and the centrosome (microtubule organizing center, MTOC), the formation and elongation of membrane protrusions (polarization), as well as directed migration of astrocytes [146,147,182,196].

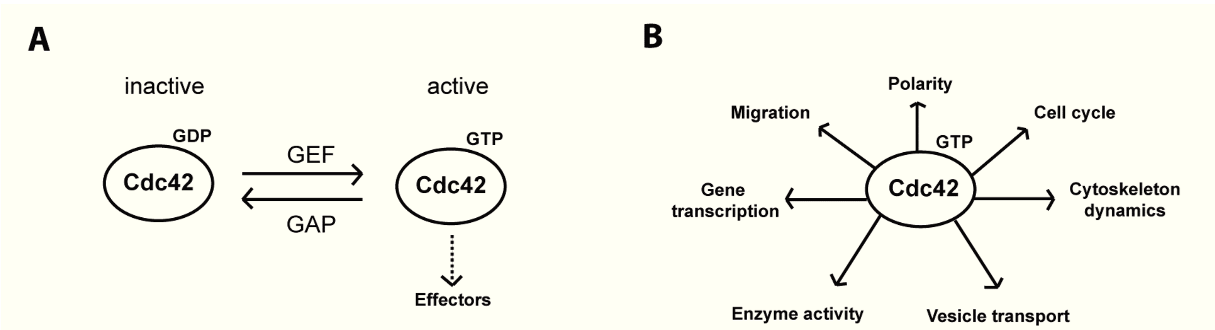

Figure 1.8 RhoGTPase activation and cellular effects. (A) Cdc42 activation is regulated by GEFs (Guanine nucleotide exchanges factors) and GAPs (GTPase activating proteins) upon external stimuli e.g. growth factors, cytokines, integrins. (B) RhoGTPase signaling activates effectors involved in a variety of cellular processes including cell polarity linked to cytoskeletal dynamics, mitosis and migration (modified from Hall [195]).

Loss-of-function studies using pharmacological inhibitors or microinjection of dominant-negative (dn) constructs revealed controversial results on the protrusion formation and polarized migration in fibroblasts and astrocytes [196-199]. Recently Seo and colleagues investigated Cdc42 signaling after spinal cord injury with pharmacological inhibition of Cdc42, and proposed impaired astrocyte migration and improved axonal regeneration based on still analysis [200]. While herein a genetic approach was chosen to address the cell-autonomous,

Cdc42-mediated effects selectively (without interfering with other RhoGTPases) and specifically by targeted deletion in astrocytes isolated from cdc42^{floxed} mice [30]. Initial loss-of-function experiments done by Stefanie Robel compared the effects of different members of the RhoGTPase protein family such as RhoA, Rac1 and Cdc42 on astrocyte polarity *in vitro* using a scratch assay. The conditional deletion of *cdc42* caused defects in MTOC re-orientation and protrusion formation of scratch-wounded astrocytes, suggesting Cdc42 to be a potent candidate for further *in vivo* studies [182]. A genetic approach to conditionally delete *cdc42* in astrocytes in combination with live imaging *in vitro* and *in vivo* allowed to investigate the role of Cdc42 in astrocyte reaction to acute injury (migration, proliferation, polarization). Indeed, genetic ablation of *cdc42 in vivo* affected not only neuronal polarity regarding cytoskeletal organization and axonal outgrowth [181], but moreover polarity cues guiding mitosis and fate of neural progenitor during embryonic development [201]. However, the regulation of astrocyte proliferation and migration by Cdc42 signaling after acute brain injury had not been studied yet.
A better understanding of how Cdc42 signaling controls these processes in all or only specific subtypes of astrocytes after injury *in vitro* compared to the situation *in vivo,* would provide novel insights in the heterogeneity of reactive astrogliosis and help to identify molecular patterns of more plastic subsets.

1.3.2 Astrocyte subpopulation with stem cell potential

The plasticity of astrocytes *in vitro* was shown by reprogramming postnatal cortical astrocytes from mice into functional neurons by retrovirus-mediated expression of neurogenic factors like neurogenin-2, Dlx2 and Mash1 [202-205]. Recently, the generation of multipotent neural stem cells derived from human cortical astrocytes by lentiviral transduction of OCT4, SOX2 and NANOG [206] additionally showed the potential of glial-derived cells for neuronal repair *in vitro* and *in vivo*.
After brain injury, reactive astrocytes share some features with radial glia in neurogenic niches including proliferative activity and re-expression of developmental markers (see Table 1-1) [17,32,113,141207]. Moreover, some reactive astrocytes acquire the ability to form self-renewing, multipotent neurospheres under pathological conditions [113,172]. The neurosphere-forming capacity of cultured reactive astrocytes isolated from injured brain regions of adult mice

together with the self-renewal and multipotency of those neurospheres, which could be passaged and differentiated into neuronal and glial lineages [113,172], further corroborates de-differentiation. Thus, reactive astrocytes serve as a source of stem cells outside of the neurogenic niches in the injured adult brain [17,208-210]. However, the number of astrocytes acquiring stem cell properties is extremely low. Therefore, it is even more important to further examine the heterogeneity of reactive astrocytes by *in vivo* live imaging after acute injury using a stab wound model.

1.3.3 Stab wound injury – Model for traumatic brain injury in mice

Traumatic brain injury (TBI) is defined as mild to severe contusive or invasive intracranial injury induced by an external force. The high TBI incidence (200.000 patients/ year in Germany [211]) amongst children, athletes and after accidents is a major cause of mortality. Depending on its severity, the clinical outcome is mainly determined by the primary brain damage as well as secondary cerebral hypoxia, edema, raised intracranial pressure and neuroinflammation causative for post-traumatic depression, epilepsy, cognitive deficits and mental disability [212]. Since therapeutic interventions for improving survival rate and neuroprotection are limited, it is mandatory to understand repair mechanisms and regenerative potential including glial cell functions after TBI. Therefore, mimicking TBI pathology in rodent models by performing a mild invasive stab wound lesion in the somatosensory cortex of mice allows to investigate acute and chronic responses of different glial cell types after TBI [11,113,114]. In contrast to other models, e.g. laser-induced lesion [213] or concussive head trauma [118,214], a stab wound injury mechanically disrupts blood vessels leading to rapid infiltration of leukocytes, activation of residing microglia, neuronal cell death followed by NG2+ cells and astrocyte response and glial scar formation (see part 1.3). As previously shown, residing microglia and quiescent astrocytes re-gain proliferative capacity, and proliferative NG2+ react by cell cycle shortening [114]. The time course of reactivity, interaction and contribution of different glial cell types, pericytes [215,216] and the cerebral vasculature during BBB repair, wound healing and neuronal regeneration is not yet entirely understood and requires further studies.

1.4 Transgenic mouse lines to study astrocyte reaction *in vitro* and *in vivo*

Herein, the stab wound model was performed in different genetically modified mouse lines (Table 1-2) to visualize astrocytes *in vivo* and to follow their reaction after injury by live imaging. A comprehensive list of generally available mouse models for targeting astrocytes in the adult brain [217] was published online by Prof. Dr. Frank Kirchhoff (see link: http://networkglia.eu/tiermodelle). In commonly used hGFAP-eGFP transgenic mice enhanced green fluorescent protein (eGFP) is driven by a human GFAP promoter (see Table 1-2) and expressed in a subset of cortical astrocytes in the adult brain. Notably, hGFAP promoter activity regulated in response to injury can cause increasing numbers of GFP+ cells. Therefore, the inducible GLAST^{CreERT2} knock-in mouse line [55] crossed with an inducible CAG-(CAT)-eGFP reporter line [218] provides several advantages for fate mapping studies of quiescent and reactive astrocytes *in vivo*: (1) GFP-labeling of a subset of GLAST+ protoplasmic astrocytes in the adult brain, (2) bright and durable fluorescent signal for single cell tracing by repetitive live imaging and (3) cytoplasmic GFP expression represents nicely the whole cell morphology with ramified processes.

In short, this mouse line uses GLAST-promoter driven expression of a modified estrogen receptor binding site fused to the Cre-recombinase (CreERT2). Upon administration of an estrogen analogue (i.e. tamoxifen), which binds cytoplasmic CreERT2 and enables its nuclear translocation, CreERT2 mediates the excision of loxP-flanked (“floxed”) DNA loci. Herein the Cre/ loxP principle is utilized on the one hand for spatio-temporally controlled expression of eGFP under the chicken β-actin (CAG) promoter [218] or activation of other reporters e.g. *R26R*-Confetti line [219] after excision of a floxed stop cassette. On the other hand, GLAST^{CreERT2} mice were chosen for loss-of-function studies, such as astrocyte-specific deletion of *cdc42* in mice carrying floxed alleles of the *cdc42* gene [30].

Thus, GLAST^{CreERT2}/ CAG-eGFP/ cdc42^{floxed} mice are well suited for these live imaging studies as astrocyte-specific induction of a fluorescent reporter allows cell tracing, as well as the targeted deletion of a specific gene of interest in the same cell population. Depending on the aim of the study, the recombination rate in GLAST^{CreERT2} mice can be adjusted by the tamoxifen dose for targeting a large pool of astrocytes – maximally 60-80% of all astrocytes [55] – or only few cells. A low density of GFP+ astrocytes is advantageous for long-term tracing of individual cells by *in vivo* imaging using two-photon laser scanning microscopy.

Table 1-2 Mouse lines used for this study of astrocyte reactions after brain injury

Mouse line	Description	References
GLAST^{CreERT2} x CAG-(CAT)-eGFP	Tamoxifen-inducible eGFP expression in cortical astrocytes (max. 60-80% of all astrocytes)	55,218
GLAST^{CreERT2} x R26R-Confetti	Tamoxifen-inducible, stochastic expression of CFP, YFP, GFP or RFP in cortical astrocytes	55,219
GLAST^{CreERT2} x cdc42^{floxed}	Conditional deletion of *cdc42* in astrocytes	30,220
hGFAP-eGFP	Expression of green fluorescent protein under human GFAP promoter in a subset of cortical astrocytes	50,221
Aldh1L1-eGFP	GFP expression in all cortical astrocytes	33,36,37

1.5 Two-photon laser scanning microscopy for live imaging in the mouse brain

By the invention of two-photon laser scanning microscopy (2pLSM), real-time imaging in living animals became applicable to follow cell dynamics and cellular interactions. Thereby, structural and developmental changes can be followed over short or long periods inside different tissues such as the brain [222-224], spinal cord [108,225,226], skin [227,228] and kidney [229]. For experimental neurobiology 2pLSM is a favorable tool due to several advantages: (1) deep tissue penetration (up to 1mm) using pulsed, near-infrared laser light, (2) avoidance of phototoxic effects, (3) high-resolution images and (4) application for repetitive live imaging over a desired time period in anaesthetized or even freely moving animals [230-232].

Two widely used methods for chronic or acute live imaging in the brain are (1) the open-skull preparation with chronic cranial window implantation (Figure 1.9) as described by [99,223,233-237] or (2) a thinned-skull preparation [238-242]. While the latter method is less invasive inducing only minimal glial reaction, astrogliosis was detected under chronically implanted windows up to one month after craniotomy [223,242]. Nevertheless, open-skull preparation is the method of choice for many functional studies, which require manipulation or topical application of substances directly onto the *dura*, but also for assessment of specific lesion paradigms, e.g. stab wound.

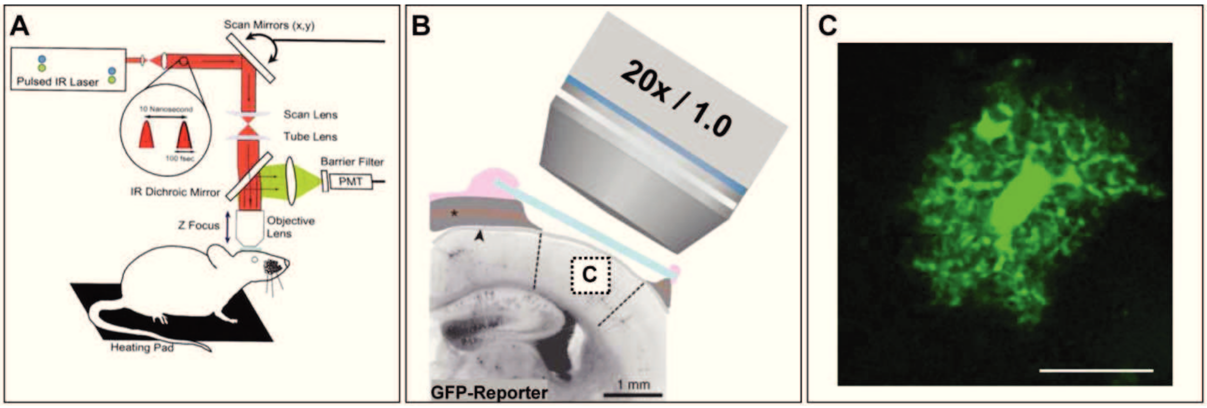

Figure 1.9 *In vivo* imaging in the cerebral cortex of adult mice. (A) Schematic illustration (modified from Goldman [243] of a 2pLSM set-up for repetitive brain imaging through a chronic cranial window (**B**, modified from Holtmaat et al. [223]) that is implanted after craniotomy (partial removal of the cranial bone; asterisk) over the dura (arrow head) in GFP-reporter mice. **(C)** Live image of a protoplasmic astrocyte with endogenous, cytoplasmic eGFP expression using GLAST^{CreERT2}/ CAG-eGFP mice and 20x / 1.0 NA objective (scale bar: 50µm).

Using 2pLSM for functional imaging in the intact brain essentially increased the knowledge about neuronal circuits [244,245], synaptic plasticity and spine dynamics [236,237,242] as well as astrocytic calcium signaling [234,246,247], the topology of the cerebral vasculature [98,248,249] and CSF circulation [99]. Moreover live 2pLSM gained novel insights into acute and chronic CNS pathologies [250], e.g. brain tumor formation and metastasis [251-253], plaque pathology and microvascular dysfunction in Alzheimer's disease [233,254], ischemic damage and associated vascular remodeling [248,255-257], cortical microhemorrage [258] as well as axonal de-/ regeneration in the spinal cord using the experimental autoimmune encephalomyelitis (EAE) model of multiple sclerosis [108,259] and a transgenic mouse model of familiar ALS [226].

Particularly with regard to the glial reaction after CNS diseases, the motility and clustering of microglia and infiltrating leukocytes during inflammatory processes in the lesioned spinal cord and cortex has been live observed using 2pLSM [224,260-262]. In contrast, little is known about the dynamics of reactive astrocytes and NG2+ cells in response to cortical injury *in vivo*. For live imaging of astrocytes in the cortex (up to 800µm deep) of anaesthetized mice, cells need to be fluorescently labeled either by application of a transient dye like sulforhodamine (SR101) [98,263], or as herein used by transgenic reporter mouse lines with stable expression of a fluorescent protein under astrocyte-specific promoter (examples listed in Table 1-2). These tools allow to follow the behavior of individual GFP+ astrocytes using repetitive *in vivo* 2pLSM, addressing the heterogeneity of astrocyte reactions after acute traumatic brain injury.

2 Aim of the study

Reactive astrocytes undergo morphological and molecular changes after injury (part 1.3). However, the identity of factors influencing the reaction of astrocytes remains unknown. The questions arose whether all astrocytes respond to an acute injury, or whether specific astrocyte subpopulations have specialized functions after injury. While proliferation and migration of astrocytes were studied *in vitro* [146] and *in situ* [113,114,155], the contribution of reactive astrocytes during glial scar formation has not yet been investigated by *in vivo* live imaging after acute brain injury. Therefore, the following key questions were addressed in my thesis:

(1) Which factors influence astrocyte migration (a) *in vitro* and (b) *in vivo*?
(2) Which factors influence astrocyte proliferation (a) *in vitro* and (b) *in vivo*?
(3) How can these processes be compared *in vitro* and *in vivo*?

To address these questions, the behavior of wildtype and *cdc42*-deficient astrocytes was monitored (a) *in vitro* by time-lapse video microscopy after scratch wound, as well as (b) *in vivo* by 2pLSM live imaging after a small punctuate wound or larger stab wound in different transgenic mouse lines (see Table 1-2). For further characterization of the proliferative astrocyte subpopulation after stab wound the live observations were validated in fixed tissue by immunohistochemistry and confocal laser scanning microscopy as well as on ultrastructural level by immuno-labeled electron microscopy (EM) in collaboration with Prof. Ingo Bechmann and Dr. Martin Krüger at the Institute for Anatomy at the University of Leipzig.

3 Results

The studies on astrocyte's behavior and recruitment after acute injury *in vitro* and *in vivo*, as well as the role of Cdc42 in these processes, are published in two separate articles in international peer-reviewed journals. For each article the experimental results are summarized (part 3.1. and 3.2.), and the contributions of all authors are given below.

3.1 The role of RhoGTPase Cdc42 in astrocyte recruitment to the injury site

This work includes the published study entitled 'Genetic Deletion of Cdc42 Reveals a Crucial Role for astrocyte recruitment to the injury site in vitro and in vivo' by Stefanie Robel*, **Sophia Bardehle***, Alexandra Lepier, Cord Brakebusch, and Magdalena Götz in *The Journal of Neuroscience* 2011, 31(35):12471–12482.
* equally contributed to this work.

In this study the intrinsic role of Cdc42 for astrocyte polarity and recruitment after injury was studied *in vitro* and *in vivo*. Therefore, *cdc42* was deleted in cultured astrocytes that were isolated from postnatal cortices of cdc42^{floxed} mice, and transduced with lentivirus encoding Cre-recombinase. As injury model, the scratch assay was used to follow the behavior of cdc42-deficient astrocytes by video time-lapse microscopy for 5 days after the lesion. While the ability to elongate protrusions towards the scratch was *per se* maintained, the lack of functional Cdc42 disturbed astrocyte polarity and led to multi-directional, randomly oriented protrusions associated with disoriented migration and impaired wound closure.
To evaluate the effect of cdc42 deletion in astrocytes in the adult mouse brain, GLAST^{CreERT2} mice were crossed with cdc42^{floxed} mice and inducible eGFP reporter mice. After tamoxifen induction and stab wound injury, brains were analyzed immunohistochemically 7 days after injury. Like *in vitro*, *cdc42*-deficient, GFP+ astrocytes were able to polarize towards the injury – *in vivo* with even enhanced protrusion length compared to controls – while reduced numbers of

recombined astrocytes were found at the injury site. Taken together, these data provide evidence that Cdc42 signaling intrinsically regulates astrocyte polarity, directional migration *(in vitro)* and their recruitment to the injury. Whether proliferation and/ or migration are involved in astrocyte recruitment *in vivo*, and to which extent this is controlled by Cdc42 was addressed by the follow-up study using *in vivo* live imaging (part 3.2).

Contributions of different authors to this publication

The experiments and data analyses were performed by Stefanie Robel and me, who equally contributed to this work (*). I did the *in vitro* time-lapse experiments including scratch assay, video microscopy and tracking analysis (Figure 4; Movie 1 and 2), as well as parts of the immunohistochemical analyses including confocal microscopy and quantifications (Figure 5 and 6). The project was initially designed by Stefanie Robel and Magdalena Götz. Alexandra Lepier contributed with viral vector design and virus production. Cord Brakebusch provided the cdc42^{floxed} mice. Stefanie Robel, Magdalena Götz and I wrote the manuscript. This project was financed by Magdalena Götz.

Neurobiology of Disease

Genetic Deletion of *Cdc42* Reveals a Crucial Role for Astrocyte Recruitment to the Injury Site *In Vitro* and *In Vivo*

Stefanie Robel,[1,2]* Sophia Bardehle,[1,2]* Alexandra Lepier,[1] Cord Brakebusch,[3] and Magdalena Götz[1,2]
[1]Physiological Genomics, Institute of Physiology, Ludwig-Maximilians University München, 80336 München, Germany, [2]Institute for Stem Cell Research, HelmholtzZentrum München, 85764 Neuherberg, Germany, and [3]Biotech Research and Innovation Centre, University of Copenhagen, 2200 Copenhagen, Denmark

It is generally suggested that astrocytes play important restorative functions after brain injury, yet little is known regarding their recruitment to sites of injury, despite numerous *in vitro* experiments investigating astrocyte polarity. Here, we genetically manipulated one of the proposed key signals, the small RhoGTPase Cdc42, selectively in mouse astrocytes *in vitro* and *in vivo*. We used an *in vitro* scratch assay as a minimal wounding model and found that astrocytes lacking Cdc42 (Cdc42Δ) were still able to form protrusions, although in a nonoriented way. Consequently, they failed to migrate in a directed manner toward the scratch. When animals were injured *in vivo* through a stab wound, Cdc42Δ astrocytes developed protrusions properly oriented toward the lesion, but the number of astrocytes recruited to the lesion site was significantly reduced. Surprisingly, however, lesions in Cdc42Δ animals, harboring fewer astrocytes contained significantly higher numbers of microglial cells than controls. These data suggest that impaired recruitment of astrocytes to sites of injury has a profound and unexpected effect on microglia recruitment.

Introduction

Astrocytes play crucial roles in the adult brain, yet the molecular mechanisms governing their specific functions are still poorly understood. Throughout the brain astrocytes occupy distinct territories (Bushong et al., 2002; Ogata and Kosaka, 2002), where they perform various functions including the regulation of blood flow in response to neural activity (Iadecola and Nedergaard, 2007; Schummers et al., 2008), requiring contact of their endfeet to blood vessels. Astrocytes are polarized toward the basement membrane around blood vessels and target proteins, such as aquaporin-4 to their endfeet (Bragg et al., 2006). If this interface fails to form properly, as is the case following a loss of β1-integrins, there results a mild reactive gliosis with all hallmarks of reactive astrogliosis except proliferation (Robel et al., 2009), highlighting the importance of astrocyte polarity. However, little is known about the role of astrocyte polarity after brain injury *in vivo*.

The reaction of astrocytes to brain injury presents as reactive astrogliosis that ranges from wound closure through astrocyte dedifferentiation, to scar formation (Ridet et al., 1997; Silver and Steindler, 2009; Sofroniew and Vinters, 2010). Astrocyte activation is characterized by hypertrophy and upregulation of many proteins, including the intermediate filaments vimentin and glial fibrillary acidic protein (GFAP), and proteins expressed at earlier developmental stages, such as nestin, Tenascin C or phosphacan (Buffo et al., 2008; Sirko et al., 2009). Interestingly, following severe injury, a large fraction of reactive astrocytes proliferate and some even regain stem cell potential (Buffo et al., 2008; Robel et al., 2011). While this dedifferentiation may be considered beneficial, reactive astrocytes also upregulate various cell surface molecules, e.g., chondroitin sulfate proteoglycans, and participate in scar formation and inhibition of axon growth across this region (Reier and Houle, 1988; Busch and Silver, 2007). Thus, astrocytes perform numerous functions in response to injury, partially differing depending on the type and size of injury (Pekny and Pekna, 2004; Sofroniew, 2009).

A key aspect common to many injuries is the increase in astrocyte number at the injury site, which has been suggested to be a result of oriented migration and proliferation (Okada et al., 2006; Buffo et al., 2008; Simon et al., 2011). Given that the presence of astrocytes at the injury site is functionally important (Sofroniew, 2009), it is critical to understand the molecular machinery governing astrocyte polarity and recruitment to the injury site *in vivo*. The small RhoGTPase Cdc42 has emerged as a

Received May 31, 2011; revised July 7, 2011; accepted July 11, 2011.
Author contributions: S.R. and M.G. designed research; S.R. and S.B. performed research; A.L. and C.B. contributed unpublished reagents/analytic tools; S.R. and S.B. analyzed data; S.R., S.B., and M.G. wrote the paper.
This research was supported by grants from the Deutsche Forschungsgemeinschaft (DFG GO 640/7-1, 8-1, 9-1; SPP-1048), including the excellence cluster Center for Integrated Protein Science Munich, the European Community (Integrated Project EuTRACC, Grant no. LSHG-CT-2007-037445), the SFB 596 and 870, and the Bundesministerium für Bildung und Forschung (Grants 01GN0503 and FKZ: 01 GN 0820); and the Helmholtz Association in the framework of the "Helmholtz Alliance for Mental Health in Ageing Society" (HELMA), the Impulse & Networking Fund of the Helmholtz Association (HA-215), the Virtual Institute for Neurodegeneration & Ageing (VH-VI-252), as well as by the Bavarian research network "ForNeuroCell." We thank foremost the Graduate School of Systemic Neuroscience for financial support of the time-lapse video microscope, without which this study would not have been possible; Alexander Pfeifer (University of Bonn) for the EGFP and Cre-IRES-EGFP lentiviral plasmids; Christian Naumann for cloning the tdTomato and tdTomato-IRES-Cre lentiviral plasmids, as well as for establishment of the time-lapse imaging; Silvia Cappello, Swetlana Sirko, Susan Buckingham, Vishnu Cuddapah, and Harald Sontheimer for critical comments on the manuscript; and Gabi Jäger, Simone Bauer, Andrea Steiner-Mezzadri, Tatiana Simon-Ebert, and Rebecca Krebs for excellent technical assistance.
*S.R. and S.B. contributed equally to this work.
S. Robel's current address: Department of Neurobiology and Center for Glial Biology in Medicine, University of Alabama at Birmingham, Birmingham, AL 35294.
Correspondence should be addressed to Magdalena Götz, Physiological Genomics, Ludwig-Maximilians University München, Pettenkoferstrasse 12, 80336 München, Germany. E-mail: Magdalena.Goetz@helmholtz-muenchen.de.
DOI:10.1523/JNEUROSCI.2696-11.2011

Table 1. First antibodies

Recognized antigen	Host-animal/ Ig subtype	Pretreatment incubation conditions	Company/Source
Cdc42	Mouse IgG3	1:100	Santa Cruz Biotechnology (sc-8401)
Cop1 (clone CM1A10)	Mouse IgG1	1:100	Gift from J. E. Rothman, Yale School of Medicine, New Haven CT
GFAP	Mouse IgG1	1:1000	Sigma (G3898)
GFAP	Rabbit	1:500	Dako/Invitrogen (Z0334)
GFP	Mouse IgG1	1:1000	Millipore (MAB3580)
GFP	Rabbit	1:1000	Invitrogen (A6455)
GFP	Chick	1:1000	Aves Lab (GFP-1020)
Iba1	Rabbit	1:500	Wako (019-19741)
NeuN	Mouse IgG1	1:100	Millipore (MAB377)
γ-Tubulin	Mouse IgG1	1:100	Sigma (T5326)
pan-Tubulin	Rat	1:10	Gift from the Department of Anatomy and Cell Biology, Ludwig-Maximilians University München
RFP	Rabbit	1:500	Millipore (AB3216)
S100	Rabbit	1:100	Sigma (S2644)
S100β	Mouse IgG1	1:500	Sigma (S2532)

key regulator of polarization, influencing directional migration in cultured fibroblasts and astrocytes (Nobes and Hall, 1999; Etienne-Manneville and Hall, 2001, 2003). However, these results were obtained using dominant-negative forms of Cdc42, and genetic deletion of *Cdc42* in fibroblasts revealed discrepancies in polarization effects and directed migration (Czuchra et al., 2005). This is probably due to inhibition of several other members of the RhoGTPase family by dominant-negative Cdc42 (Czuchra et al., 2005). Therefore, we set out to determine the role of astrocyte polarity by investigating the Cdc42 function in astrocytes *in vitro* and *in vivo* using genetic tools to delete *Cdc42*.

Materials and Methods

Animals and surgical procedures

C57BL/6J//129/Sv-Cdc42 mice carrying alleles for *Cdc42* flanked by loxP sites (Wu et al., 2006) were mated to mice expressing a Cre-recombinase estrogen receptor fusion protein in the GLAST locus (Mori et al., 2006). To label recombined cells, the CAG-CAT-EGFP reporter line, expressing the CMV (β-actin promoter) and the loxP flanked *chloramphenicol acetyltransferase* (*CAT*) gene upstream of the EGFP cassette (Nakamura et al., 2006) have been used. Mice of either sex were included in the analysis.

All animal procedures were performed in accordance with the Policies on the Use of Animals and Humans in Neuroscience Research, revised and approved by the Society of Neuroscience and the state of Bavaria under license number 55.2-1-54-2531-23/04 or 55.2-1-54-2531-144-07. Tamoxifen was administered as described previously (Mori et al., 2006). For stab wound injury, animals were deeply anesthetized and fixed in a stereotactic frame. Stab wounds were placed into the somatosensory cortex of the right hemisphere (1.5–2 mm long, 0.2 mm wide and 0.5–0.6 mm deep).

Histological procedures

Adult animals were deeply anesthetized and transcardially perfused with PBS followed by 4% PFA in PBS (100 ml/animal). Brains were postfixed in the same fixative for at least 2 h to maximal overnight at 4°C, washed in PBS, and embedded in 4% agarose for cutting 60 μm vibratome sections.

For immunofluorescent labeling, sections were incubated overnight at 4°C in PBS containing the first antibody, 0.5% Triton X-100 (TX) and 10% normal goat serum (NGS), washed in PBS, and incubated for 2 h at room temperature in 0.5% TX and 10% NGS containing the secondary antibody. After washing in PBS, sections were mounted on glass slides and embedded in Aqua-Polymount and covered by a glass coverslip.

Primary and secondary antibodies are listed in Table 1 and Table 2.

Table 2. Secondary antibodies

Antibody	Host species	Label	Dilutions	Company
α-Chick	Goat	Alexa Fluor 488	1:500	Invitrogen (A11039)
α-Chick	Donkey	FITC	1:200	Dianova (703095155)
α-Rabbit	Donkey	Alexa Fluor 488	1:500	Invitrogen (A21206)
		Cy3	1:500	Dianova (711165152)
		Alexa Fluor 594	1:500	Invitrogen (A21207)
	Goat	Cy3	1:500	Dianova (111165144)
		Biotinylated	1:200	Vector (BA-1000)
α-Mouse IgG1	Goat	Alexa Fluor 488	1:500	Invitrogen (A21121)
		Alexa Fluor 594	1:500	Invitrogen (A21125)
		Biotinylated	1:200	South.B. (1070-08)
α-Mouse IgG2a	Goat	Alexa Fluor 488	1:500	Invitrogen (A-21131)
		Alexa Fluor 594	1:500	Invitrogen (A-21135)
α-Mouse IgG	Goat	Alexa Fluor 488	1:500	Invitrogen (A11029)
		Cy3	1:500	Dianova (115165166)
		Cy5	1:500	Dianova (115176072)
	Donkey	Alexa Fluor 594	1:500	Invitrogen (A-21203)

The terminal deoxynucleotidyl transferase dUTP nick end labeling (TUNEL) assay was performed using an *in situ* cell death detection kit (Roche) in accordance with the manufacturer's instructions.

The cresyl violet (Nissl) staining was performed as follows. Free-floating vibratome sections were mounted and dried on glass slides before they were dehydrated and washed in xylene two times for 10 min to remove lipid-rich structures. After rehydration, sections were stained in a 0.1% cresyl violet solution spiked with acetic acid for 3 min, then washed, dehydrated, and cleared in xylene, before they were embedded in Permount mounting medium and covered by a glass coverslip.

Lentivectors and lentiviral preparation

Lentiviral expression plasmids contained the sequence for *EGFP* or *Cre-IRES-EGFP* under the CMV promoter (Pfeifer et al., 2001). To avoid any differences in expression levels of the fluorescent proteins, we modified these constructs such that the red fluorescent protein tdTomato was placed directly behind the CMV promoter (LV-CMV-tdTomato and LV-CMV-tdTomato-IRES-Cre), thus resulting in comparable signal intensities. To generate the tdTomato-IRES-Cre vector, the Cre-IRES-EGFP plasmid was digested using PstI and SalI to remove the IRES-EGFP cassette. The IRES sequence was amplified with SpeI linkers and placed in front of the Cre sequence into the SpeI restriction site. The tdTomato sequence was then placed behind the CMV promoter by digestion of the CMV-IRES-Cre vector using XbaI, resulting in the lentiviral vector CMV-tomato-IRES-Cre. The tdTomato control construct was generated by replacing the EGFP cassette behind the CMV promoter with the sequence encoding tdTomato.

The lentiviral expression plasmids described above, pCMVΔR8.91 packaging vector (Zufferey et al., 1997), and the pVSVG or pLCMV envelope vector, were cotransfected into 293T cells for production of lentiviral particles as described previously (Naldini et al., 1996). Titers were determined on 293T cells, and for most experiments, 8×10^6 viral particles were used per 500 μl cell suspension.

In vitro *scratch injury assay*

The gray matter of the cerebral cortex from 3–4 postnatal mice (5–7 d old) was dissected and mechanically dissociated in Hanks' buffered saline solution containing 10 mM HEPES. After washing in DMEM medium supplemented with 10% fetal calf serum, 10 mM HEPES, and Penicillin/Streptomycin, a single cell suspension was plated into T75 flasks coated with poly-L-ornithine (PLO), and the medium was changed every other day. After reaching confluence, progenitor cells on top of the astrocyte monolayer were removed by thoroughly shaking the cell culture flask, and astrocytes were passaged onto PLO-coated coverslips or directly into PLO-coated 24-well plates for time-lapse experiments. Astrocyte cultures were transduced by the use of lentiviral particles during the splitting step after resuspension of the cells, and directly plated at a density of 70,000 cells per well on plastic or 100,000 cells per well on glass coverslips. Plates were placed into the incubator for 24 h at 37°C and 5% CO_2 before the medium replacement.

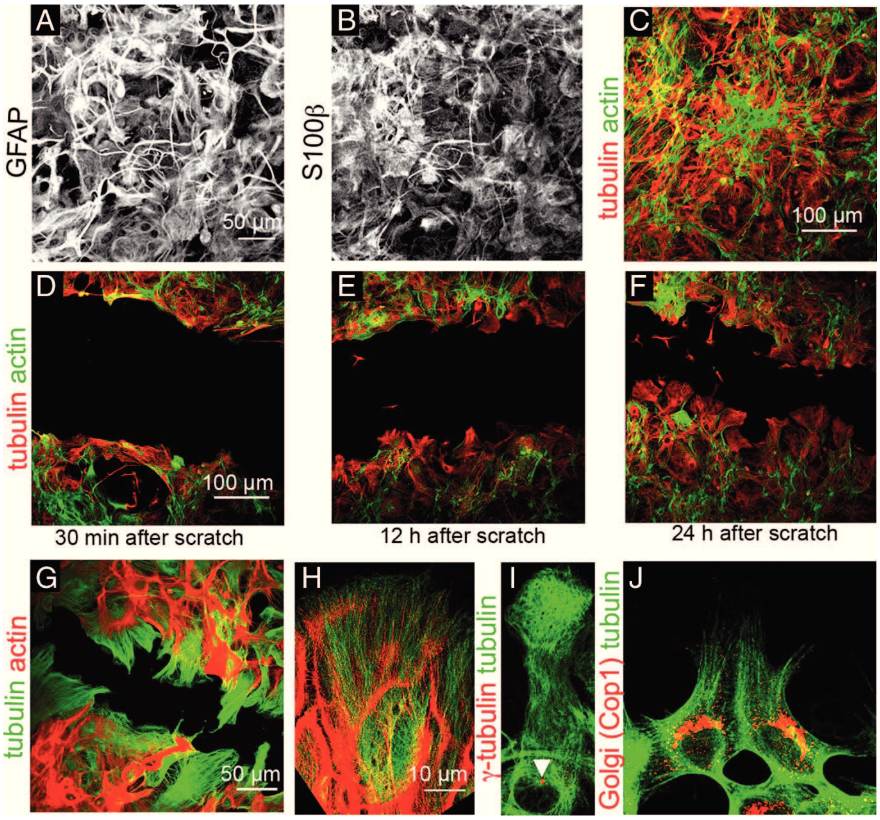

Figure 1. Astrocytes *in vitro* react to injury by polarization. Postnatal astrocyte cultures were positive for GFAP (***A***) and/or S100β (***B***). After scratching, cells in the monolayer (***C***) reacted to the injury and reduced the size of the gap over time (***D–F***). Astrocytes at the scratch formed an extension into the cell-free area (***G–J***). These protrusions were rich in tubulin and stabilized by the actin cytoskeleton (***G, H***). Centrosomes (MTOCs, arrowhead in ***I***) or Golgi (***J***) of polarized cells were reoriented facing the injury area.

Two weeks later, Cdc42 protein loss could be confirmed by immunocytochemistry exclusively in cells transduced by the lentiviruses containing the Cre recombinase (see Fig. 2).

At the earliest, 2 weeks after viral transduction and 1 week after confluence had been reached, *in vitro* scratch wound experiments were started following a published protocol (Etienne-Manneville, 2006). Briefly, the confluent astrocyte monolayer was scratched once from the left to the right wall of the well with a sterile 10 μl plastic tip, resulting in a cell-free cleft ~500 μm wide.

For time-lapse experiments, primary astrocyte cultures were prepared from cortices of postnatal *Cdc42$^{fl/fl}$* mice (postnatal days 5–7, 3–4 animals per experiment) as described above. Two weeks after transduction with tdTomato or tdTomato-IRES-Cre lentivirus, scratch assay experiments combined with video time-lapse microscopy were started. Before scratching the confluent monolayer, Hoechst 33342 dye (Invitrogen) was added to the culture medium at a final concentration of 1 μg/ml, and incubated for 20 min at 37°C with 5% CO_2. Cells were washed twice with prewarmed culture medium and scratched 2 h later. The plate was then placed into the incubation chamber (37°C, 8% CO_2) of an Observer Z1 (Zeiss) fluorescence microscope. Imaging procedures were controlled using AxioVision Rel. 4.7 software for acquisition of phase contrast images every 10 min, and fluorescence images once per hour, for 5 d using a 20× objective and an AxioCam HR camera. To control for potential effects due to Cre toxicity, we also transduced astrocytes cultured from WT (C57BL/6) with the Cre-containing virus, and found no signs of toxicity even 2 weeks after transduction. Moreover, changes were observed neither in the orientation of migration toward the scratch nor in the tortuosity.

For analysis of fixed cells, cultures were either immunostained or labeled for actin filaments by phalloidin-Alexa Fluor 488 (Invitrogen) that was added to the secondary antibody solution.

Data analysis

Results are presented as the mean calculated between different animals (at least three sections per animal and three animals for each time point unless stated differently) or between independent cultures. The variation between animals or cultures is depicted as SEM with one data point representing one animal.

Based on a Gaussian distribution, the data were statistically analyzed by performing an unpaired *t* test. Means were considered significantly different according to the *p* value: $*p \leq 0.05$, $**p \leq 0.01$, and $***p \leq 0.001$. Calculations and statistical analysis were done with Excel and GraphPad Prism 3.0, 4.0, or 5.0. Means were considered significantly different as indicated above.

Quantifications after stab wound in vivo. For analysis of astrocyte protrusion formation after a stab wound injury *in vivo*, lesion size and astrocyte proliferation were assessed using confocal images taken with a Zeiss LSM700 confocal microscope. Length and width of EGFP-positive cells, as well as the longest process toward the stab wound, was measured using ZEN 2008/2009 software (Zeiss). To analyze Nissl+ neuronal number in stab wound lesions, slices were imaged using the Stereo Investigator (mbf Bioscience) software interfaced with an upright Olympus BX-51 microscope. Traces were drawn around regions of interest using a Plan Apo 10× objective corrected for bright-field observation. Counting was performed using a Plan Apo 40× objective. The Stereo Investigator (mbf Bioscience) software was also used to quantify microglia number in confocal images taken using a Leica SP5 microscope.

Quantifications after scratch wound in vitro. Scratched astrocyte cultures were stained for microtubules that were then observed using a fluorescence microscope (Olympus, BX61) with a 60× objective. Reorientation of the centrosome [microtubule organizing center (MTOC)] in astrocyte cultures after scratch wound was quantified by separating the area around the nucleus into 4 equal quadrants that joined in the center of the nucleus of the cell of interest. The quadrants were placed with one quadrant facing the scratch and the median of each 90° angle located either perpendicular or parallel to the scratch. MTOCs were scored as reoriented when they were located in the quadrant facing the scratch. Transduced cells in the first row adjacent to the scratch that displayed one major protrusion three times longer than wide were scored as "protruding cells." The data were obtained from three independent preparations from different litters. For each preparation and time point, two different coverslips and at least 100 transduced cells per coverslip were analyzed and one coverslip was considered a single data point.

Images from time-lapse video microscopy were assembled into a movie and analyzed using the AxioVision Rel. 4.8 software (Zeiss). Quantifications include virus-transduced cells that expressed the red fluorescent protein tomato and lined the front of the scratch. Hoechst labeled nuclei were tracked for three defined time points (1, 3, 5 d). The individual tracking paths of every selected cell were used to calculate the following parameters: mean velocity, straight distance, total distance (equals the path length) and tortuosity (equates to the quotient of total distance and straight distance). Protrusion number and transduced cell polarity was assessed 12, 24, 48, and 120 h post-injury (p.i.) using red fluorescence images. For protrusion turnover, the presence or absence of each single protrusion was analyzed at a first and a second time point for three different periods 0–24 h p.i., 24–48 h p.i. and 48–120 h p.i.

Results

Polarity of astrocytes after scratch injury *in vitro*

Previous studies used a scratch wound assay after injection of dominant-negative and constitutively active constructs to demonstrate a role for the small RhoGTPase Cdc42 in astrocyte polarity (Etienne-Manneville and Hall, 2001, 2003; Etienne-Manneville et al., 2005). In the present study, we used the same assay to examine the effects of *Cdc42* genetic deletion in astrocytes. Toward this aim, mouse astrocytes were obtained from the postnatal cerebral cortex and grown to full confluence to allow for astrocyte maturation. After 3–4 weeks in culture, cells presented with a flat morphology and could be labeled with antibodies against the astrocyte proteins GFAP (Fig. 1*A*) and/or S100β (Fig. 1*B*). In accordance with previous observations (Etienne-Manneville, 2006), after injuring the monolayer (Fig. 1*C*), astrocytes extended processes toward the cell-free scratch region and subsequently migrated and populated the scratch over a 24 h period (Fig. 1*D–F*). These scratch-oriented processes had tubulin-positive fibers in the leading tips and were stabilized by the actin cytoskeleton (Fig. 1*G,H*) at 24 h p.i. The formation of protrusions was accompanied by reorientation of both the centrosome (MTOC) labeled by γ-tubulin (Fig. 1*I*) and the Golgi apparatus labeled by Cop1 (Fig. 1*J*) toward the injury site, starting as early as 4 h after scratch in some cells.

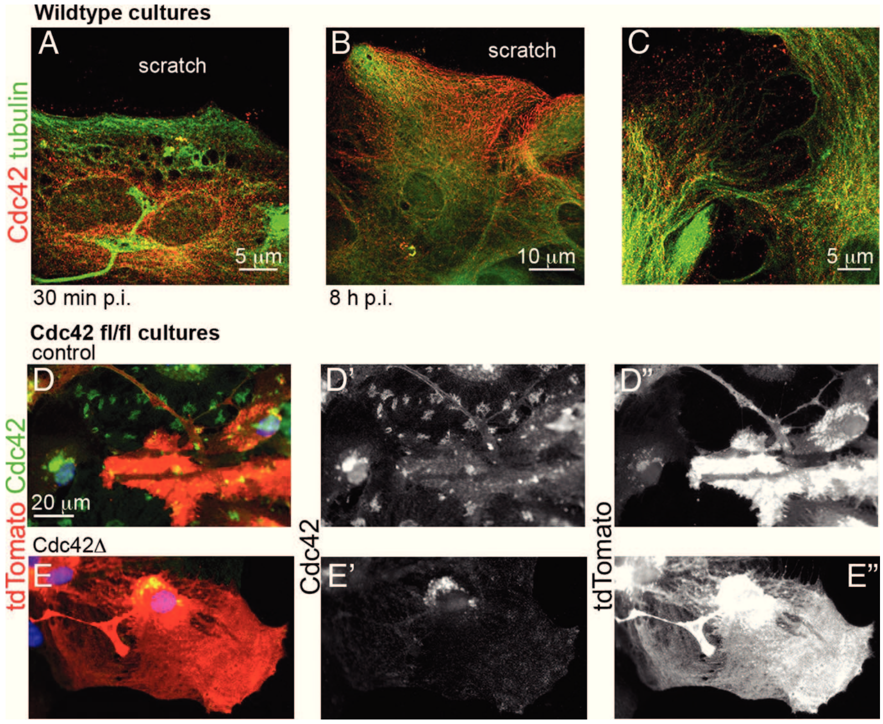

Figure 2. Localization of Cdc42 and protein loss after gene deletion. ***A***, Cdc42 protein is distributed around the nuclei of cells shortly after scratching the monolayer. ***B***, ***C***, Eight hours later, Cdc42 is relocalized toward the leading edge (***B***) and to the tips of tubulin filaments (***C***). ***C–E''***, Two weeks after transduction with control- or Cre-virus, Cdc42 protein expression was examined. Lower-magnification pictures of not completely confluent cultures show diffuse Cdc42 staining and enrichment of the protein as dots at cell borders and within the cells in control-transduced and nontransduced cells (***D–D''***). In contrast, Cdc42 was absent in all these places in tomato-IRES-Cre transduced cells (***E–E''***). Strong red fluorescence around the nuclei of transduced cells breaking through into the green channel could be observed in control and Cdc42Δ cultures. Since this effect was also observed in live imaging experiments, it appears to be intrinsic clustering of the tdTomato protein in the Golgi compartment.

To examine Cdc42 expression in this culture model, astrocytes were stained for Cdc42 at different time points after monolayer injury (Fig. 2*A–C*). Before and shortly after the scratch, endogenous Cdc42 protein was found mainly around the nuclei of astrocytes located at the scratch wound (Fig. 2*A*), whereas after 8 h, the protein relocalized toward the leading edge of astrocytes facing the scratch (Fig. 2*B,C*). This is similar to what has been reported after injecting constructs encoding Cdc42-GFP fusion proteins (Etienne-Manneville and Hall, 2001; Osmani et al., 2010). High-power magnification revealed that Cdc42 was enriched at the tips of newly formed processes (Fig. 2*C*).

Deletion of Cdc42 reveals a crucial role in orientation of cells toward scratch injury *in vitro*

To investigate the role of Cdc42 in astrocyte polarization, we used a genetic deletion designed to avoid potential nonspecific effects of constitutively active and dominant-negative constructs. Postnatal mouse astrocytes containing both alleles of the *Cdc42* gene flanked by loxP sites (Wu et al., 2006) were cultured and transduced with lentiviruses containing the sequence for either Cre-IRES-EGFP/tdTomato-IRES-Cre (Cdc42Δ cultures) or EGFP/tdTomato alone (control cultures; for control of Cre toxicity, see Materials and Methods). Two weeks after transduction, control and Cdc42Δ cultures were stained for Cdc42 (Fig. 2*D–E''*). Cre-transduced cells lacked specific staining (Fig. 2*E–E''*), thereby confirming that the *Cdc42* gene was successfully deleted and Cdc42 protein levels were substantially reduced after lentiviral transduction.

After wounding the confluent astrocyte monolayer (for experimental design, see Fig. 3*A*), the reaction of astrocytes was followed in control and Cdc42Δ cultures. As expected, most of the astrocytes lining the scratch in control cultures formed long polarized protrusions during the first 24 h (Fig. 3*B*). In contrast, transduced astrocytes in Cdc42Δ cultures appeared less organized, with multiple protrusions extending randomly from cells (Fig. 3*C–E*).

To examine the development of this effect more quantitatively, we defined protrusions as (1) cell extensions that were at least three times longer than wide and (2) oriented into the cell-free scratch. We then assessed their appearance at different times after injury. Cells were scored as "unipolar protruding" when they formed a protrusion into the scratch without obvious extensions into other directions. After 30 min, only a small percentage of control- or Cre-transduced astrocytes had formed a protrusion into the scratch (7 $\pm$ 0.8% of control-transduced cells with protrusion 0.5 h p.i., n (cultures) = 6). Over time, an increasing number of control-transduced cells formed protrusions into the cell-free area, and at 24 h p.i., more than half of the cells were clearly elongated toward the injury site (55.2 $\pm$ 2.4% control-transduced cells with protrusion 24 h p.i., n = 6). In contrast, significantly fewer Cre-transduced Cdc42Δ cells formed unipolar protrusions oriented into the scratch at this time (21.6 $\pm$ 3.0% Cre-transduced cells with protrusion 24 h p.i., n = 6, $p \leq 0.0001$). In addition to this significant reduction of Cdc42Δ unipolar cells with scratch oriented protrusions we also noted many Cdc42Δ

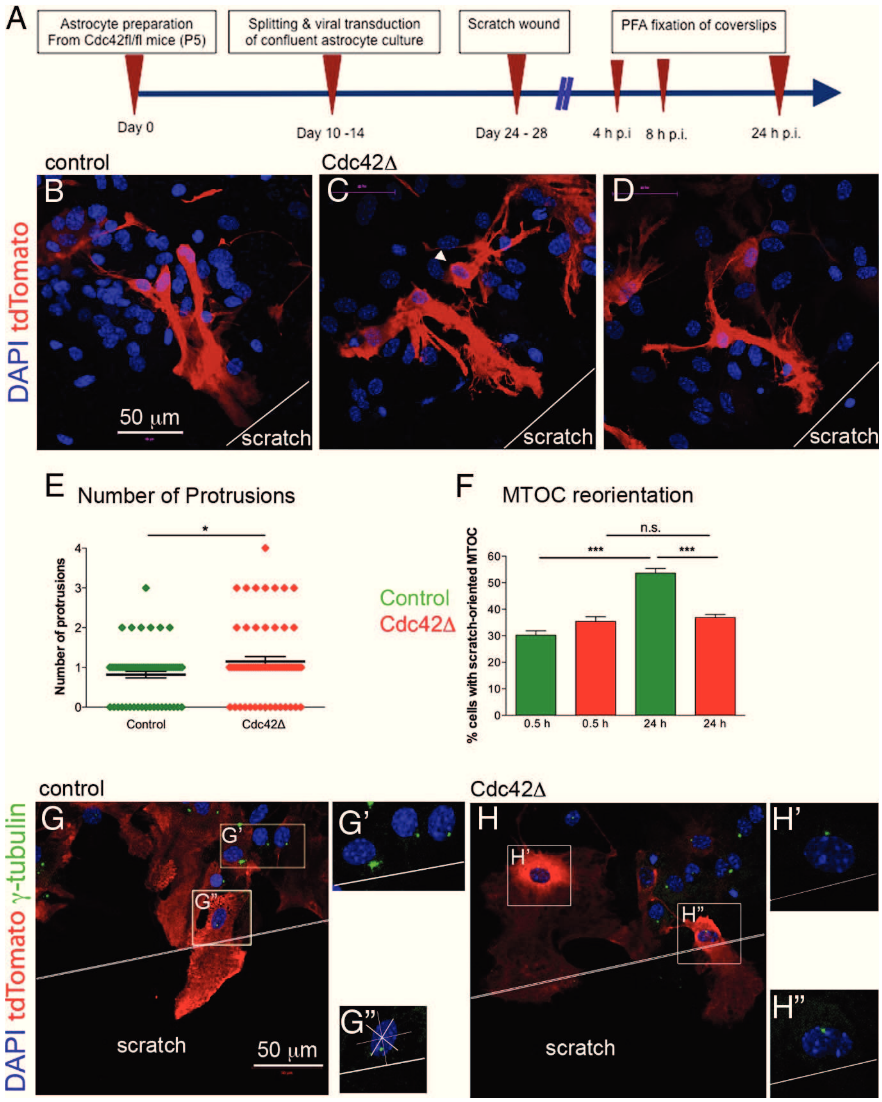

Figure 3. Cdc42 is involved in orienting protrusions and the MTOC toward a scratch wound *in vitro*. ***A–D***, Astrocytes of postnatal *Cdc42*$^{fl/fl}$ mice were cultured in a monolayer, transduced with Cre-IRES-tdTomato or tdTomato virus and scratch wounded 2 weeks later (***A***). In control cultures most cells formed long unipolar protrusions toward the direction of the scratch (***B***). Cdc42Δ cultures were characterized by misoriented cells (white arrowhead in ***C***) and many cells with multiple protrusions directed into various directions around the cell body (***D***). ***E***, Quantification of the number of protrusions per cell is shown (this quantification was done according to the experimental scheme in Fig. 3*A* at 24 h p.i.). ***F***, Quantification of MTOC reorientation 24 h p.i. shows a significant reduction in MTOC reorientation after deletion of Cdc42. ***G–H″***, The majority of first row astrocytes had MTOCs oriented toward the scratch (***G***, ***G′***, ***G″***), whereas MTOCs of Cre-transduced cells were randomly located around the nucleus (***H***, ***H′***, ***H″***). To quantify MTOC orientation, the nucleus was divided into 4 quadrants and MTOCs located in the quadrant facing the scratch were scored as oriented (***G″***). P5, Postnatal day 5.

unipolar cells with protrusions oriented parallel or even away from the scratch (see example in Fig. 3*C*) as well as cells with multiple protrusions (see example in Fig. 3*D*). Indeed, significantly more Cdc42Δ cells had a higher number of protrusions than control cells (Fig. 3*E*), clearly demonstrating that the reduced number of unipolar cells orienting toward the scratch is not due to a failure of process formation. We therefore asked whether this defect might be due to defects in polarization.

Previously, it has been shown that astrocytes place their MTOC in front of their nucleus toward the direction of a scratch injury, and this appears to be a prerequisite for oriented protrusion formation (Etienne-Manneville and Hall, 2001). To investigate whether the reorientation of the MTOC was disturbed, we used the same assay (Fig. 3*A*) and compared the number of reoriented MTOCs in control- and Cre-transduced astrocytes (Fig. 3*F–H″*). Since the MTOC is located close to the nucleus, the area around the nucleus was separated into 4 equal quadrants and placed such that one quadrant was facing the scratch with each 90° angle being either perpendicular or parallel to the scratch (Fig. 3*G″*). In nonoriented cells, the MTOC should be located randomly around the nucleus, i.e., in 25% of all cases in any of the 4 quadrants. Only cells with MTOCs clearly belonging to a given nucleus were included in the quantification, and they were scored as reoriented when they were located in the quadrant facing the scratch (Fig. 3*G″*).

At 30 min after wounding MTOCs were facing the scratch in a random manner. As soon as 4 h p.i., some control-transduced astrocytes adjacent to the scratch started to reorient their MTOC toward the scratch (data not shown). This proportion increased even further at 24 h p.i. (Fig. 3*F*,*G″*). Comparable to control cells, at the start of the experiment, MTOCs of Cdc42Δ astrocytes were randomly facing the scratch area. However, at 24 h p.i., the number of reoriented MTOCs within Cdc42Δ astrocytes did not increase further (Fig. 3*F*,*H–H″*), indicating that Cdc42 is required for MTOC orientation toward the scratch.

Loss of Cdc42 causes impaired migration after scratch injury *in vitro*

The above data suggest that Cdc42 deletion leads to defects in the initial orientation of astrocytes toward the scratch. However, as these data were obtained in fixed cultures, we next used time-lapse video microscopy to observe protrusion formation dynamics in relation to cell migration of virally transduced cells over several days (Fig. 4*A*).

As expected, control-transduced astrocytes and nontransduced astrocytes adjacent to the scratch formed unipolar protrusions, translocated their cell bodies, and retracted their rear sides to migrate into the scratch. Within 5 d, astrocytes in control cultures had completely closed the 500 μm wide scratch (Fig. 4*B*; Movie 1). However, Cdc42Δ astrocytes migrated virtually randomly and were often overtaken by WT cells (Fig. 4*B*; Movie 2). To clarify the causes for these defects after loss of Cdc42, we examined astrocyte migration and focused on protrusion formation, stability, and orientation, as well as nuclear translocation, as these are all crucial steps in cell migration and scratch wound closure.

Consistent with the data from still analysis described above, protrusion formation per se was not impaired in Cdc42Δ astrocytes compared with control cells (66 ± 6% of control-transduced cells and 72 ± 4% of Cre-transduced cells formed protrusions 24 h p.i., $n = 3$), while protrusion orientation was remarkably different in Cdc42Δ astrocytes that had a higher number of protrusions that were randomly oriented compared with control cells (Fig. 3*C–E*; data not shown). To understand the cause for the increase in protrusion number in Cdc42Δ astrocytes, we examined protrusion turnover. Within the first 24 h p.i., protrusion turnover was comparable between Cdc42Δ and control astrocytes (Fig. 4*C*). Thereafter, the number of instable protrusions per cell decreased significantly in control astrocytes, due to stabilization of previously formed protrusions. This was not the case for Cdc42Δ astrocyte protrusions, which retained a higher turnover rate at 48 h p.i. (Fig. 4*C*). Thus, Cdc42Δ astrocytes have difficulties in stable maintenance of protrusions over time.

Since defects in process maintenance may affect migration, we next tracked nuclei of control- or Cre-transduced cells over a period of 5 d with hourly distance measurement (132 data points) depicted in a tracking path (Fig. 4*D*). A starting position and an end position was defined for three different time points (1, 3, 5 d p.i.), and based on the fluorescent images taken each hour, the software performed automated tracking. As evidenced by the examples shown in Figure 4*D*, the tracking paths of control astrocytes had a straight linear appearance, whereas the majority of Cdc42Δ cells took a rather coiled path (Fig. 4*D*). Consistent with this impression, the straight distance migrated (shortest path from the starting position to the end position, Fig. 4*E*) was significantly reduced for Cdc42Δ astrocytes to virtually half of the straight distance covered by control cells over the same period (Fig. 4*F*). Conversely, the total migration distance, represented by the overall migration distance of a cell including forward, backward, and sideward movements (Fig. 4*E*), was comparable between control and Cdc42Δ astrocytes (Fig. 4*G*). Consistent with the equivalent migration distance between control and Cdc42Δ cells, the average velocity was also not significantly different between control and Cdc42Δ cells at 1, 3, and 5 d p.i. (Fig. 4*H*). In summary, the overall ability of Cdc42Δ cells to migrate was not impaired, but directed migration toward the scratch was aberrant.

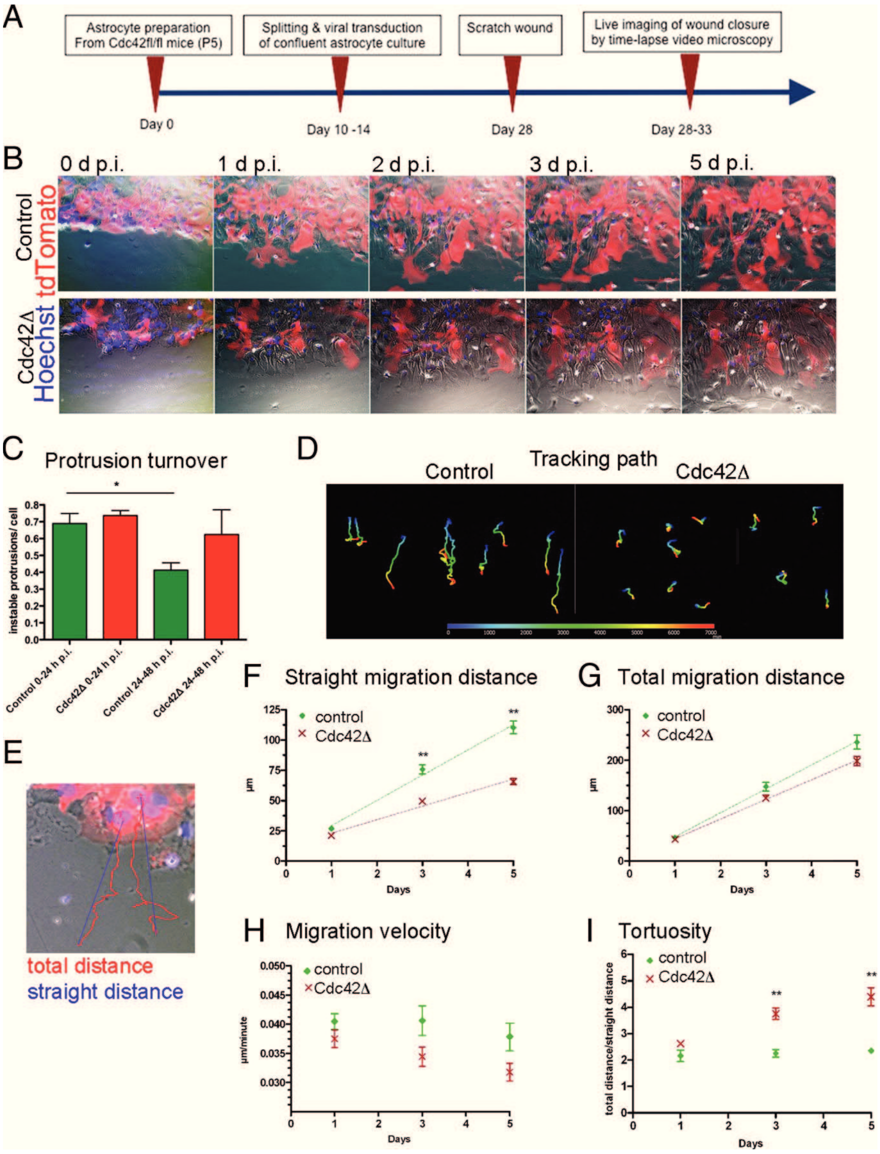

Figure 4. Reactive astrocytes lacking Cdc42 show abnormal migration behavior *in vitro*. ***A***, The migratory behavior of *Cdc42*$^{fl/fl}$ astrocytes transduced with lentiviral particles encoding tdTomato-IRES-Cre or tdTomato alone was analyzed using the *in vitro* scratch wound assay combined with time-lapse video microscopy. Movie gallery (3 channel overlap: phase contrast; blue, Hoechst live dye; red, tdTomato reporter) of the progression of wound closure by scratch-activated astrocytes 0, 1, 2, 3, and 5 d p.i. ***B***, Nontransduced and control-transduced cells filled the scratch within 5 d, while Cdc42Δ cells showed migration deficits. ***C***, Quantification of the protrusion turnover rate revealed an increase in instable protrusions in Cdc42Δ cells. ***D***, Migration paths recorded by tracking the nuclear translocation over 5 d, show disoriented movements of Cdc42Δ astrocytes when compared with control cells. ***E***, Schematic representation of total migration distance (nuclear path) and straight distance (direct route); both parameters were measured for transduced astrocytes at the scratch 1, 3 and 5 d p.i. ***F–H***, Analysis of the tracking data revealed a reduction of the straight nuclear migration distance in the Cdc42Δ culture 3 d p.i and later (***F***), but no difference in total migration distance (***G***) and mean velocity (***H***) between control and Cdc42Δ cells. An increase in tortuosity at 3 and 5 d p.i. further confirmed the orientation defect of migrating Cdc42Δ astrocytes (***I***).

If cells migrate the same total distance at the same speed, but cover less straight distance, their migration pathway would likely be rather coiled and curved. This was measured as the tortuosity, the quotient of total and straight distance. An absolute linear movement in one direction (with identical straight and total distance) would have a tortuosity value of 1. The tortuosity of control-infected astrocytes was 2.5 ± 0.3, i.e., their path was 2.5 times longer than a direct route from start to end. Cdc42Δ cells exhibited continuously increased tortuosity values from day 1 (2.6 ± 0.2) to day 5 (4.4 ± 0.6) that reached almost double the tortuosity values of control cells (Fig. 4*I*). Thus, loss of Cdc42 in astrocytes resulted in significantly increased directional changes, despite an overall equal capacity for migration as reflected in the comparable total migration distance and velocity.

The role of Cdc42 in astrocytes at a stab wound injury *in vivo*

These results demonstrate that Cdc42Δ astrocytes can extend protrusions and migrate at normal speed, but they do so in an undirected manner that ultimately impairs wound closure *in*

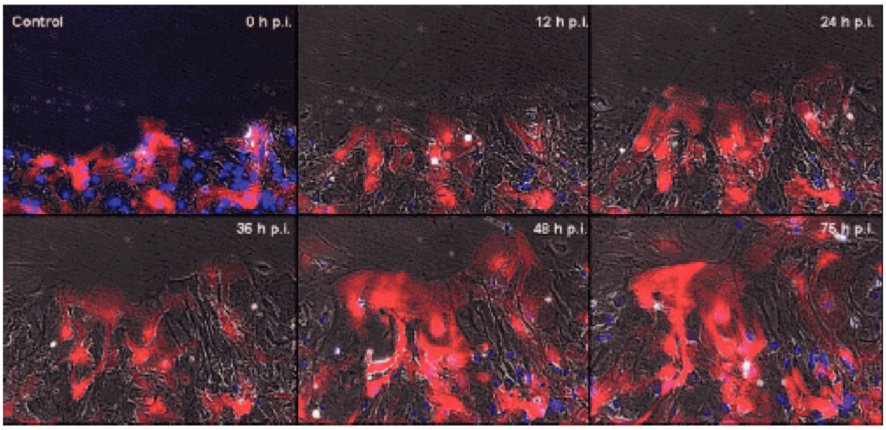

Movie 1. Astrocyte polarization and migration after *in vitro* scratch wound. Scratch-wounded astrocyte monolayer, followed over 3 d by time-lapse video microscopy. Nontransduced cells and control-transduced cells (expressing the red fluorescent protein tdTomato) polarize perpendicular to the scratch, and thereafter migrate into the cell-free cleft to fill up the wound.

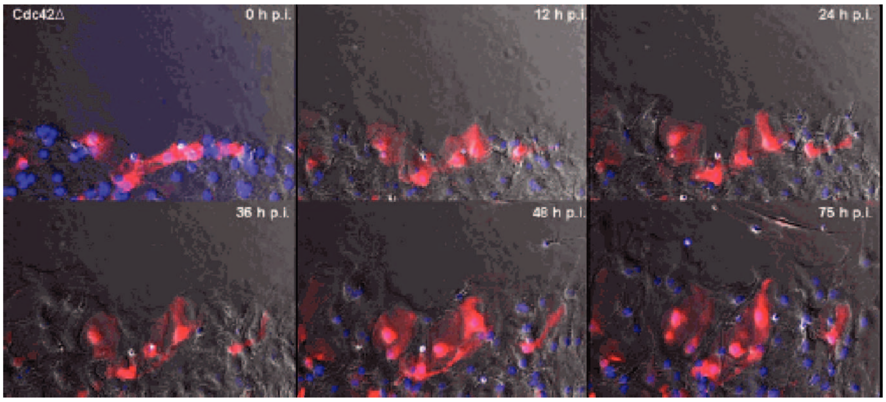

Movie 2. Astrocytes lacking Cdc42 show deficits in polarized migration. After scratching an astrocyte monolayer, Cdc42-deficient cells (expressing the red fluorescent protein tdTomato) show impaired scratch-directed polarization and migration. Wild-type cells (cells that do not express tdTomato) bypass impaired Cdc42Δ astrocytes.

vitro. This raises the question of whether the defects observed in Cdc42Δ astrocytes in the scratch wound assay *in vitro* can be observed *in vivo*, where astrocytes react to a complex milieu of signals released by multiple cell types. To examine the behavior of Cdc42Δ astrocytes *in vivo*, we used the stab wound lesion model in the adult mouse cerebral cortex (Buffo et al., 2005, 2008), and monitored the polarity reaction and recruitment of astrocytes toward the site of this acute traumatic injury.

Astrocytes also reacted *in vivo* to injury by altering their morphology assuming a bipolar shape within 7 d p.i. (compare Fig. 5*A*,*B*). To examine the full morphology of protoplasmic astrocytes beyond their GFAP+ processes (for differences between GFAP-immunostaining and fully cytoplasmic extensions, see Wilhelmsson et al., 2006), an EGFP reporter mouse line was crossed to the Tamoxifen-inducible *GLAST::CreERT2* line, which allows the induction of genetic recombination in astrocytes (Mori et al., 2006; Buffo et al., 2008). Protoplasmic astrocytes in the gray matter of the cerebral cortex normally possess many fine, radially arranged processes (Fig. 5*C*). After stab wound injury however, many EGFP-labeled astrocytes became elongated and extended long processes toward the injury border at 7 d p.i. (Fig. 5*B*,*D*). This reaction was reminiscent of the "palisading zone," a defined region next to the injury core described previously in mouse models of epilepsy (Oberheim et al., 2008). After stab wound, elongated astrocytes were only detected within an approximate area of 200 μm around the lesion site, while further away, reactive astrocytes retained their radial symmetry and did not become polarized (Fig. 5*E*). As observed by GFAP-immunostaining (Fig. 5*A*,*B*), also analysis of full morphology revealed that the polarity reaction and formation of the palisading zone developed gradually with few astrocytes beginning to elongate and extending processes toward the injury border at 3 d p.i., while more than one third of reactive astrocytes proximal to the injury border had an elongated and polar morphology with long processes oriented toward the injury site at 7 d p.i., Figs. 5*D*, 6).

To examine the role of Cdc42 in polarization of astrocytes toward the injury site *in vivo*, *Cdc42* was conditionally deleted in astrocytes in the adult brain using the *GLAST::CreERT2* mouse line crossed to the above described line with loxP sites flanking exon 2 of the *Cdc42* gene. Recombination was achieved by administration of the estrogen analog Tamoxifen to 2- to 3-month-old mice heterozygous for *GLAST::CreERT2*, positive for the EGFP-reporter, and homozygous (referred to as Cdc42Δ), heterozygous, or-negative (referred to as control) for the floxed *Cdc42* allele. Four weeks after Tamoxifen administration, when Cdc42 protein should be largely gone, a stab wound was placed in the gray matter of the cerebral cortex (Fig. 6*A*). First, we examined expression of GFAP, an intermediate filament characteristically upregulated in parenchymal astrocytes in response to injury. As expected, a high number of recombined astrocytes close to the injury site expressed GFAP in control animals (93.5 ± 2.0 GFAP+ EGFP+ cells among EGFP, n (animals) = 3; Fig. 6*B*). After deletion of Cdc42, a comparable number of astrocytes upregulated GFAP (95.9 ± 1.7% GFAP+ EGFP+ cells among EGFP in Cdc42Δ, $n = 3$, $p = 0.43$; Fig. 6*C*) and showed a hypertrophic morphology, suggesting that overall injury-induced reactivity was not disturbed by the loss of Cdc42.

Next, we examined the polarization of astrocytes by quantifying cells that had formed an elongated protrusion at 7 d p.i., when the palisading zone was well established in the control. Accordingly, 39.2 ± 1.7% ($n = 3$) of the EGFP+ control cells in the palisading zone had formed a protrusion oriented toward the injury (Fig. 6*D*). Surprisingly, this number was significantly enhanced in Cdc42Δ astrocytes (68.4 ± 3.6%, $n = 4$, $p \leq 0.001$; Fig. 6*E*). Cdc42Δ astrocytes were more elongated (83.3 ± 6.8, $n = 5$), with a significant increase in total length compared with control astrocytes (57.6 ± 6.3 μm in control, $n = 3$, $p \leq 0.044$; quantified according to the panel depicted in Fig. 6*F*). This was an effect of the stab wound injury, as no differences in astrocyte size or morphology were observed in the contralateral hemispheres (data not shown). Thus, in sharp contrast to the *in vitro* response, the change toward a bipolar morphology is even more pronounced in astrocytes lacking Cdc42.

In response to injury, astrocyte number increases around the lesion site (Sofroniew and Vinters, 2010). Given that Cdc42-

deficient astrocytes showed impaired directed migration *in vitro*, we asked whether astrocyte recruitment toward the injury site *in vivo* would also be affected. We quantified the number of EGFP+ cells in the hemisphere contralateral to the injury to control for recombination efficiency, and observed an equal number of cells in control and Cdc42Δ brains (99.7 ± 17.8% of recombined cells in Cdc42Δ brains, $n = 8$, relative to recombined cell number in control brains, $n = 6$, $p = 0.99$), demonstrating equal recombination rates. However, within the palisading zone around the stab wound (0–100 μm from the injury core) the number of Cdc42Δ EGFP+ cells was reduced to less than half (236.8 ± 51.1 cells per mm^2 in control, versus 95.5 ± 9.2 in Cdc42Δ, $n = 4$, $p = 0.0347$), suggesting a severe defect in astrocyte recruitment toward the injury site in the absence of Cdc42.

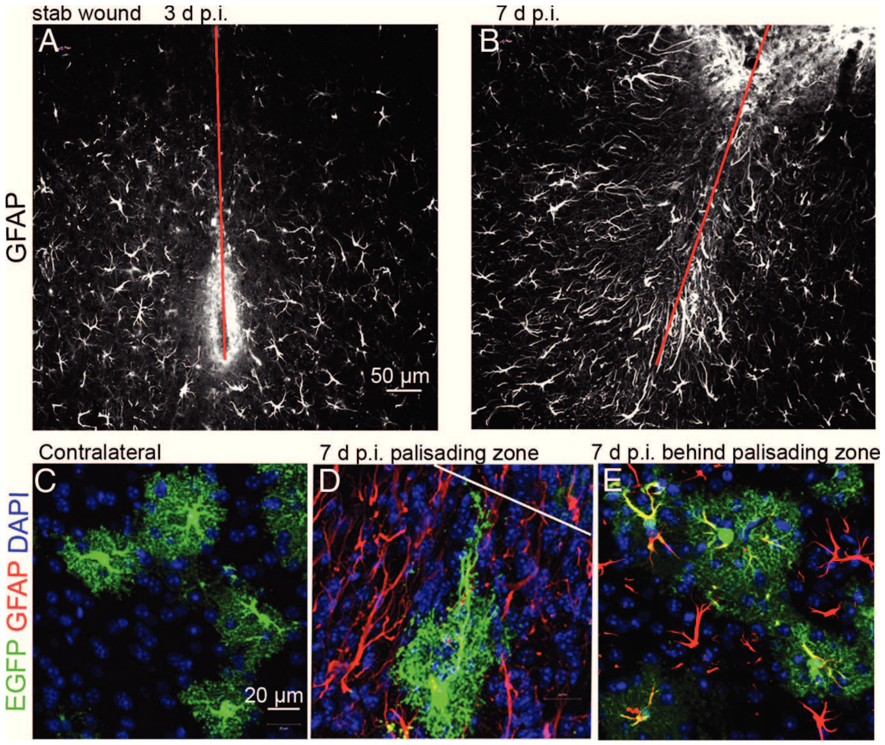

Figure 5. Astrocytes change their morphology after acute injury *in vivo*. ***A***, ***B***, After stab wound injury, GFAP+ astrocytes were clearly hypertrophic at 3 d p.i. (***A***). At 7 d p.i. astrocytes formed a palisading zone directly around the lesion (***B***). The red line outlines the lesion core in ***A*** and ***B***. ***C***, EGFP labeling of single astrocytes revealed their morphology in greater detail. Gray matter astrocytes in the intact cerebral cortex have a star-like morphology with few main processes that ramify into many fine branches. ***D***, ***E***, At 7 d p.i., 2 types of reactive astrocytes were observed. ***D***, Directly at the lesion site astrocytes extended a few thick processes toward the injury site. ***E***, Distal from the injury site GFAP+, reactive astrocytes were not elongated. The white line in ***D*** indicates the lesion site.

Astrocyte-specific loss of Cdc42 leads to increased microglia number at the stab wound injury *in vivo*

Notably, while we observed a strong decrease in the proportion of recombined astrocytes at the injury site, only approximately one third of all astrocytes were recombined in both controls and fl/fl mice (27.5 ± 2.7% in control 25.9 ± 4.8% in Cdc42Δ, $n = 3$, $p = 0.78$). We then considered whether even such a small 15% decrease in the total population of reactive astrocytes at the injury site might be sufficient to affect other cell types surrounding the injury site. Microglia are the resident immune cells of the brain and are activated and recruited toward injury, most likely interacting with astrocytes throughout reactive gliosis (Hanisch and Kettenmann, 2007). To understand whether the reaction of microglia to injury was changed after loss of Cdc42 in the recombined astrocytes at 7 d p.i., we quantified Iba1-positive microglia. Contralateral to the injury site, the number of microglia was similar between control and Cdc42Δ brains (9023 ± 1494 Iba1+ cells per mm^3 in control and 7916 ± 665 Iba1+ cells per mm^3 in Cdc42Δ, $p = 0.54$; Fig. 7*A*,*B*). As expected, the number of microglia dramatically increased directly at the lesion (Fig. 7*C*,*D*). In the control, microglia number relative to the contralateral hemisphere was approximately fivefold higher at a distance of 100–250 μm from the injury site and tenfold higher directly at the injury site (0–100 μm) (Fig. 7*C*,*E*). This increase was even more pronounced after astrocyte-specific deletion of *Cdc42*. Here, a 12.5-fold increase in microglia was observed (Fig. 7*D*,*E*; $n = 3$, $p \leq 0.031$). Interestingly, the increase in microglia number was observed precisely in the region where astrocyte numbers were decreased (see above), but not at further distant sites (Fig. 7*E*). Thus, even though only a subset of astrocytes was affected in recruitment to the injury site, these changes were sufficient to affect the microglia reaction.

The proper reaction of astrocytes and microglia postinjury is thought to be essential for protection of the brain from primary neuronal loss. Since both of these cell types are changed after loss of Cdc42, we next examined neuronal number at the injury site (Fig. 7*F*). The pan-neuronal marker NeuN is typically downregulated in neurons surrounding the injury site (data not shown), therefore we used cresyl violet for neuronal somata detection (see red arrow in Fig. 7*G*,*H*; Fig. 7*G*, inset) and compared neuronal cell number in close proximity to the injury site to a similar brain region at >500 μm distant from the injury. Notably, neuron number was reduced to approximately one-third within 100 μm around the stab wound at 3 and 7 d p.i. ($n = 6$, Fig. 7*F*–*H*), but at 100–200 μm distant from the injury, their number was comparable to far distant regions (93.7 ± 13.2% neurons in control, 82.5 ± 9.4% neurons in brains with Cdc42Δ astrocytes, normalized to neuronal number distal to the injury site, $n = 3$, $p = 0.53$), indicating a rather concise region of neuronal death in close vicinity to the injury site. In brains with recombined astrocytes depleted of Cdc42 (Fig. 7*G*), neuron number was comparably reduced to within 100 μm of the injury site at 3 or 7 d p.i. (Fig. 7*F*,*H*, $n = 8$, $p = 0.48$). This is consistent with a comparable number of apoptotic cells detected by TUNEL, 3 d p.i. (9685 ± 4634 TUNEL cells per mm^3 in control brains, 7277 ± 1490 TUNEL cells per mm^3 in brains with Cdc42Δ astrocytes, $n = 6$, $p = 0.63$), indicating that primary neuronal death in response to injury is not affected by the modest reduction of astrocyte recruitment achieved by inducible Cdc42 deletion in ~30% of adult astrocytes.

Discussion

Here, we demonstrate an essential role for the small RhoGTPase Cdc42 for recruitment of astrocytes to an injury site *in vitro* and *in vivo*. While injury-oriented process formation was impaired2 in the absence of Cdc42 *in vitro*, it appeared normal *in vivo*. In

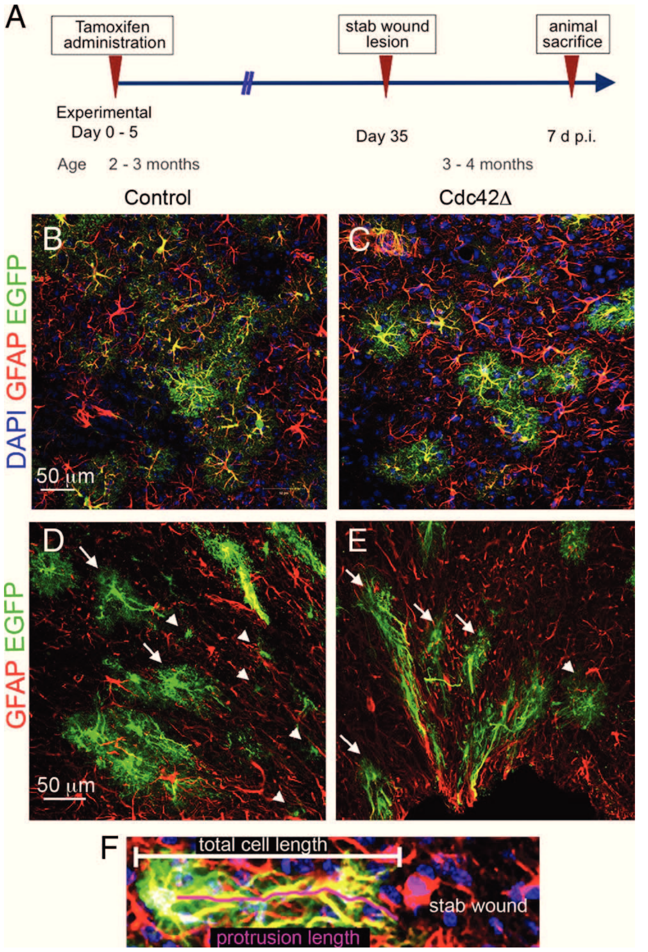

Figure 6. The effects of *Cdc42* deletion in astrocytes on their morphology at the injury site *in vivo*. ***A***, Genetic recombination was induced in 2- to 3-month-old animals that were stab wound injured 4 weeks later and killed 7 d p.i. following the schedule in ***A***. ***B–E***, Astrocytes at the injury site strongly upregulated GFAP in control (***B***) and Cdc42Δ (***C***) brains. In control brains, ~40% of recombined EGFP+ astrocytes formed a protrusion (white arrows, nonprotruding cells are highlighted by a white arrowhead) within the palisading zone (***D***). This number was increased in Cdc42Δ animals (***E***). ***F***, Measurements of protrusion and cell length were done.

contrast, the increase in astrocyte number at the injury site could not be compensated for *in vivo*. Most importantly, even a modest (based on the recombination frequency of ~30%) reduction in astrocyte recruitment to the injury site resulted in a significant increase in microglia number at the injury site, suggesting a crucial role of astrocytes in reducing microglia number at the injury site.

Polarity and migration of astrocytes after injury *in vitro*

Scratch injury *in vitro* is a well established assay used to monitor directed cell migration. Astrocytes *in vitro* polarize toward a scratch by positioning the centrosome/MTOC between their nucleus and their leading edge and forming directed protrusions before migration into the cell-free scratch (Etienne-Manneville and Hall, 2001, 2003; Etienne-Manneville et al., 2005; Höltje et al., 2005; Etienne-Manneville, 2006; Peng et al., 2008; Ang et al., 2010). Consistent with previous experiments using dominant-negative (Dn)Cdc42, genetic deletion of *Cdc42* in astrocytes *in vitro* resulted in MTOC misorientation and a decreased number of cells exhibiting scratch oriented unipolar protrusions, thereby supporting the idea that Cdc42 affects astrocyte polarity *in vitro* (Etienne-Manneville and Hall, 2001; Etienne-Manneville, 2008a,b; Li and Gundersen, 2008; Bartolini and Gundersen, 2010). However, we could not confirm all the defects previously observed after DnCdc42 (Etienne-Manneville and Hall, 2001; Czuchra et al., 2005); for example protrusion formation was undisturbed after genetic deletion of Cdc42 in astrocytes *in vitro* and *in vivo*. Conversely, Cdc42Δ cells often appeared multipolar with multidirectional protrusions around the cell body soon after the scratch. This discrepancy could be due to the dominant-negative constructs affecting other RhoGTPases, since they bind to corresponding guanine nucleotide exchange factors (GEFs) with a higher affinity than endogenous RhoGTPases, preventing effector interaction and subsequent signaling (Feig, 1999). As GEFs are often shared by several RhoGTPase members (Schmidt and Hall, 2002; Rossman et al., 2005), DnCdc42 may also affect Rac1, which is localized to the leading edge of scratch-activated cells by Cdc42-dependent Pak activity, and is responsible for protrusion formation (Cau and Hall, 2005).

Cell migration is governed by the ability to extend, retract, and stabilize membrane protrusions in a defined direction. This can occur in a noncoordinated manner, resulting in random migration, or in a coordinated manner, resulting in directed migration in response to environmental cues (Etienne-Manneville, 2008a). Indeed, tracking Cdc42Δ astrocyte nuclei revealed that overall migration was not impaired. However, their tracking paths into the scratch were coiled showing that their directionality was lost. We conclude that in Cdc42Δ astrocytes an initial polarization defect leads to randomly oriented MTOCs that subsequently cause disoriented movement.

Defects in astrocyte recruitment to the site of brain injury after Cdc42 deletion in astrocytes of the adult brain

Here, we unravel a hitherto unrecognized role of the small RhoGTPase Cdc42 in astrocyte recruitment to the injury site *in vivo*, without affecting overall astrocyte reactivity (Okada et al., 2006; Herrmann et al., 2008), since *GFAP* upregulation and hypertrophic response after injury were normal. Interestingly, in contrast to what has been found *in vitro*, the polarity reaction of astrocytes in the palisading zone adjacent to the injury site was not impaired by *Cdc42* deletion, but even enhanced with more cells elongated toward the injury. This discrepancy highlights the limitations of the *in vitro* scratch assay and the complex nature of cellular interactions and multiple signaling pathways after injury *in vivo*. While astrocytes in the scratch wound assay are exposed to a cell-free scratch, and almost exclusively astrocyte-released autocrine signals, astrocytes are exposed to a much larger repertoire of signals released from a multitude of cells *in vivo*, including degenerating neurons, oligodendrocytes and their progenitor cells, the NG2 glia, microglia, and invading cells from the blood system. Indeed, we found that microglia numbers were significantly increased surrounding the stab wound site, thus possibly representing a source of additional signals mediating orientation of palisading astrocytes toward the injury site. Therefore, the *in vitro* assay is well suited to examine cell-autonomous effects, but extrapolation to the *in vivo* situation may not always be possible.

Mechanisms controlling Cdc42 activation and localization to the leading edge of the cell are still poorly understood, but ADP ribosylation factor 6 (Arf6)-dependent membrane traffic is such a crucial factor for recruitment of Cdc42 to the leading edge (Osmani et al., 2010). Moreover, Cdc42 is a downstream effector of integrin signaling (Etienne-Manneville and Hall, 2001; Osmani et al., 2006; Etienne-Manneville, 2008b). Interestingly, interference with β1-integrin-mediated signaling at postnatal stages by genetic deletion results in reactive astrogliosis even in

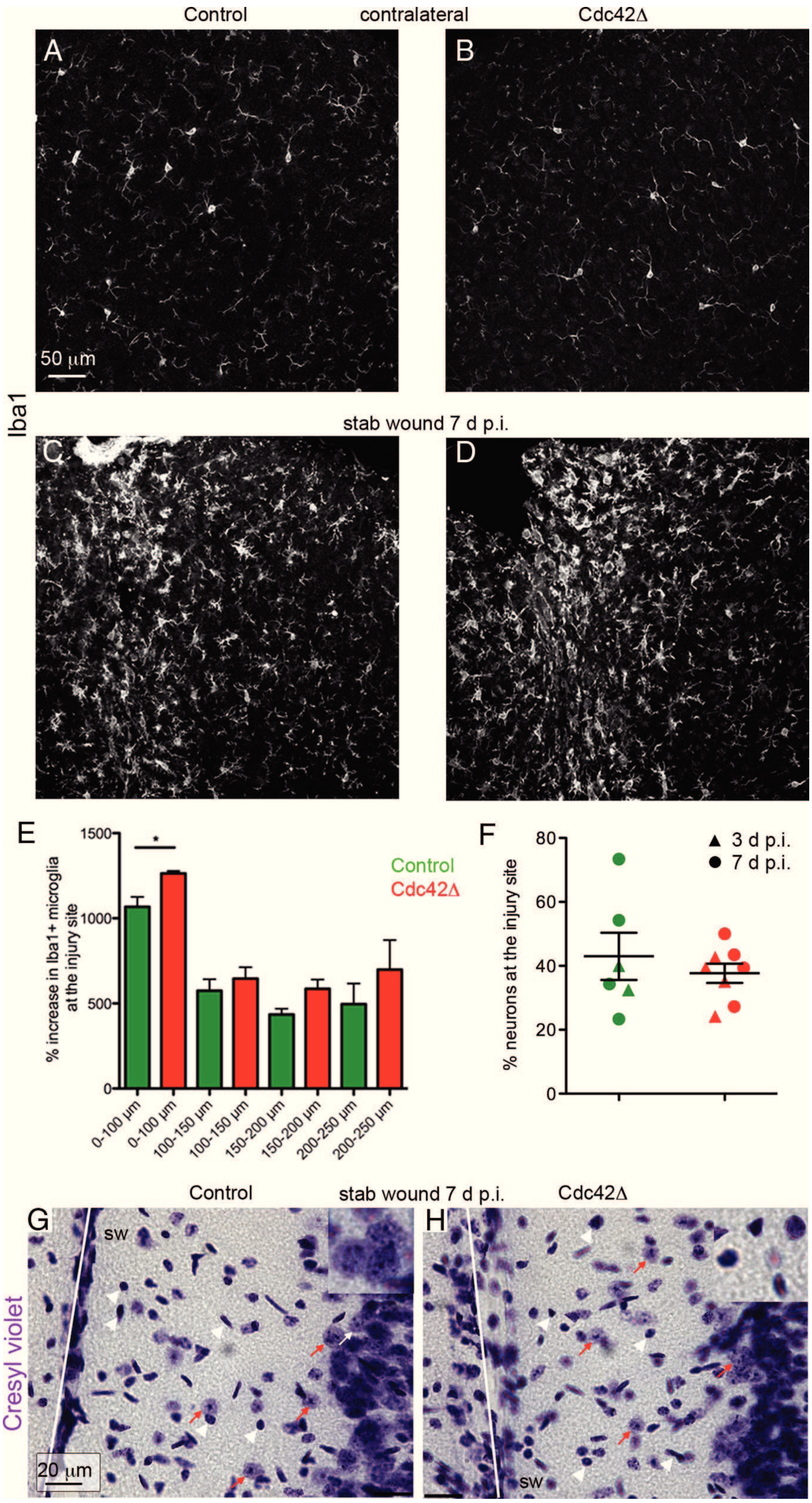

Figure 7. The effects of *Cdc42* deletion in astrocytes on microglia and neurons at the injury site *in vivo*. ***A–E***, Iba1-labeled microglial cells are shown in brains with control (***A***, ***B***) or Cdc42Δ (***C***, ***D***) astrocytes 7 d p.i. There were comparable numbers of resting Iba1+ microglia in the contralateral hemispheres of control (***A***) and Cdc42Δ (***B***) brains. The microglia number significantly increased close to the injury site in brains with control (***C***) or Cdc42Δ (***D***) astrocytes, but numbers were increased even further after deletion of *Cdc42* in astrocytes (***E***). ***F–H***, Neurons were visualized by cresyl violet staining as pale purple cells (***G***, ***H***; indicated by red arrows and enlarged in the inset in ***G***), and stereotactic counting of these revealed no significant difference after deletion of *Cdc42* at the injury site (***F***). Neuronal numbers at the injury site were normalized to numbers quantified in a distal unaffected region (***F***). Small or shrunken dark purple cells were excluded from the quantitative analysis as they represent glial and/or dying cells (see white arrowheads in ***H***). sw, Stab wound.

the uninjured brain *in vivo* (Robel et al., 2009), and interference with integrin signaling in astrocytes *in vitro* blocks protrusion formation and polarity (Etienne-Manneville and Hall, 2001; Osmani et al., 2006; Peng et al., 2008). Notably, *in vivo*, palisading zone formation and bipolar orientation could also occur in the absence of β1-integrins in astrocytes (data not shown), further supporting the concept of alternative pathways in astrocyte orientation *in vitro* (requiring β1-integrins and Cdc42) and *in vivo* (not requiring either of these). However, other integrins may be compensating in the absence of Cdc42 to mediate effects on astrocyte polarity via other effector pathways (Holly et al., 2000; Lemons and Condic, 2008). For example, α6β4 integrins interact with intermediate filaments (Rezniczek et al., 1998), which are strongly upregulated after brain injury in astrocytes and may play a key role in stabilizing palisading bipolar astrocytes at the site of injury *in vivo*. In addition, the basement membrane receptor dystroglycan has been shown to be necessary for astrocyte polarization (Peng et al., 2008), and could act as a redundant mechanism for reactive astrocyte polarization *in vivo*.

Although Cdc42Δ astrocytes were polarized *in vivo*, the increase in astrocyte number surrounding the injury site was severely impaired, with less than half of the recombined Cdc42-deficient astrocytes found at the injury site. This is not due to developmental defects, as *Cdc42* was deleted in fully mature astrocytes in the adult brain by Tamoxifen-mediated recombination using *GLAST::CreERT2* mice (Mori et al., 2006; Buffo et al., 2008). We therefore conclude that Cdc42 plays a specific and non-redundant role after brain injury in regulating astrocyte recruitment to the lesion site. Most importantly, recruiting fewer astrocytes to the injury site also affects another cell type as detailed below. It will therefore be important to unravel the precise mechanisms of Cdc42-dependent astrocyte recruitment *in vivo*. Both directed cell migration and proliferation have been implicated in this process (Okada et al., 2006; Auguste et al., 2007; Buffo et al., 2008; Sofroniew and Vinters, 2010), and only live *in vivo* imaging will be able to directly determine which of these processes is defective in the absence of Cdc42.

Consequences of reduced astrocyte recruitment after injury

Activated astrocytes contribute to scar formation not only by increasing in number, but also by releasing a multitude of molecules, such as chondroitin sulfate proteoglycans, cytokines, and mitogens (Buffo et al., 2010) that act on other cell types. Therefore, a key question was to what extent even a small change in the number of recruited astrocytes may impact other cell types. Indeed, reduction of half of all recombined astrocytes (~15% of all astrocytes), resulted in a significant increase in microglia number at the injury site. These observations support quantitative signaling between reactive astrocytes and microglia. Indeed, reactive astrogliosis in the uninjured brain as elicited by *β1-integrin* deletion (Robel et al., 2009) also affected microglial cells, and astrocyte-conditioned medium has been shown to affect the state of microglia activation (Schilling et al., 2001; Kim et al., 2010), consistent with direct signaling from activated astrocytes to microglia. In addition, Cdc42-deficient astrocytes may be defective in their release of signaling molecules due to possible alterations in their secretory activity (Harris and Tepass, 2010). To reveal the precise role of microglia in this context, it will be interesting to investigate whether they are in a "beneficial" state (Thored et al., 2009; Kettenmann et al., 2011) to compensate for the reduction in astrocytes, or whether the increase in microglia is an indicator of an increased detrimental inflammatory reaction due to the defects in Cdc42-deficient astrocytes. Further analysis of reactive astrocytes and microglial cells in this context will be required to determine their exact activation and signaling state. Thus, conditional deletion of *Cdc42* in astrocytes will serve as a useful model to further study interaction between glial cell types *in vivo* with the aim of dissecting pathways eliciting the beneficial or adverse roles. Beyond the precise mechanisms, this analysis highlights the key role of reactive astrocytes at the injury site and the profound effect of even small alterations in their number.

References

Ang SF, Zhao ZS, Lim L, Manser E (2010) DAAM1 is a formin required for centrosome reorientation during cell migration. PLoS One 5:e13064.

Auguste KI, Jin S, Uchida K, Yan D, Manley GT, Papadopoulos MC, Verkman AS (2007) Greatly impaired migration of implanted aquaporin-4-deficient astroglial cells in mouse brain toward a site of injury. FASEB J 21:108–116.

Bartolini F, Gundersen GG (2010) Formins and microtubules. Biochim Biophys Acta 1803:164–173.

Bragg AD, Amiry-Moghaddam M, Ottersen OP, Adams ME, Froehner SC (2006) Assembly of a perivascular astrocyte protein scaffold at the mammalian blood-brain barrier is dependent on alpha-syntrophin. Glia 53:879–890.

Buffo A, Vosko MR, Ertürk D, Hamann GF, Jucker M, Rowitch D, Götz M (2005) Expression pattern of the transcription factor Olig2 in response to brain injuries: implications for neuronal repair. Proc Natl Acad Sci U S A 102:18183–18188.

Buffo A, Rite I, Tripathi P, Lepier A, Colak D, Horn AP, Mori T, Götz M (2008) Origin and progeny of reactive gliosis: A source of multipotent cells in the injured brain. Proc Natl Acad Sci U S A 105:3581–3586.

Buffo A, Rolando C, Ceruti S (2010) Astrocytes in the damaged brain: molecular and cellular insights into their reactive response and healing potential. Biochem Pharmacol 79:77–89.

Busch SA, Silver J (2007) The role of extracellular matrix in CNS regeneration. Curr Opin Neurobiol 17:120–127.

Bushong EA, Martone ME, Jones YZ, Ellisman MH (2002) Protoplasmic astrocytes in CA1 stratum radiatum occupy separate anatomical domains. J Neurosci 22:183–192.

Cau J, Hall A (2005) Cdc42 controls the polarity of the actin and microtubule cytoskeletons through two distinct signal transduction pathways. J Cell Sci 118:2579–2587.

Czuchra A, Wu X, Meyer H, van Hengel J, Schroeder T, Geffers R, Rottner K, Brakebusch C (2005) Cdc42 is not essential for filopodium formation, directed migration, cell polarization, and mitosis in fibroblastoid cells. Mol Biol Cell 16:4473–4484.

Etienne-Manneville S (2006) In vitro assay of primary astrocyte migration as a tool to study Rho GTPase function in cell polarization. Methods Enzymol 406:565–578.

Etienne-Manneville S (2008a) Polarity proteins in migration and invasion. Oncogene 27:6970–6980.

Etienne-Manneville S (2008b) Polarity proteins in glial cell functions. Curr Opin Neurobiol 18:488–494.

Etienne-Manneville S, Hall A (2001) Integrin-mediated activation of Cdc42 controls cell polarity in migrating astrocytes through PKCzeta. Cell 106:489–498.

Etienne-Manneville S, Hall A (2003) Cdc42 regulates GSK-3beta and adenomatous polyposis coli to control cell polarity. Nature 421:753–756.

Etienne-Manneville S, Manneville JB, Nicholls S, Ferenczi MA, Hall A (2005) Cdc42 and Par6-PKCzeta regulate the spatially localized association of Dlg1 and APC to control cell polarization. J Cell Biol 170:895–901.

Feig LA (1999) Tools of the trade: use of dominant-inhibitory mutants of Ras-family GTPases. Nat Cell Biol 1:E25–E27.

Hanisch UK, Kettenmann H (2007) Microglia: active sensor and versatile effector cells in the normal and pathologic brain. Nat Neurosci 10:1387–1394.

Harris KP, Tepass U (2010) Cdc42 and vesicle trafficking in polarized cells. Traffic 11:1272–1279.

Herrmann JE, Imura T, Song B, Qi J, Ao Y, Nguyen TK, Korsak RA, Takeda K, Akira S, Sofroniew MV (2008) STAT3 is a critical regulator of astrogliosis and scar formation after spinal cord injury. J Neurosci 28:7231–7243.

Holly SP, Larson MK, Parise LV (2000) Multiple roles of integrins in cell motility. Exp Cell Res 261:69–74.

Höltje M, Hoffmann A, Hofmann F, Mucke C, Grosse G, Van Rooijen N, Kettenmann H, Just I, Ahnert-Hilger G (2005) Role of Rho GTPase in astrocyte morphology and migratory response during in vitro wound healing. J Neurochem 95:1237–1248.

Iadecola C, Nedergaard M (2007) Glial regulation of the cerebral microvasculature. Nat Neurosci 10:1369–1376.

Kettenmann H, Hanisch UK, Noda M, Verkhratsky A (2011) Physiology of microglia. Physiol Rev 91:461–553.

Kim JH, Min KJ, Seol W, Jou I, Joe EH (2010) Astrocytes in injury states rapidly produce anti-inflammatory factors and attenuate microglial inflammatory responses. J Neurochem 115:1161–1171.

Lemons ML, Condic ML (2008) Integrin signaling is integral to regeneration. Exp Neurol 209:343–352.

Li R, Gundersen GG (2008) Beyond polymer polarity: how the cytoskeleton builds a polarized cell. Nat Rev Mol Cell Biol 9:860–873.

Mori T, Tanaka K, Buffo A, Wurst W, Kühn R, Götz M (2006) Inducible gene deletion in astroglia and radial glia—a valuable tool for functional and lineage analysis. Glia 54:21–34.

Nakamura T, Colbert MC, Robbins J (2006) Neural crest cells retain multipotential characteristics in the developing valves and label the cardiac conduction system. Circ Res 98:1547–1554.

Naldini L, Blömer U, Gallay P, Ory D, Mulligan R, Gage FH, Verma IM, Trono D (1996) In vivo gene delivery and stable transduction of nondividing cells by a lentiviral vector. Science 272:263–267.

Nobes CD, Hall A (1999) Rho GTPases control polarity, protrusion, and adhesion during cell movement. J Cell Biol 144:1235–1244.

Oberheim NA, Tian GF, Han X, Peng W, Takano T, Ransom B, Nedergaard M (2008) Loss of astrocytic domain organization in the epileptic brain. J Neurosci 28:3264–3276.

Ogata K, Kosaka T (2002) Structural and quantitative analysis of astrocytes in the mouse hippocampus. Neuroscience 113:221–233.

Okada S, Nakamura M, Katoh H, Miyao T, Shimazaki T, Ishii K, Yamane J, Yoshimura A, Iwamoto Y, Toyama Y, Okano H (2006) Conditional ablation of Stat3 or Socs3 discloses a dual role for reactive astrocytes after spinal cord injury. Nat Med 12:829–834.

Osmani N, Vitale N, Borg JP, Etienne-Manneville S (2006) Scrib controls Cdc42 localization and activity to promote cell polarization during astrocyte migration. Curr Biol 16:2395–2405.

Osmani N, Peglion F, Chavrier P, Etienne-Manneville S (2010) Cdc42 localization and cell polarity depend on membrane traffic. J Cell Biol 191:1261–1269.

Pekny M, Pekna M (2004) Astrocyte intermediate filaments in CNS pathologies and regeneration. J Pathol 204:428–437.

Peng H, Shah W, Holland P, Carbonetto S (2008) Integrins and dystroglycan regulate astrocyte wound healing: the integrin beta1 subunit is necessary for process extension and orienting the microtubular network. Dev Neurobiol 68:559–574.

Pfeifer A, Brandon EP, Kootstra N, Gage FH, Verma IM (2001) Delivery of the Cre recombinase by a self-deleting lentiviral vector: efficient gene targeting in vivo. Proc Natl Acad Sci U S A 98:11450–11455.

Reier PJ, Houle JD (1988) The glial scar: its bearing on axonal elongation and transplantation approaches to CNS repair. Adv Neurol 47:87–138.

Rezniczek GA, de Pereda JM, Reipert S, Wiche G (1998) Linking integrin alpha6beta4-based cell adhesion to the intermediate filament cytoskeleton: direct interaction between the beta4 subunit and plectin at multiple molecular sites. J Cell Biol 141:209–225.

Ridet JL, Malhotra SK, Privat A, Gage FH (1997) Reactive astrocytes: cellular and molecular cues to biological function. Trends Neurosci 20:570–577.

Robel S, Mori T, Zoubaa S, Schlegel J, Sirko S, Faissner A, Goebbels S, Dimou L, Götz M (2009) Conditional deletion of beta1-integrin in astroglia causes partial reactive gliosis. Glia 57:1630–1647.

Robel S, Berninger B, Götz M (2011) The stem cell potential of glia: lessons from reactive gliosis. Nat Rev Neurosci 12:88–104.

Rossman KL, Der CJ, Sondek J (2005) GEF means go: turning on RHO GTPases with guanine nucleotide-exchange factors. Nat Rev Mol Cell Biol 6:167–180.

Schilling T, Nitsch R, Heinemann U, Haas D, Eder C (2001) Astrocyte-released cytokines induce ramification and outward K+ channel expression in microglia via distinct signalling pathways. Eur J Neurosci 14:463–473.

Schmidt A, Hall A (2002) Guanine nucleotide exchange factors for Rho GTPases: turning on the switch. Genes Dev 16:1587–1609.

Schummers J, Yu H, Sur M (2008) Tuned responses of astrocytes and their influence on hemodynamic signals in the visual cortex. Science 320:1638–1643.

Silver DJ, Steindler DA (2009) Common astrocytic programs during brain development, injury and cancer. Trends Neurosci 32:303–311.

Simon C, Götz M, Dimou L (2011) Progenitors in the adult cerebral cortex: cell cycle properties and regulation by physiological stimuli and injury. Glia 59:869–881.

Sirko S, Neitz A, Mittmann T, Horvat-Bröcker A, von Holst A, Eysel UT, Faissner A (2009) Focal laser-lesions activate an endogenous population of neural stem/progenitor cells in the adult visual cortex. Brain 132:2252–2264.

Sofroniew MV (2009) Molecular dissection of reactive astrogliosis and glial scar formation. Trends Neurosci 32:638–647.

Sofroniew MV, Vinters HV (2010) Astrocytes: biology and pathology. Acta Neuropathol 119:7–35.

Thored P, Heldmann U, Gomes-Leal W, Gisler R, Darsalia V, Taneera J, Nygren JM, Jacobsen SE, Ekdahl CT, Kokaia Z, Lindvall O (2009) Long-term accumulation of microglia with proneurogenic phenotype concomitant with persistent neurogenesis in adult subventricular zone after stroke. Glia 57:835–849.

Wilhelmsson U, Bushong EA, Price DL, Smarr BL, Phung V, Terada M, Ellisman MH, Pekny M (2006) Redefining the concept of reactive astrocytes as cells that remain within their unique domains upon reaction to injury. Proc Natl Acad Sci U S A 103:17513–17518.

Wu X, Quondamatteo F, Lefever T, Czuchra A, Meyer H, Chrostek A, Paus R, Langbein L, Brakebusch C (2006) Cdc42 controls progenitor cell differentiation and beta-catenin turnover in skin. Genes Dev 20:571–585.

Zufferey R, Nagy D, Mandel RJ, Naldini L, Trono D (1997) Multiply attenuated lentiviral vector achieves efficient gene delivery in vivo. Nat Biotechnol 15:871–875.

3.2 Live imaging of astrocyte responses to acute brain injury

The presented work on *in vivo* imaging of reactive astrocytes after traumatic brain injury is published in the article entitled 'Live imaging of astrocyte responses to acute injury reveals selective juxtavascular proliferation' by **Sophia Bardehle**, Martin Krüger, Felix Buggenthin, Julia Schwausch, Jovica Ninkovic, Hans Clevers, Hugo J Snippert, Fabian J Theis, Melanie Meyer-Luehmann, Ingo Bechmann, Leda Dimou and Magdalena Götz in *Nature Neuroscience* 2013, 16(5):580-6.

In this study, *in vivo* 2pLSM was used to trace single GFP+ astrocytes in living GLAST^{CreERT2}/ CAG-eGFP mice and other transgenic lines for days and weeks after acute cortical injury. Depending on the lesion size, a heterogeneous behavior of astrocytes was observed, which was classified according to the morphological changes into different subsets including cells with hypertrophic somata, polarizing cells, dividing cells or cells that remained stable. Different than expected, astrocyte migration was not observed after stab wound injury. Instead, only a small subset of astrocytes divided, and was preferentially located in direct contact with blood vessels. Verified by immunohistochemical and ultrastructural analyses, the majority of proliferating astrocytes were in juxtavascular position. The role of Cdc42 in reactive astrocytes was investigated by astrocyte-specific deletion in adult GLAST^{CreERT2} mice crossed to cdc42^{floxed} mice, which led to an attenuated response of astrocytes after stab wound with reduced – but preserved juxtavascular – proliferation. In conclusion, *in vivo* live imaging revealed (1) the heterogeneity of reactive astrocytes, (2) modest astrocyte recruitment solely by a minor pool of proliferating astrocytes, (3) which were found in a specific vascular niche. These findings add novel insights to mechanisms of astrogliosis, and suggest a small, plastic subset of reactive astrocytes with stem cell potential might be involved in ambiguous aspects of glial scar formation.

Contributions of different authors to this publication

All experiments (animal operations, 2pLSM, immunohistochemistry) and data analyses were performed by me (except for electron microscopy, migration and volume analyses). Martin Krüger and Ingo Bechmann carried out the electron microscopy. Felix Buggenthin and Fabian J. Theis assisted in image registration for migration analysis and data processing for volume analysis (Suppl. Figures 2 and 3). Julia Schwausch, Jovica Ninkovic, Hans Clevers and Hugo J. Snippert supplied the GLAST/confetti mouse strain (Suppl. Figure 9). Melanie Meyer-Luehmann provided access to the 2pLSM and expert advice on imaging. Leda Dimou initially established the *in vivo* two-photon microscopy technique together with me. Magdalena Götz together with Leda Dimou designed the project. I wrote the manuscript together with Magdalena Götz, who coordinated and financed the project. Further funding was provided by Fabian J. Theis and Ingo Bechmann.

nature neuroscience

Live imaging of astrocyte responses to acute injury reveals selective juxtavascular proliferation

Sophia Bardehle[1,2], Martin Krüger[3], Felix Buggenthin[4,5], Julia Schwausch[2], Jovica Ninkovic[2], Hans Clevers[6], Hugo J Snippert[6], Fabian J Theis[4,5], Melanie Meyer-Luehmann[7,8], Ingo Bechmann[3], Leda Dimou[1,2] & Magdalena Götz[1,2,9]

Astrocytes are thought to have important roles after brain injury, but their behavior has largely been inferred from postmortem analysis. To examine the mechanisms that recruit astrocytes to sites of injury, we used *in vivo* two-photon laser-scanning microscopy to follow the response of GFP-labeled astrocytes in the adult mouse cerebral cortex over several weeks after acute injury. Live imaging revealed a marked heterogeneity in the reaction of individual astrocytes, with one subset retaining their initial morphology, another directing their processes toward the lesion, and a distinct subset located at juxtavascular sites proliferating. Although no astrocytes actively migrated toward the injury site, selective proliferation of juxtavascular astrocytes was observed after the introduction of a lesion and was still the case, even though the extent was reduced, after astrocyte-specific deletion of the RhoGTPase Cdc42. Thus, astrocyte recruitment after injury relies solely on proliferation in a specific niche.

The diversity of functions proposed for reactive astrocytes after brain injury[1–5] underlines the inadequacy of our current understanding of astrocyte responses to brain damage. Thus, both beneficial roles, such as restoration of ionic homeostasis in the extracellular milieu, wound healing and limitation of inflammation[2,5], and deleterious functions, such as scar formation[4], have been attributed to astrocyte reactions to brain injury. However, very little is known about how astrocytes perform such functions. Do all astrocytes participate in all of these processes or are some astrocytes specialized for particular tasks, such as limiting the invasion of immune cells, antigen presentation[6] or scar formation? The answer to this question obviously has a bearing on whether, and how, one can selectively promote beneficial and inhibit adverse functions following brain injury. For example, if a certain subset of astrocytes is involved in scar formation, it might be beneficial to constrain their activity specifically. To form a scar, astrocytes must accumulate around the injury site, and it is thought that astrocytes do so by actively migrating toward the lesion and, under some conditions, proliferating nearby[5,6]. However, this concept of astrocyte recruitment is largely based on *postmortem* immunohistochemical analyses[7,8], as astrocyte migration and dynamic orientation toward an injury site have so far only been studied *in vitro* using the scratch-wound assay[9,10]. If, when and how astrocyte migration occurs after injury *in vivo*, and to what degree it might contribute to increasing astrocyte numbers around the injury site, have not yet been investigated by live imaging *in vivo*. Similarly, other important aspects of astrocyte behavior in response to injury, such as the extent of cell death or proliferation, can only be assessed by live imaging. This also holds true for the crucial issue of functional heterogeneity. Protein and gene expression analyses have suggested an element of heterogeneity among astrocytes reacting to injury, with, for example, only subsets upregulating specific intermediate filaments, such as nestin[3,11] or MHC molecules[6]. However, it is entirely unknown whether such subpopulations are actually committed to specific functions, such as migration or interaction with immune cells, or whether all astrocytes can take on all of these functions over time.

To tackle these questions, it is essential to follow single, identifiable astrocytes by live imaging. We used *in vivo* two-photon laser-scanning microscopy (2pLSM)[12,13] to visualize and monitor astrocyte reactions over time via an implanted cranial window, following acute traumatic brain injury (TBI) inflicted by localized stabbing of the somatosensory cortex as previously described[7,10]. Using the progeny (referred to as GLAST/eGFP mice) of crosses between the GLAST^{CreERT2} knock-in mouse line[14] (Cre recombinase is expressed in the endogenous *Glast* (also known as *Slc1a3*) locus) and an inducible enhanced (e)GFP reporter strain[15] allowed us to label protoplasmic astrocytes in the gray matter[7] with GFP (**Supplementary Movie 1**), and to continuously observe changes in the behavior of GFP^+ astrocytes for up to 28 d after the time of injury (**Figs. 1** and **2**).

RESULTS

Astrocytes react heterogeneously to TBI

We assessed the morphology of GFP^+ astrocytes by live 2pLSM during the first imaging session on the day of the operation

[1]Physiological Genomics, Institute of Physiology, Ludwig-Maximilians University Munich, Munich, Germany. [2]Institute for Stem Cell Research, Helmholtz Zentrum Munich, Neuherberg, Germany. [3]Institute of Anatomy, University of Leipzig, Leipzig, Germany. [4]Institute of Bioinformatics and Systems Biology, Helmholtz Zentrum Munich, Neuherberg, Germany. [5]Department of Mathematics, Technical University Munich, Germany. [6]Hubrecht Institute, Koninklijke Nederlandse Akademie van Wetenschappen and University Medical Center Utrecht, Connecticut Utrecht, The Netherlands. [7]Adolf Butenandt Institute, Department of Biochemistry, Ludwig-Maximilians University Munich, Munich, Germany. [8]Neurocenter, Department of Neurology, University of Freiburg, Freiburg, Germany. [9]Munich Cluster for Systems Neurology (SyNergy), Munich, Germany. Correspondence should be addressed to M.G. (magdalena.goetz@helmholtz-muenchen.de).

Received 11 October 2012; accepted 27 February 2013; published online 31 March 2013; doi:10.1038/nn.3371

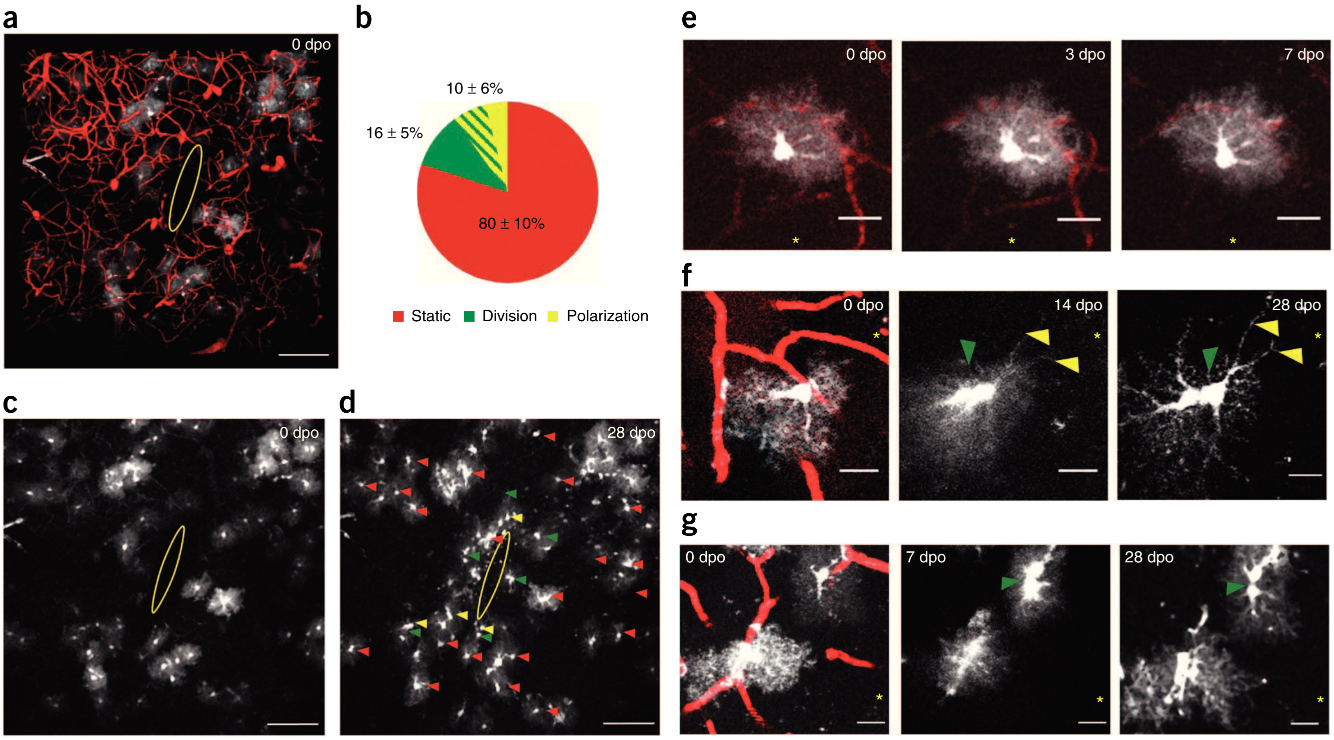

Figure 1 Live imaging of astrocyte responses to a punctate lesion. (**a**) GFP-labeled astrocytes (white) in the vicinity of a punctate lesion (yellow ellipse) in the somatosensory cortex of GLAST/eGFP mice, imaged live by 2pLSM at 0 dpo. Blood vessels are labeled with Texas Red–dextran, and the image shows a three-dimensional view of a 200-µm-deep *x*-*y*-*z* stack. (**b**) Astrocyte behavior was classified into three categories on the basis of the morphological changes observed by 7 d after wounding: cells retained a stable morphology (static), became polarized and/or underwent division ($n = 5$ mice, mean ± s.e.m.). (**c**–**g**) Repeated observations of the same cells within 300 µm of the lesion from 0 dpo (**c**) up to 28 dpo (**d**; 200-µm-deep *z* projection) revealed a markedly heterogeneous reaction: the majority of cells retained a stable morphology (**d**, red arrowheads; an example is shown in **e**), and only a few cells became polarized toward the injury site (**d**, yellow arrowheads; example in **f**) and/or underwent cell division (**d**, green arrowheads; examples in **f**,**g**). The yellow asterisks in **e**–**g** indicate the lesion site. Scale bars represent 100 µm (**a**,**c**,**d**) and 20 µm (**e**–**g**).

(0 d post-operation (dpo), typically 30 min after injury). At this time, all GFP$^+$ cells exhibited the round and bushy morphology typical of protoplasmic astrocytes (**Fig. 1a**,**c**,**e**–**g**). We inflicted relatively small 'punctate' lesions (200 µm long and 800 µm deep) on GLAST/eGFP mice (the lesion size was defined as the cell-free area that was devoid of blood vessels labeled with Texas Red–conjugated dextran; **Fig. 1a**). Virtually all astrocytes could be reliably identified during the course of the entire experiment, and little or no cell death was observed. Most astrocytes (80% of 102 cells from 5 mice) maintained their morphology for up to 4 weeks after wounding (static; **Fig. 1b**,**d**,**e**), in spite of the fact that GFAP was upregulated in virtually all of the astrocytes close to the injury site, as revealed by immunohistochemical analysis at 7 d after injury (**Supplementary Fig. 1**).

We were unable to detect any migration of astrocytes toward punctate wounds, even after close examination using blood vessels as stable landmarks. To detect even small cell movements, we precisely superimposed images of the same cells acquired at different time points, after correction for tissue contraction. This confirmed that astrocyte positions remained stable and provided no evidence for cell migration (**Supplementary Fig. 2**). However, we did observe signs of hypertrophy, polarization or proliferation of astrocytes, as previously described *in vitro*[9,10,16]. In about half of all astrocytes (42%), the soma was enlarged and cell processes were thicker at 7 dpo than at 0 dpo, indicating that the cells had entered a hypertrophic state (**Supplementary Fig. 3d**). Some cells (10%) formed elongated processes (defined as at least threefold longer than the radius of the cell) that were directed toward the lesion site (polarization; **Fig. 1b**,**d**,**f**). Such changes were not observed after cranial window insertion without prior injury of the cortex (**Supplementary Fig. 4**). We also observed astrocytes that had divided (16%; **Fig. 1b**), typically at 5–7 dpo (**Fig. 1d**,**f**,**g**). Each of these proliferating astrocytes generated no more than two daughter cells, which remained close together for the entire time of observation, even up to 4 weeks (**Fig. 1f**,**g**). Most cell divisions were found within 100 µm of the injury (**Supplementary Fig. 5b**), and polarization preceded 38% of all cell divisions (**Fig. 1b**,**f**), that is, the majority of the cells that proliferated were not polarized, but divided as round bushy astrocytes (**Fig. 1g**). Notably, the somata of most dividing astrocytes were located directly adjacent to a blood vessel (**Fig. 1f**,**g**, and **Supplementary Movies 2** and **3**), whereas others made contact with vessels by means of extended processes (**Fig. 1e**). This difference cannot be accounted for by differences in the local density of blood vessels, as only a minority of the astrocytes (33%, see below) were in direct contact with the vasculature via their cell somata. Such cells have been referred to as perivascular astrocytes[17,18].

To determine whether these astrocytes may be particularly prone to resume proliferation after more extensive injury, we made incisions (stab wounds) of about 1 mm long and 800 µm deep before insertion of the cranial window (**Fig. 2a**). This type of injury activated astrocytes over a wider area, as almost all of the astrocytes within 300 µm of the injury site upregulated GFAP (*postmortem* analysis; **Supplementary Fig. 6**). Moreover, in this case, a greater fraction of astrocytes than in mice with punctate wounds (86% ± 7%) became hypertrophic (**Fig. 2b** and **Supplementary Fig. 3a**,**d**), as revealed by a marked increase in the mean volume of cell somata (**Supplementary Fig. 3b**). These values are based on direct comparison of measurements for 12 individual cells

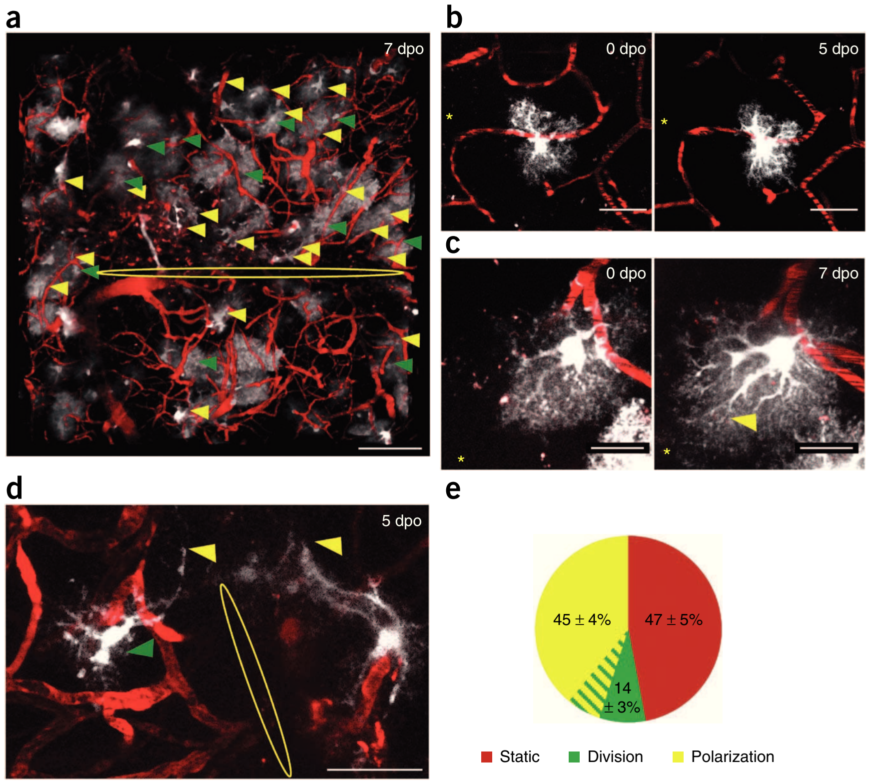

Figure 2 Live imaging of astrocyte responses to a stab wound. (**a**) Heterogeneous reaction of GFP⁺ astrocytes within 300 μm of a large stab wound (yellow ellipse) was observed live at 7 dpo by 2pLSM (the image shows a three-dimensional view of a 450-μm-deep *x-y-z* stack) using Texas Red–dextran to label blood vessels. (**b**) Example of a cell that became hypertrophic, but essentially retained its initial morphology and maintained its position. These cells with static position and no polarization or proliferation were the largest population, as depicted in the pie chart in **e**. (**c**,**d**) Examples of cells that polarized toward the lesion (yellow arrowheads in **a**, **c** and **d**) and/or showed cell divisions that were identifiable as newly appearing cell duplets at 5 dpo (green arrowheads in **a** and **d**). (**e**) The pie chart summarizes the behavior of astrocytes within 300 μm of the stab wound, as assessed on the basis of morphological changes occurring between 0 and 7 dpo ($n = 3$ mice, mean ± s.e.m.). Scale bars represent 100 μm (**a**), 50 μm (**b**,**d**) and 20 μm (**c**). The lesion site is marked by the yellow ellipse (**a**,**d**) or with yellow asterisks (**b**,**c**).

from three mice imaged at the indicated times, which yielded a mean volume ratio of 3 ± 0.4, whereas control cells maintained their initial volume (**Supplementary Fig. 3c**). Thus, after more extensive injury, the somata of virtually all astrocytes increased in size (**Fig. 2b** and **Supplementary Fig. 3a,d**), although this was not necessarily associated with a change in overall morphology (**Fig. 2b**).

Moreover, a subset of astrocytes (45%) within 300 μm of a large stab wound became polarized. Polarization typically occurred within 3–5 dpo (**Fig. 2c–e** and **Supplementary Movie 4**), with processes extending up to 111 μm (mean ± s.e.m., 69 ± 5 μm, $n = 3$ mice), that is, more than threefold longer than the average radius of protoplasmic astrocytes at 0 dpo (≤30 μm, 25 ± 0.5 μm, $n = 3$ mice). Notably, none of the astrocytes, not even the polarized ones, exhibited any detectable signs of movement toward the injury site (≤5 μm over 7 d; **Supplementary Fig. 2** and **Supplementary Movie 5**). Just as in the case of the smaller punctate wound, only a subset of astrocytes in the region of the larger stab wound divided within 7 dpo (14%; **Fig. 2a,d,e**), and never generated more than two daughter cells. However, the induction of astrocyte proliferation was no longer restricted to the immediate vicinity (<100 μm) of the injury, but occurred over a larger area around the stab wound (**Supplementary Fig. 5**). Again, the vast majority of astrocyte divisions observed by live imaging after a stab wound (71%, $n = 8$ cells) occurred in cells whose somata were directly apposed to a blood vessel (**Fig. 3a–c**).

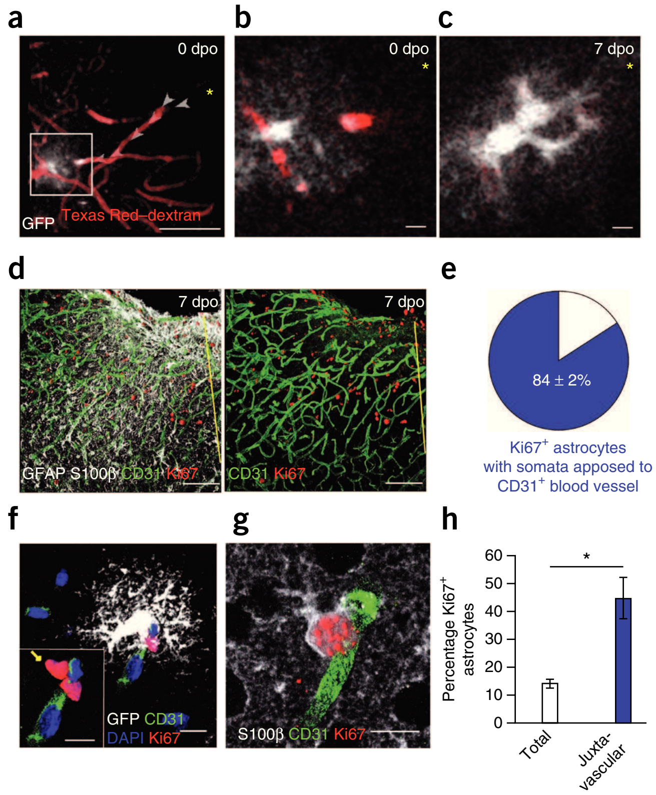

Figure 3 Astrocyte proliferation adjacent to blood vessels. (**a**,**b**) Live imaging of a GFP⁺ astrocyte 30 min after localized wounding on 0 dpo (close-up in **b**, see **Supplementary Movie 2**) revealed direct contact between the cell soma and a blood vessel (0 dpo, arrowheads). (**c**) The same cell imaged 7 d later (7 dpo) showed up as a cell duplet, indicating that the astrocyte had undergone cell division in close proximity to the vasculature (**Supplementary Movie 3**). The yellow asterisks in **a**–**c** indicate the lesion site. (**d**–**h**) Quantitative analysis by immunolabeling confirmed proliferation (Ki67⁺ nuclei) of astrocytes, which were labeled with GFAP and S100β (**d**,**g**) or with GFP (**f**), close to CD31⁺ endothelial cells of cerebral blood vessels 7 d after infliction of a stab wound. (**e**) The majority of astrocytes with Ki67⁺ nuclei were in direct contact with blood vessels (mean ± s.e.m.); examples are shown for juxtavascular proliferating astrocytes labeled with GFP (**f**) or S100β (**g**) from GLAST/eGFP mice. The yellow arrow in the insert of **f** indicates the Ki67⁺ nucleus of the GFP⁺ cell shown in white in **f**. (**h**) Astrocytes that were directly apposed to blood vessels showed a higher proliferation rate than the total astrocyte population (mean ± s.e.m., unpaired *t* test, $^*P = 0.040$). Scale bars represent 100 μm (**a**,**d**) and 20 μm (**b**,**c**,**f**,**g**).

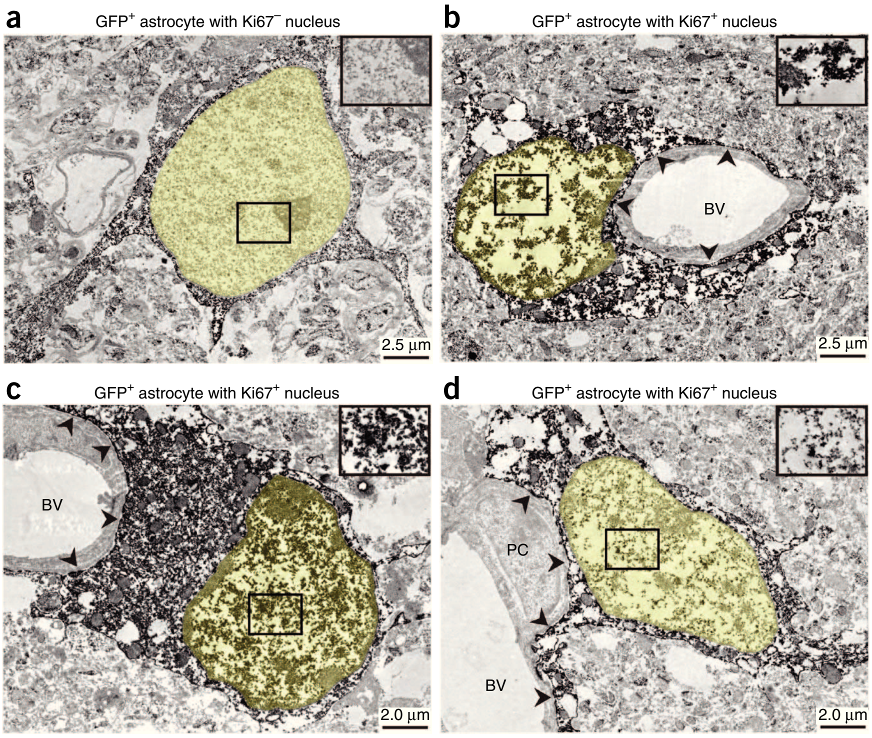

Figure 4 Juxtavascular locations of proliferating astrocytes. (**a**–**d**) Immunoelectron microscopy of GFP+ astrocytes from *Aldh1l1-eGFP* mice after stab wounding (7 dpo), identified by double-labeling for GFP− and Ki67-DAB, confirmed proliferation of astrocytes in direct contact with cerebral blood vessels (BVs). Positive DAB labeling resulted in the expected granular staining pattern visible in the cytoplasm of GFP+ astrocytes, as well as in Ki67+ nuclei of proliferating cells (**b**–**d**). Although most parenchymal astrocytes (**a**) did not proliferate, a proliferating subset of GFP+ Ki67+ astrocytes was found preferentially in juxtavascular locations, where cell somata made direct contacts with the fused glio-vascular basement membrane (marked with arrowheads in **b**–**d**) at brain capillaries and post-capillary vessels. The nuclei of astrocytes are shaded in yellow. Insets show close-ups of boxed regions in the respective nuclei, with typical DAB grains indicative of Ki67 immunoreactivity (**b**–**d**), whereas the nucleus in **a** is Ki67−. PC, pericyte.

Taken together, our *in vivo* imaging data reveal a marked lack of migration of reactive astrocytes, as well as a notable heterogeneity of response, with subsets of astrocytes polarizing toward the injury site, and a rather specific subset of astrocytes with their soma in direct contact with the vasculature showing a particular tendency to proliferate.

Preferentially juxtavascular astrocytes proliferate

To examine the locations of proliferating astrocytes independently of GLAST^{CreERT2}-mediated recombination, we used immunostaining to detect actively proliferating (Ki67+) cells (mostly microglia and NG2 glia[8]) that were astrocytes (S100β+ and/or GFAP+) and with their soma in direct vicinity to endothelial cells (CD31+) lining the blood vessels (**Fig. 3d**). Although only 33% of all astrocytes (1,049 cells, 3 mice) were located with their somata directly adjacent to CD31+ endothelial cells, 84% of all proliferating (Ki67+) astrocytes (194 cells, 5 mice; **Fig. 3e**) were found to display such direct apposition to a blood vessel (**Fig. 3f,g**). Indeed, among astrocytes whose somata were in direct contact with a blood vessel, the fraction that proliferated within 7 d of stab wounding was threefold higher (45%) than in the astrocyte population as a whole (14%; **Fig. 3h**), further supporting the concept that astrocytes in this position are more prone to divide than others.

However, direct apposition, as defined at the light microscopic level, may well overlook intervening cells or even misinterpret the position of cells in relation to the different basement membranes surrounding the blood vessels[19]. To clarify the exact location of dividing astrocytes, we used pre-embedding immunoelectron microscopy to determine the location of dividing (Ki67+) astrocytes labeled by GFP in *Aldh1l1-eGFP* mice[20,21] 7 d after stab wounding. GFP+ cells with or without Ki67 labeling were localized in vibratome sections (**Supplementary Fig. 7**) and further processed for electron microscopy (**Fig. 4**). Although many Ki67-negative astrocytes were found in the parenchyma (**Fig. 4a**), the somata of Ki67+ GFP+ astrocytes were

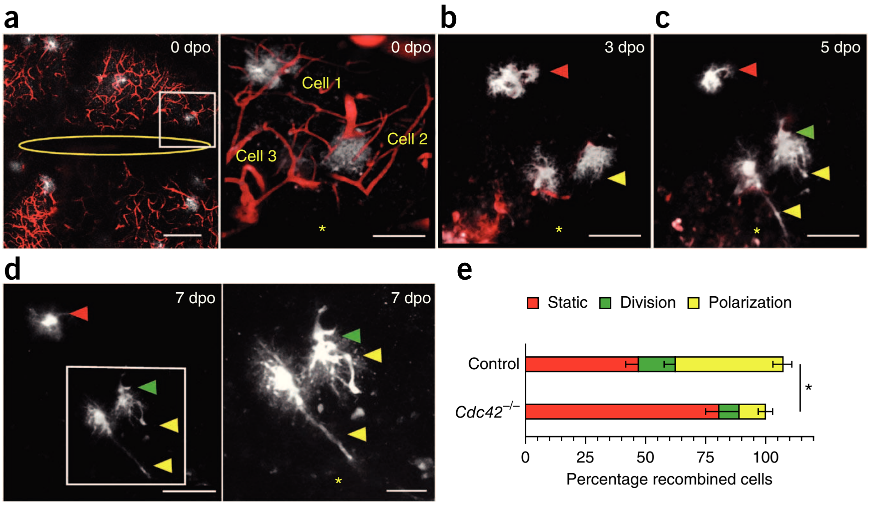

Figure 5 Live imaging of *Cdc42*−/− astrocytes following stab wounding. (**a**–**d**) The behavior of *Cdc42*−/− astrocytes labeled with GFP was observed live by 2pLSM in GLAST/eGFP *Cdc42*$^{loxP/loxP}$ mice after stab wounding. A heterogeneous reaction of astrocytes following injury was also detected in *Cdc42*−/− astrocytes. Although many cells retained a static morphology (cell 1, **a**; red arrowhead, **b**–**d**), a few cells polarized toward the lesion site (cells 2 and 3, **a**; yellow arrowheads, **b**–**d**) or underwent division (green arrowhead, **c**,**d**). Boxed regions in **a**,**d** are enlarged in right panels. Scale bars represent 100 μm (**a**, left), 50 μm (**a**, right; **b**,**c**; **d**, left) and 25 μm (**d**, right). (**e**) Compared with control mice with normal Cdc42 expression, fewer *Cdc42*−/− astrocytes in the vicinity of a stab wound exhibited morphological changes or showed signs of polarization, implying that the ability of these astroglia to respond to injury was impaired ($n = 3$ mice per group, mean ± s.e.m., one-way ANOVA, $*P = 0.0373$). The lesion site is marked with yellow asterisks.

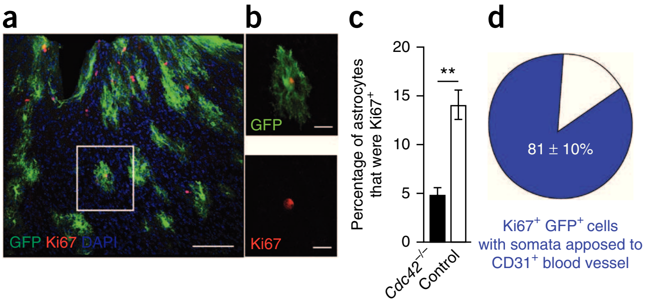

Figure 6 Proliferation defect in *Cdc42*$^{-/-}$ astrocytes following injury. (**a**–**c**) Immunolabeling of astrocytes in GLAST/eGFP *Cdc42*$^{loxP/loxP}$ mice revealed a significant decrease in the numbers of proliferating (Ki67^{+} nuclei) *Cdc42*$^{-/-}$ GFP^{+} astrocytes observed after stab wounding (7 dpo, higher magnification of boxed region shown in **b**) compared with the proliferation rate of control astrocyte with normal Cdc42 expression (mean ± s.e.m., unpaired *t* test, $^{**}P = 0.001$). (**d**) Most of the proliferating *Cdc42*$^{-/-}$ astrocytes were located in direct contact with a blood vessel (mean ± s.e.m.). Scale bars represent 100 μm (**a**) and 25 μm (**b**).

always closely associated with blood vessels (**Fig. 4b**–**d**). In many cases, the Ki67^{+} nucleus was only separated by a small astrocytoplasmic bridge from the neighboring blood vessel, and no other cells or processes could be detected between the soma of the Ki67^{+} astrocyte and the fused glio-vascular basement membrane surrounding the vessels (**Fig. 4b**–**d**). Most proliferating astrocytes (n = 14 cells) were found at capillaries or postcapillary vessels that were anatomically defined, for example, by their diameter, the presence of smooth muscle cells and basement membrane architecture[19]. Some astrocytes were located in close proximity to pericytes (**Fig. 4d**), but were always separated from these by the fused glio-vascular basement membrane, thereby clearly determining their position as juxtavascular, rather than perivascular[19]. As no additional basement membrane was detected on the parenchymal side of Ki67^{+} GFP^{+} astrocytes, a putative location in the perivascular (Virchow-Robin) space could always be ruled out, and their position was, by definition, juxtavascular, that is, inside the brain parenchyma proper (**Supplementary Fig. 8**).

Astrocyte proliferation occurs clonally

Live observations of astrocyte duplets suggested that each pair represented the daughter cells derived from the division of a single mother cell. Given that virtually no cell migration was observed, it seems highly unlikely that a different cell could have adventitiously moved into apposition with a previously identified cell in the interval between two successive imaging sessions. Nevertheless, we wished to confirm the clonal nature of astrocyte duplets directly, using an independent technique. To this end, we crossed GLAST^{CreERT2} mice with the multicolor *R26R-Confetti* reporter strain[22] (referred to as GLAST/Confetti mice), which allows for inducible labeling of astrocytes with one of four different fluorescent proteins, membrane-bound cyan fluorescent protein, nuclear GFP, or cytoplasmic yellow or red fluorescent protein. To perform a clonal analysis on the progeny of reactive astrocytes, we treated adult mice with low doses of tamoxifen, which induced sparse labeling of less than 25 astrocytes of each color per hemisphere of the cerebral cortex (**Supplementary Fig. 9**). Although no astrocyte duplets were detected in control, non-lesioned brains or in the contralateral hemisphere of clonally induced GLAST/Confetti mice subjected to unilateral stab wounding, cell duplets of each of the four colors were found in the ipsilateral, lesioned hemisphere, and were always unicolored (defined as pairs of cell somata of the same color ≤5 μm apart, 20 sections from 3 animals). Given that all astrocyte duplets (n = 18 duplets in 2 brains at 7 dpo; **Supplementary Fig. 9b**–**e**) appeared close to the injury site (<500 μm away) and were always of a single color, we concluded that each duplet was the product of a single cell division.

The absence of any larger clusters of cells of the same color confirms the observation, based on repeated imaging of live cells, that a given astrocyte undergoes no more than a single division over the course of our experiments, although the possibility of a further division rapidly followed by cell death cannot formally be excluded. With regard to the extent of astrocyte expansion after injury, both live imaging and clonal labeling revealed that the increase in astrocyte numbers was limited. Only a minority of astrocytes divides at all, each generating just two daughter cells, and no cells migrated into the area adjacent to the wound.

Effect of *Cdc42* deletion on astrocyte reactions to injury

However, even small changes in the number of astrocytes can have substantial effects on microglia activation[10] or leukocyte immigration[5]. We set out to explore the role of a candidate molecule that might participate in regulating the proliferation of juxtavascular astrocytes, the population responsible for increasing astrocyte numbers after stab wounding. The small RhoGTPase Cdc42 is a major signaling mediator that is involved in many proliferative pathways[23,24] and has been implicated in astrocyte recruitment by polarized cell migration *in vitro*[9,10]. Thus, deletion of the *Cdc42* gene in astrocytes allowed us to further test for possible changes in cell position or the formation of processes.

To investigate the intrinsic role of Cdc42 in astrocyte reactions to injury, we monitored GFP-labeled astrocytes lacking Cdc42 by live imaging in tamoxifen-induced *GLAST/eGFP Cdc42*$^{loxP/loxP}$ mice[10] after inflicting a stab wound injury about 1 mm in length (**Fig. 5**). Live observation by 2pLSM revealed that the number of *Cdc42*$^{-/-}$ astrocytes that extended elongated processes toward the injury site was markedly lower than that observed in *GLAST/eGFP Cdc42*$^{+/+}$ controls (*Cdc42*$^{-/-}$, 11%; *Cdc42*$^{+/+}$, 45%; three mice per genotype; **Fig. 5**). The incidence of cell division among *Cdc42*$^{-/-}$ astrocytes was likewise reduced (*Cdc42*$^{-/-}$, 8.5%; *Cdc42*$^{+/+}$, 14%; **Fig. 5c**–**e**), and those cells that did divide were restricted to within 100 μm of the injury. In control mice, dividing astrocytes were found up to 300 μm from the site of the wound.

Immunohistochemical analysis of similarly lesioned GLAST/eGFP *Cdc42*$^{loxP/loxP}$ mice confirmed the proliferation defect in *Cdc42*$^{-/-}$ astrocytes (**Fig. 6a**–**c**). Only 5% of *Cdc42*$^{-/-}$ astrocytes (1,031 cells, n = 5 mice; **Fig. 6c**) are actively dividing (Ki67^{+} nuclei) at 7 dpo, compared with 14% of astrocytes (1,049 cells, n = 3 mice; **Fig. 6c**) in control mice with normal Cdc42 expression. Although deletion of *Cdc42* in astrocytes impaired the frequency of polarization and proliferation, the proliferating subset of astrocytes was still found preferentially in juxtavascular positions (81%, n = 6 mice; **Fig. 6d**). Thus, even when proliferation of the juxtavascular subset is impaired, astrocytes located at other sites apparently do not compensate for that. This is compatible with the notion that the population of reactive astrocytes is made up of distinct subsets dedicated to specific tasks, such as proliferation or polarization.

DISCUSSION

The ability to repeatedly examine the same small area of tissue *in vivo* using live imaging can provide new insights into the detailed pathology of diverse CNS disorders, including Alzheimer's disease[25], multiple sclerosis[26] and axonal degeneration in the spinal cord[27–29]. We used this technique to monitor the reaction of astroglia to TBI and discovered a marked degree of heterogeneity in astrocyte behavior. Although most astrocytes became hypertrophic and upregulated GFAP after stab wounding (**Supplementary Figs. 1**, **3** and **6**), only subsets of them polarized or proliferated. In stark contrast with data obtained *in vitro* with scratch wound assays[9,10,16], our *in vivo* observations revealed that most astrocytes in the lesioned region, including those that polarized toward the injury site or proliferate, stayed in their initial positions after TBI. Thus, not only do astrocytes remain in their region of developmental origin, for example, in the cerebral cortex[30], and expand in number by proliferation during postnatal stages[31], they do not even migrate for short distances over periods from days to weeks after TBI, at least not in the gray matter of the cerebral cortex.

Technical considerations

Before considering these observations further, it is important to rule out possible technical artifacts. Clearly, inducible genetic recombination does not allow one to label all astrocytes, but rather provides the opportunity to adjust the density of GFP-labeled astrocytes to levels that are optimal for imaging purposes. Thus, although most astrocytes express GLAST (and 60–80% of all astrocytes coexpress the Cre recombinase from the GLAST locus[14]), a subset of astrocytes with lower levels of GLAST expression[32] will not be labeled by inducible genetic recombination. To rule out the possibility that our observations reported are applicable only to the subset of astrocytes with higher levels of GLAST (and thus CreERT2), we performed three sets of control experiments: live imaging after stab wounding of *Aldh1l1-eGFP* mice, in which the entire astrocyte population is labeled[20,21] (**Supplementary Fig. 10a**–**e** and **Supplementary Movie 6**), live imaging in *GFAP-eGFP* mice[33], in which the astrocytes with the highest GFAP expression levels are labeled (**Supplementary Fig. 10f**–**h**), and immunostaining to verify the results obtained in the above-mentioned transgenic lines. Live imaging of the control mouse lines confirmed the immobility of most astrocytes, as no cell migration was observed in these strains either. Furthermore, we confirmed the juxtavascular location of proliferating astrocytes by live imaging and immunostaining in both of the transgenic mouse lines. Thus, our results were confirmed in three independent mouse lines and can reasonably be applied to the entire astrocyte population. In this regard, the behavior of GLAST/eGFP–labeled astrocytes may be viewed as representative of that of astrocytes in general.

We were also able to rule out several technical concerns in regard to our 2pLSM imaging technique, as we were able to clearly visualize the migration of other glial populations, such as NG2 glia, toward injury sites (A. von Streitberg, C. Straube, M.G. & L.D., unpublished data), consistent with previous observations of microglial cells[13,34]. Thus, most glial cells readily migrated to injury sites in the gray matter of the cerebral cortex after stab wound injury, whereas astrocytes failed to do so. It will be interesting to examine whether this also holds true for white matter regions or other injury conditions, and whether astrocytes generally do not migrate in the mammalian brain *in vivo*.

Astrocyte recruitment to injury sites

Our findings that astrocytes did not migrate have marked implications for the mechanism of recruitment to sites of injury, as they imply that astrocyte numbers increase after TBI solely as a result of proliferation. Notably, the increase in astrocyte numbers after such stab wound injury is relatively modest (about 20%), which is consistent with the limited amount of proliferation that we observed. In this context, it is important to stress that the increase observed by GFAP immunostaining in many pathological samples does not reflect an increase in astrocyte numbers, but rather upregulation of GFAP expression. In many, if not most, brain regions, astrocytes are GFAP negative under normal, healthy conditions, as is the case in the gray matter of the cerebral cortex[33,35]. Thus, the enormous increase in GFAP$^+$ cells may give a misleading impression, considering that total astrocyte numbers showed only a modest increase.

The astrocytes that proliferated and generated two daughter cells, which remained close together, were mainly found at juxtavascular locations. Astrocytes whose somata lie directly adjacent to blood vessels have been described previously in the retina[18] and somatosensory cortex in mouse[17], and have been referred to as perivascular astrocytes. On the basis of our electron microscopic data, which localized the somata of proliferating astrocytes in regard to the glio-vascular basement membrane in the juxtavascular parenchyma rather than to a perivascular (Virchow-Robin) space (enclosed between two basement membranes), we refer to these as the juxtavascular subset of astrocytes given the earlier localization of pericytes[19] and microglia[26,36]. It will now be important to determine whether this population is widespread in the CNS or has a more restricted, possibly even region-specific, distribution.

These data raise the question of the functional relevance of this class of astrocytes. When proliferating astrocytes were selectively ablated by expression of herpes simplex virus thymidine kinase (HSV-TK) under the control of the *Gfap* promoter, leukocyte infiltration was markedly enhanced[37], prompting the suggestion that juxtavascular astrocytes, and their expansion after injury, may be important for limiting invasion of these cells into the brain. As recent data also imply that pericyte-derived cells contribute to fibrotic scar formation[38], it is tempting to speculate that juxtavascular astrocytes may also limit migration and/or proliferation of these cells. Thus, this juxtavascular subset of astrocytes is in a privileged position to interact with cells invading injured brain areas[26,38,39]. Taken together, our live-imaging data, which reveal that a rather special type of astrocytes is the major contributor to proliferation after TBI, prompts new ideas about the role of astrocytes in this specific location. Likewise, one may have to reconsider the issue of a direct contribution of astrocytes to scar formation, given their limited increase in number and failure to migrate to the actual injury site. However, it will certainly be of interest to apply this analysis to other injury models, such as stroke or selective inflammatory lesions, to observe astrocyte behavior under these different conditions, given that their patterns of gene expression also differ markedly[6].

Astrocyte heterogeneity

Irrespective of the exact function of the juxtavascular astrocytes, our observation of a specific subset of astrocytes proliferating after stab wound injury reveals a notable functional heterogeneity in astrocyte behavior. This heterogeneity also extends further, as we observed a distinct subset of astrocytes that polarized toward the lesion site, whereas others retained their bushy morphology despite clearly reacting to injury by becoming hypertrophic. As we were able to follow reactive astrocytes for days and weeks after injury, we could verify that subsets of astrocytes retained their bushy morphology at all times after injury, rather than extending long polarized processes and retracting them again.

Astrocytes that did polarize typically extended their elongated processes toward the injury site between 3 and 5 d after stab wounding, and maintained them for several weeks, as has been described in epilepsy models[40]. Notably, the proportion of astrocytes that proliferated did not increase as a function of the injury size, although a higher proportion of astrocytes polarized toward a larger injury.

This further supports the idea that at least three different sets of astrocytes react in distinct ways to stab wound injury. This is important because it provides a basis for selective regulation of the different subsets of astrocytes, not only to unravel their specific functions, but eventually to modulate these functions with a view to improving outcomes after brain injury. Our data therefore not only revise the current view of astrocyte recruitment to injury[2,5], but also highlight the heterogeneity of astrocyte behavior, which suggests a division of labor in response to local lesions, and provide the basis for new approaches to ameliorating functional deficits following injury.

METHODS

Methods and any associated references are available in the online version of the paper.

Note: Supplementary information is available in the online version of the paper.

ACKNOWLEDGMENTS

We are indebted to C. Brakebusch for the *Cdc42*$^{loxP/loxP}$ mice, S. Robel for initial help in setting up the two-photon live-imaging procedure, and C. Straube and S. Falkner for sharing their imaging expertise. We would also like to thank R. Waberer, C. Meyer, D. Franzen, I. Mühlhahn and G. Jäger for technical assistance, and M. Hübener, D.E. Bergles, J. McCarter and P. Hardy for critical comments on the manuscript. We thank the DFG (German Research foundation) whose support (particularly via the Leibniz Prize and SFB 870) allowed us to invest into this new experimental area and for funding M.G. and F.J.T. by SPP1356 and I.B. by DFG-FOR 1336. In addition, this work was supported by the BMBF (Ministry of Science and Education) to M.G. and F.J.T., the Helmholtz Association (Helmholtz Alliance ICEMED to M.G., I.B. and F.J.T.; Helmholtz Alliance on Systems Biology to M.G. and F.J.T.), the Emmy Noether Program of the DFG (ME 3542/1-1 to M.M.-L.), the European Research Council (starting grant 'LatentCauses' to F.J.T.) and Munich Cluster for Systems Neurology. The Initial Training Network Edu-GLIA (PITN-GA-2009-237956) funded by the European Commission under the Seventh Framework Program (FP7) provided a wonderful discussion platform for glial research.

AUTHOR CONTRIBUTIONS

S.B. performed all of the experiments and data analyses (except for electron microscopy) and wrote the manuscript. M.K. and I.B. carried out electron microscopy. F.B. and F.J.T. assisted in data processing and volume analysis (**Supplementary Figs. 2** and **3**). J.S., J.N., H.C. and H.J.S. supplied the GLAST/confetti mouse strain (**Supplementary Fig. 9**). M.M.-L. provided access to the 2pLSM and expert advice on imaging. L.D. initially established the *in vivo* two-photon microscopy technique and taught it to S.B. M.G., together with L.D., designed the project and experiments, discussed the results and wrote the manuscript. M.G. coordinated and directed the project.

COMPETING FINANCIAL INTERESTS

The authors declare no competing financial interests.

1. Hellal, F. *et al.* Microtubule stabilization reduces scarring and causes axon regeneration after spinal cord injury. *Science* **331**, 928–931 (2011).
2. Pekny, M. & Nilsson, M. Astrocyte activation and reactive gliosis. *Glia* **50**, 427–434 (2005).
3. Robel, S., Berninger, B. & Götz, M. The stem cell potential of glia: lessons from reactive gliosis. *Nat. Rev. Neurosci.* **12**, 88–104 (2011).
4. Silver, J. & Miller, J.H. Regeneration beyond the glial scar. *Nat. Rev. Neurosci.* **5**, 146–156 (2004).
5. Sofroniew, M.V. Molecular dissection of reactive astrogliosis and glial scar formation. *Trends Neurosci.* **32**, 638–647 (2009).
6. Zamanian, J.L. *et al.* Genomic analysis of reactive astrogliosis. *J. Neurosci.* **32**, 6391–6410 (2012).
7. Buffo, A. *et al.* Origin and progeny of reactive gliosis: a source of multipotent cells in the injured brain. *Proc. Natl. Acad. Sci. USA* **105**, 3581–3586 (2008).
8. Simon, C., Götz, M. & Dimou, L. Progenitors in the adult cerebral cortex: cell cycle properties and regulation by physiological stimuli and injury. *Glia* **59**, 869–881 (2011).
9. Etienne-Manneville, S. *In vitro* assay of primary astrocyte migration as a tool to study Rho GTPase function in cell polarization. *Methods Enzymol.* **406**, 565–578 (2006).
10. Robel, S., Bardehle, S., Lepier, A., Brakebusch, C. & Götz, M. Genetic deletion of Cdc42 reveals a crucial role for astrocyte recruitment to the injury site *in vitro* and *in vivo*. *J. Neurosci.* **31**, 12471–12482 (2011).
11. Sirko, S. *et al.* Reactive glia in the injured brain acquire stem cell properties in response to Sonic hedgehog. *Cell Stem Cell* (in the press) (2013).
12. Holtmaat, A. *et al.* Long-term, high-resolution imaging in the mouse neocortex through a chronic cranial window. *Nat. Protoc.* **4**, 1128–1144 (2009).
13. Nimmerjahn, A., Kirchhoff, F. & Helmchen, F. Resting microglial cells are highly dynamic surveillants of brain parenchyma *in vivo*. *Science* **308**, 1314–1318 (2005).
14. Mori, T. *et al.* Inducible gene deletion in astroglia and radial glia—a valuable tool for functional and lineage analysis. *Glia* **54**, 21–34 (2006).
15. Nakamura, T., Colbert, M.C. & Robbins, J. Neural crest cells retain multipotential characteristics in the developing valves and label the cardiac conduction system. *Circ. Res.* **98**, 1547–1554 (2006).
16. Höltje, M. *et al.* Role of Rho GTPase in astrocyte morphology and migratory response during *in vitro* wound healing. *J. Neurochem.* **95**, 1237–1248 (2005).
17. McCaslin, A.F., Chen, B.R., Radosevich, A.J., Cauli, B. & Hillman, E.M. *In vivo* 3D morphology of astrocyte-vasculature interactions in the somatosensory cortex: implications for neurovascular coupling. *J. Cereb. Blood Flow Metab.* **31**, 795–806 (2011).
18. Reichenbach, A. & Wolburg, H. Astrocytes and ependymal glia. in *Neuroglia*, 2nd edn. (Kettenmann, H. & Ransom, B.R.) 19–35 (Oxford University Press, 2005).
19. Krueger, M. & Bechmann, I. CNS pericytes: concepts, misconceptions and a way out. *Glia* **58**, 1–10 (2010).
20. Cahoy, J.D. *et al.* A transcriptome database for astrocytes, neurons and oligodendrocytes: a new resource for understanding brain development and function. *J. Neurosci.* **28**, 264–278 (2008).
21. Heintz, N. Gene expression nervous system atlas (GENSAT). *Nat. Neurosci.* **7**, 483 (2004).
22. Snippert, H.J. *et al.* Intestinal crypt homeostasis results from neutral competition between symmetrically dividing Lgr5 stem cells. *Cell* **143**, 134–144 (2010).
23. Fuchs, S. *et al.* Stage-specific control of neural crest stem cell proliferation by the small rho GTPases Cdc42 and Rac1. *Cell Stem Cell* **4**, 236–247 (2009).
24. Warner, S.J., Yashiro, H. & Longmore, G.D. The Cdc42/Par6/aPKC polarity complex regulates apoptosis-induced compensatory proliferation in epithelia. *Curr. Biol.* **20**, 677–686 (2010).
25. Meyer-Luehmann, M. *et al.* Rapid appearance and local toxicity of amyloid-beta plaques in a mouse model of Alzheimer's disease. *Nature* **451**, 720–724 (2008).
26. Davalos, D. *et al.* Fibrinogen-induced perivascular microglial clustering is required for the development of axonal damage in neuroinflammation. *Nat. Commun.* **3**, 1227 (2012).
27. Ertürk, A. *et al.* Three-dimensional imaging of the unsectioned adult spinal cord to assess axon regeneration and glial responses after injury. *Nat. Med.* **18**, 166–171 (2012).
28. Misgeld, T., Nikic, I. & Kerschensteiner, M. *In vivo* imaging of single axons in the mouse spinal cord. *Nat. Protoc.* **2**, 263–268 (2007).
29. Dibaj, P. *et al.* *In vivo* imaging reveals rapid morphological reactions of astrocytes towards focal lesions in an ALS mouse model. *Neurosci. Lett.* **497**, 148–151 (2011).
30. Tsai, H.H. *et al.* Regional astrocyte allocation regulates CNS synaptogenesis and repair. *Science* **337**, 358–362 (2012).
31. Ge, W.P., Miyawaki, A., Gage, F.H., Jan, Y.N. & Jan, L.Y. Local generation of glia is a major astrocyte source in postnatal cortex. *Nature* **484**, 376–380 (2012).
32. Regan, M.R. *et al.* Variations in promoter activity reveal a differential expression and physiology of glutamate transporters by glia in the developing and mature CNS. *J. Neurosci.* **27**, 6607–6619 (2007).
33. Nolte, C. *et al.* GFAP promoter-controlled EGFP-expressing transgenic mice: a tool to visualize astrocytes and astrogliosis in living brain tissue. *Glia* **33**, 72–86 (2001).
34. Fuhrmann, M. *et al.* Microglial *Cx3cr1* knockout prevents neuron loss in a mouse model of Alzheimer's disease. *Nat. Neurosci.* **13**, 411–413 (2010).
35. Middeldorp, J. & Hol, E.M. GFAP in health and disease. *Prog. Neurobiol.* **93**, 421–443 (2011).
36. Mathiisen, T.M., Lehre, K.P., Danbolt, N.C. & Ottersen, O.P. The perivascular astroglial sheath provides a complete covering of the brain microvessels: an electron microscopic 3D reconstruction. *Glia* **58**, 1094–1103 (2010).
37. Bush, T.G. *et al.* Leukocyte infiltration, neuronal degeneration, and neurite outgrowth after ablation of scar-forming, reactive astrocytes in adult transgenic mice. *Neuron* **23**, 297–308 (1999).
38. Göritz, C. *et al.* A pericyte origin of spinal cord scar tissue. *Science* **333**, 238–242 (2011).
39. Prodinger, C. *et al.* CD11c-expressing cells reside in the juxtavascular parenchyma and extend processes into the glia limitans of the mouse nervous system. *Acta Neuropathol.* **121**, 445–458 (2011).
40. Oberheim, N.A. *et al.* Loss of astrocytic domain organization in the epileptic brain. *J. Neurosci.* **28**, 3264–3276 (2008).

ONLINE METHODS

Mice, tamoxifen treatment and surgical procedures. Adult (2–3 month old) male mice obtained from crosses between GLAST^{CreERT2} and either CAG-CAT-eGFP (GLAST/eGFP)[14,15], *Cdc42$^{loxP/loxP}$* (ref. 41), *R26R-Confetti* reporter mice (GLAST/Confetti)[22] or *Aldh1l1-eGFP* mice[20,21] were used. Tamoxifen was administered by adding it to food (400 mg per kg, LasVendi) in the case of GLAST/eGFP mice. To induce low rates of recombination, GLAST/Confetti mice received a single intraperitoneal injection of 80 μg of tamoxifen per gram of body weight (stock solution: 40 mg ml^{-1} tamoxifen in corn oil with 10% ethanol) 1 week before surgery.

For repeated imaging, a cranial window was prepared as described previously[12] using tamoxifen-induced GLAST/eGFP and GLAST/eGFP *Cdc42$^{loxP/loxP}$* mice. In brief, mice were anesthetized with an intraperitoneal injection of midazolam (5 mg per kg of body weight), medetomidine (0.5 mg per kg) and fentanyl (0.05 mg per kg), and a unilateral craniotomy (diameter of 3 mm) was positioned between cranial sutures bregma and lambda above the somatosensory cortex. Punctate wounds were inflicted by inserting a lancet-shaped knife into the cortex to a depth of 0.8 mm; to produce stab lesions, the lancet was moved 1 mm in a lateral direction. The craniotomy was covered with a permanent glass cover slip (5-mm diameter) and sealed with dental acrylic (Paladur, Heraeus). Anesthesia was antagonized with an intraperitoneal injection of atipamezol (2.5 mg per kg), flumazenil (0.5 mg per kg) and naloxone (1.2 mg per kg).

For immunohistochemical analysis of GLAST/eGFP and GLAST/Confetti mice, 2–3-month-old mice were subjected to stab wounds no sooner than 1 week after the last tamoxifen dose. GLAST/eGFP *Cdc42$^{loxP/loxP}$* mice were analyzed 3 weeks after induction of recombination to ensure clearance of endogenous Cdc42 protein.

All animal experiments were performed in accordance with the Guidelines on the Use of Animals and Humans in Neuroscience Research, revised and approved by the Society of Neuroscience, and licensed by the State of Upper Bavaria.

2pLSM. Anesthetized mice were injected intravenously (tail vein) with 50 μl of a solution (10 mg ml^{-1}) of Texas Red–conjugated dextran (70 kDa; Molecular Probes D1864) to label blood vessels. Head-bar fixed, anesthetized and craniotomized mice were placed on a heated stage, and imaging was performed with an Olympus FV1000MPE microscope equipped with a multi-photon, near-infrared, pulsed MaiTai HP DeepSee laser (Spectra Physics) equipped with a water immersion objective (20× 1.0 NA), an FV10-MRG filter (barrier filter = 495–540 nm, dichromatic mirror = 570 nm, BA 575–630 nm) and internal photomultiplier tube detectors. Emission of intrinsic eGFP signal (astrocytes in green channel) and Texas Red–conjugated dextran (vasculature in red channel) was simultaneously scanned using an excitation wavelength of 910 nm (depth-adjusted laser power <50 mW). Optical sections with a resolution of 512 × 512 pixels in the *x-y* dimension were acquired at *z* increments of 5 μm to a depth of maximally 500 μm below the dura. Labeled blood vessels served as landmarks for repetitive imaging of *z* stacks obtained for the same field of view. The low density of GFP-labeled astrocytes, which was controlled by adjusting the tamoxifen dose, enabled reliable identification and continuous tracing of single cells selected at 0 dpo (first imaging time point 30 min after injury), and these cells were repeatedly monitored at various intervals thereafter (3, 5, 7, 14, 21 or 28 dpo). A maximum of five imaging sessions was performed per mouse. All imaging experiments were performed without detectable phototoxic side effects.

Immunohistochemistry. Mice were anesthetized and transcardially perfused with 4% paraformaldehyde (PFA, vol/vol) in phosphate-buffered saline (PBS) for 20 min. Brains were post-fixed in 4% PFA for 1 h after dissection. Staining of vibratome sections (60 μm thick) was performed as described previously[10] using chick antibody to GFP (1:500, Aves Lab, GFP-1020), mouse antibody to GFAP (1:500, Sigma, G3893), mouse antibody to S100β (1:500, Sigma, S2532), rabbit antibody to Ki67 (1:100, Thermo Fisher Clone, SP6 RM-9106-S), rat antibody to CD31 (1:500, BD, 550274) and rabbit antibody to red fluorescent protein (1:500, Rockland, 600-401-379) as primary antibodies, and fluorophore-coupled (1:500) antibody to chick Alexa488 (Invitrogen, A11039) and antibody to mouse Alexa488 (Invitrogen, A11029) or Cy3 (Dianova 115-165-003), antibody to rabbit Cy3 (Dianova, 711-165-152) and antibody to rat A647 (Invitrogen, A-21247) as secondary antibodies. Nuclei were stained with DAPI (1:10,000, Sigma, D9564) for 5 min at 20–25 °C. Slides were analyzed with a Zeiss LSM710 confocal laser-scanning microscope using water-immersion objectives (25× 0.8 NA and 40× 1.1 NA).

Data processing and image registration. For visualization and analysis of 2pLSM data, Olympus FV10-ASW 2.0 and ImageJ 1.45q software was used. Cell migration was analyzed using labeled blood vessels as landmarks to bring three-dimensional images of the same area imaged at different time points into register with each other. The color channels of image stacks obtained at different time points were split into four separate grayscale image stacks showing astrocytes and blood vessels at 0 dpo and later time points. Channel splitting and merging was performed with ImageJ[42]. Rigid three-dimensional registration was performed on blood vessel images with elastix 4.5, using day 0 as the fixed and the second time point as the shifted image (**Supplementary Fig. 2a**)[43]. This step resolved linear shifts in *x*, *y* and *z* directions, as well as rotations. Next, transformed images were brought into register using an elastic b-spline method[44,45] to correct for tissue deformation. The calculated transformation parameters were then applied to the stack of images from the GFP channel for the second time point, as well as to a control grid (**Supplementary Fig. 2a**). Areas of the image that revealed no change relative to the control grid indicated that registration was unreliable because of the lack of blood vessel labeling. Such regions were not used for evaluation of astrocyte migration. Channel splitting and the two-step registration procedure made it possible to precisely overlay different three-dimensional image stacks on the basis of the landmark information provided by the blood vessels. Analysis of superimposed, registered four-color stacks never detected any cell body displacements in images acquired at different time points (**Supplementary Fig. 2b–m**).

To validate the visual evaluation of cellular hypertrophy, we used a semi-automatic image processing pipeline to measure the volume of individual GFP-labeled cell somata (n = 12 hypertrophic cells from three mice, n = 11 control cells from four mice) at two different time points based on three-dimensional live-imaging data (**Supplementary Fig. 3**). For each image stack, optical sections were smoothed with a two-dimensional Gaussian filter (sigma = 0.5) to remove noise. Cell somata were identified by manual three-dimensional thresholding using the ImageJ plug-in 3d object counter v2.0 (ref. 46). The high variability in GFP intensities, influenced by tissue depth, wound reaction, laser power and optical window quality, made it necessary to manually adjust thresholds for each individual cell in three-dimensional *z* stacks to reliably determine the size of cell somata. The volume (in μm^3) of each segmented soma was computed by multiplying the sum of segmented voxels by the calibration in *x*, *y* and *z* direction. Volume ratios were calculated for cell pairs (n > 10) by dividing the value for the later time point (5 or 7 dpo) by the value at 0 dpo. A cell was defined as hypertrophic if the volume of the soma increased by more than 10% in the period after injury. All hypertrophic cells used in this analysis displayed volume ratios >1.5.

Immunoelectron microscopy. For electron microscopy, mice were killed and transcardially perfused using a fixative containing 0.1% glutaraldehyde (vol/vol) and 4% PFA. The tissue was post-fixed in the fixative for 4 h. After that, mouse brains were cut into consecutive 60-μm sections on a vibratome (Leica Microsystems) in cooled PBS. After thorough rinsing, unspecific binding of the antibodies was blocked by incubation in PBS containing 5% goat serum (vol/vol). Chick antibody to GFP (1:200, Aves Lab, GFP-1020) and rabbit antibody to Ki67 (1:200 dilution, Thermo Fisher Clone, SP6 RM-9106-S) primary antibodies were incubated overnight at 4 °C. Following thorough rinsing, the appropriate biotinylated secondary antibodies (1:250, Dianova; antibody to rabbit, 111-065-003; antibody to chick, 103-065-155) were incubated with the tissue for 2 h at 20–25 °C. The sections were then rinsed again, and bound antibodies were visualized with the DAB reaction, using a staining kit (Vector Laboratories) according to the manufacturer's protocol. Omission of primary antibodies resulted in the absence of specific staining. Vibratome sections were further processed and embedded in Durcupan (Sigma Aldrich) as described previously[39]. To restrict the ultrastructural analysis precisely to areas of the stab wound, the lesion site was identified by light microscopy and the blocks of resin were trimmed down to the respective region before ultra-thin sectioning so as to ensure that ultra-thin sections encompassed the lesion site only. Sections (60 nm thick) were prepared on an ultramicrotome (Leica Microsystems), transferred to formvar-coated grids and stained with lead citrate for 6 min. Ultrastructural analysis was performed using a Zeiss SIGMA electron microscope equipped with a STEM detector and Atlas software (Zeiss NTS).

Quantification and statistical analyses. Immunohistochemical analysis was done on multi-channel, confocal three-dimensional stacks, using Zeiss ZEN 2010 software and the Cell Counter plug-in for ImageJ 1.45q. Quantifications on fixed sections were done on 3–6 mice (≥3 sections each) per group. The sample size was justified by significance testing and experience from previous immunohistochemical analyses. Results are represented as means ± s.e.m. calculated between different mice. The single-cell analyses are based on live imaging of a total number of 102 cells from five mice with punctate wounds, 68 cells from three mice with stab wounds, and 25 cells from three *Cdc42*$^{-/-}$ mice with stab wounds. Statistics was performed with GraphPad Prism 4.0. For statistical analysis, data were first tested for their distribution and, if normally distributed, the unpaired, two-tailed Student's *t* test was used; otherwise nonparametric, one-way ANOVA was used for comparing mean values that were considered significantly different.

41. Wu, X. *et al.* Cdc42 controls progenitor cell differentiation and beta-catenin turnover in skin. *Genes Dev.* **20**, 571–585 (2006).
42. Abramoff, M.D., Magalhães, P.J. & Ram, S.J. Image processing with ImageJ. *Biophotonics Int.* **11**, 36–42 (2004).
43. Klein, S., Staring, M., Murphy, K., Viergever, M.A. & Pluim, J.P. elastix: a toolbox for intensity-based medical image registration. *IEEE Trans. Med. Imaging* **29**, 196–205 (2010).
44. Klein, S., Staring, M. & Pluim, J.P. Evaluation of optimization methods for nonrigid medical image registration using mutual information and B-splines. *IEEE Trans. Image Process.* **16**, 2879–2890 (2007).
45. Metz, C.T., Klein, S., Schaap, M., van Walsum, T. & Niessen, W.J. Nonrigid registration of dynamic medical imaging data using nD + t B-splines and a groupwise optimization approach. *Med. Image Anal.* **15**, 238–249 (2011).
46. Bolte, S. & Cordelieres, F.P. A guided tour into subcellular colocalization analysis in light microscopy. *J. Microsc.* **224**, 213–232 (2006).

Live imaging of astrocyte responses to acute injury reveals selective juxtavascular proliferation

Sophia Bardehle[1,2], Martin Krüger[3], Felix Buggenthin[4], Julia Schwausch[2], Jovica Ninkovic[2], Hans Clevers[5], Hugo J. Snippert[5], Fabian J. Theis[4], Melanie Meyer-Luehmann[6,7], Ingo Bechmann[3], Leda Dimou[1,2] and Magdalena Götz[1,2,8 *]

SUPPLEMENTARY INFORMATION

SUPPLEMENTARY FIGURES

Supplementary Figure 1

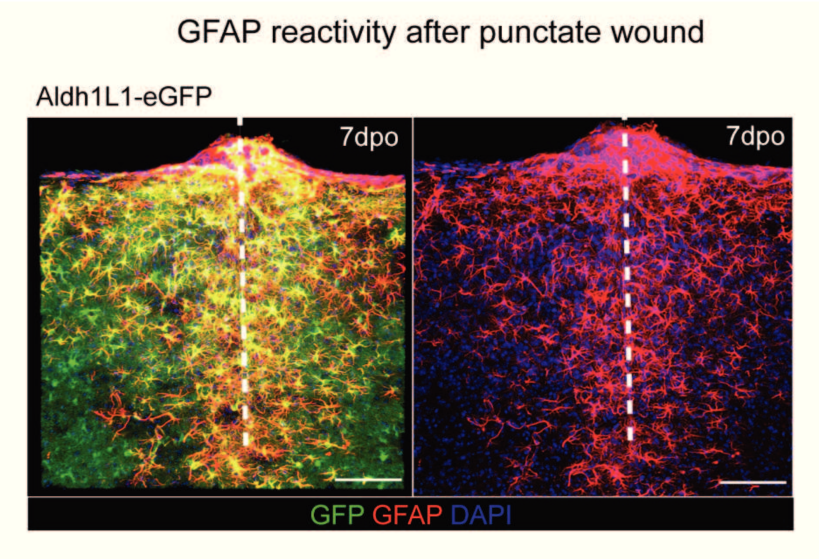

Supplementary Figure 1 Reactive astrocytes up-regulate GFAP after a small punctate wound. Immunohistochemistry for GFAP in lesioned cortical sections of Aldh1L1-eGFP mice, which express GFP in all astrocytes[19,20] (green in the left panel) reveals that almost all astrocytes within a radius of 300 µm of a 'punctate' wound (dashed white line) also express GFAP (red in the panel on the right, yellow in the merged panel on the left) at 7 dpo. Scale bars: 100 µm

Nature Neuroscience: doi:10.1038/nn.3371

Supplementary Figure 2

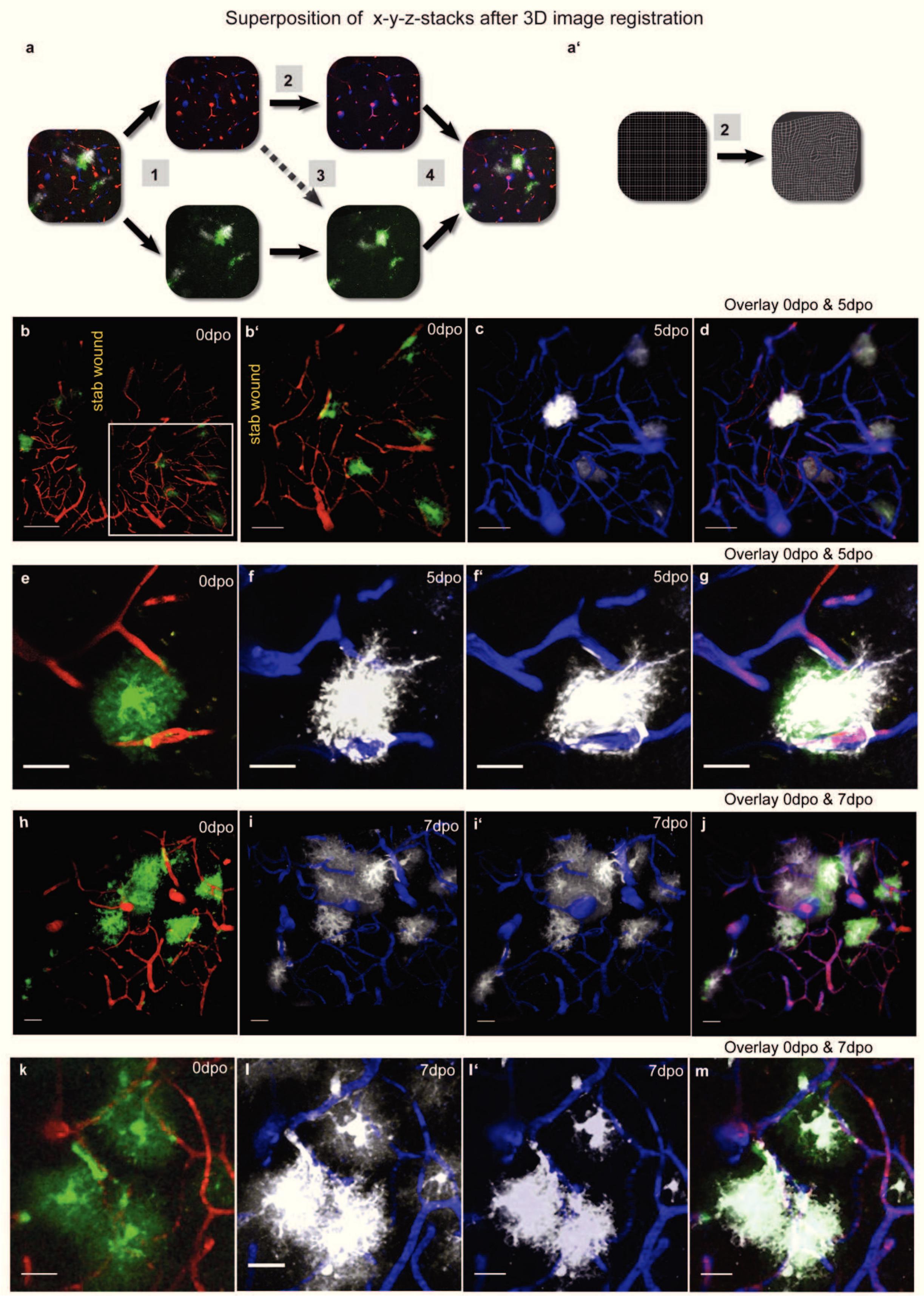

Supplementary Figure 2 Precise superimposition of 3D image stacks acquired at different time points indicates no astrocyte migration. (**a**) Workflow for image registration

Nature Neuroscience: doi:10.1038/nn.3371

of 3-dimensional (3D) image data: (1) Raw data from 2-channel image stacks obtained at two different time points are split into four grayscale stacks. (2) The data for the channel showing the distribution of blood vessels (BV) at day 0 (reference image) and a later time point (corrected image) are brought into register (see Methods). (3) The calculated transformation required to achieve this is then applied to the data from the GFP channel (astrocytes) for the later time point. (4) Finally, registered 4-channel image stacks with overlapping blood vessel (BV) landmarks and GFP+ astrocytes from two different time points are superimposed (for further details see Methods). (**a'**) Control grid used for computed registration parameters. The calculated transformation from step 2 (**a**) applied to a 3D grid with dimensions equal to the original images. (**b-m**) Precisely superimposed 3D images obtained at two different time points after cortical lesion show no change in the localization of GFP+ astrocytes between day 0 (**b**; the area in the inset is shown in **b'**, and at a higher magnification in **e**, **h** and **k**; green: GFP; red: BV) and 5dpo (original image: **f**; after registration: **c**, **f'**; white: GFP; blue: BV) or 7 dpo (original image: **i** and **l**; after registration: **i'**, **l'**; white: GFP, blue: BV). The merged 4-channel stacks (**d**, **g**, **j**, **m**) provide no evidence for astrocyte migration after stab wounding. Scale bars: 100 µm (**b**), 50 µm (**b'-d**), 25 µm (**e-m**).

Nature Neuroscience: doi:10.1038/nn.3371

Supplementary Figure 3

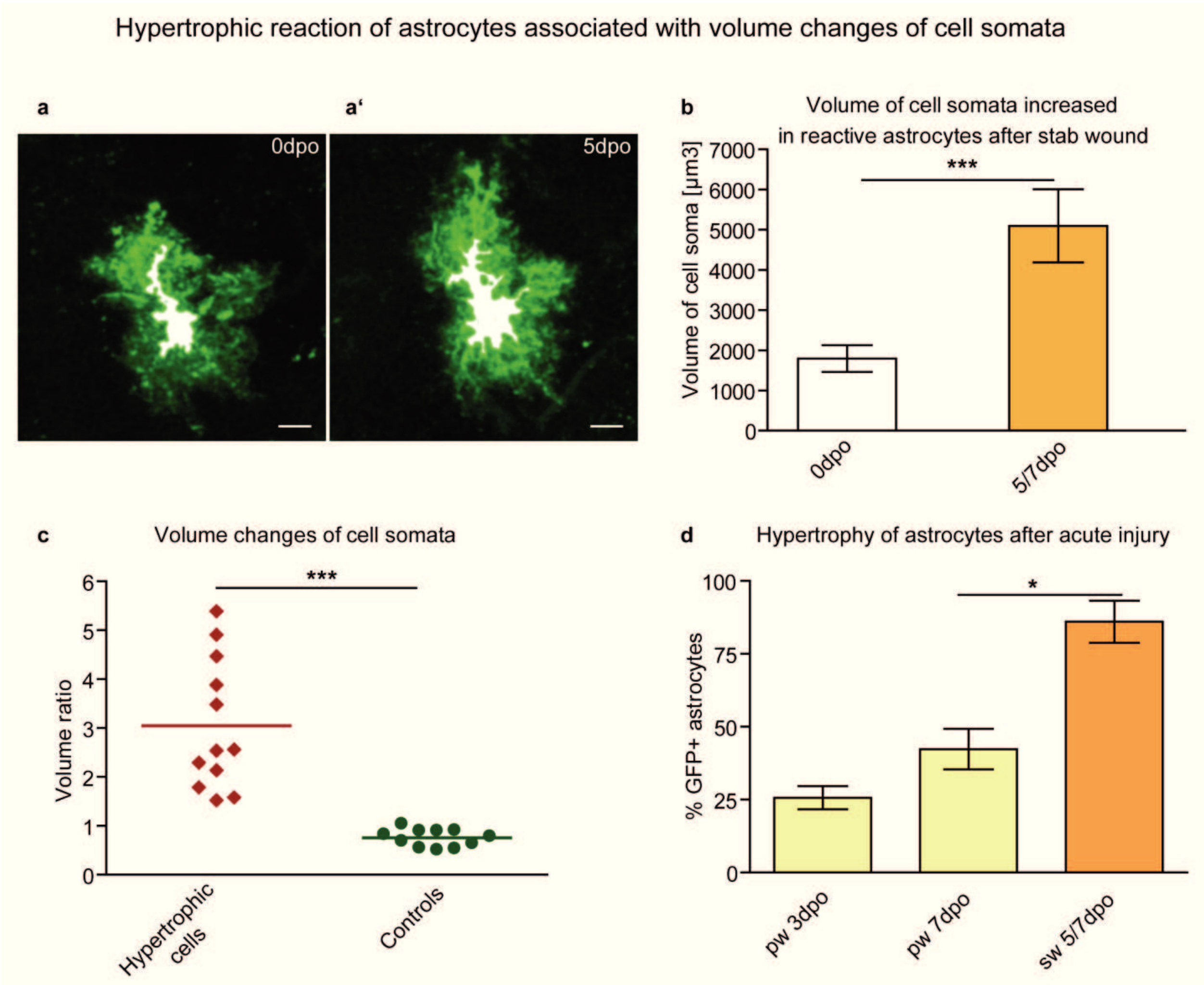

Supplementary Figure 3 Hypertrophic reaction of astrocytes is indicated by an increase in the mean volume of cell somata. (**a, a'**) Live images (z-stack projection of 40 µm depth) of the same GFP+ astrocyte (green channel, z-projection) acquired on the day of the operation (0dpo; **a**) and 5 days later (5 dpo; **a'**) reveal that the cell becomes hypertrophic after stab wounding, as indicated by swelling of the cell soma (white channel) and thickening of the major processes. Cell somata were defined and their volumes quantified using a semi-automatic approach (see Methods). (**b**) The volumes of the same cell somata were measured at 0dpo and 5 or 7dpo (n=12 cells in 3 animals; mean ± SEM; paired t-test; ***p=0.0005). (**c**) Volume ratios of cells from animals with stab wounds (n=12 cells from 3 animals), measured at the indicated time points, were significantly higher than those determined for a control population of astrocytes from animals that had been subjected to a punctate wound (n=11 cells from 4 animals), with volumes of the latter remaining essentially unchanged (unpaired t-test, ***p=0.0001). (**d**) The majority of GFP+ astrocytes within a 300-µm radius of a large stab wound (sw) were classified as hypertrophic (86 %, 5/7 dpo), while only 26 % (3 dpo) to 42 % (7 dpo) of such cells become hypertrophic after a punctate wound (pw; >100 cells, n=3 animals, mean±SEM, unpaired t-test, *p=0.012). Scale bar: 20 µm (**a**, **a'**)

Nature Neuroscience: doi:10.1038/nn.3371

Supplementary Figure 4

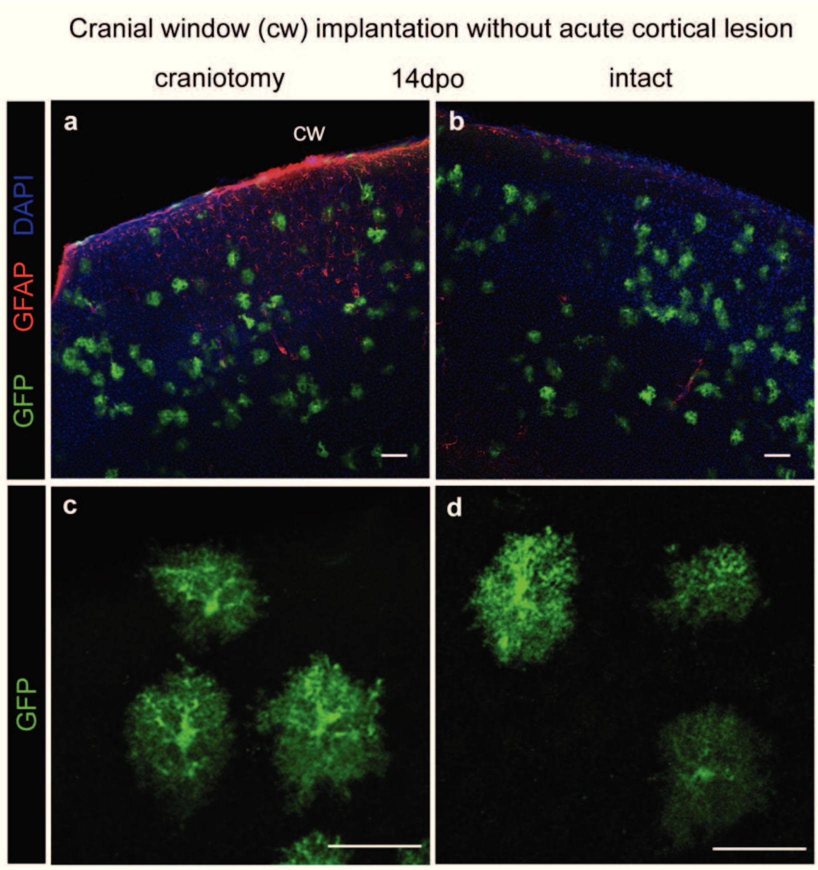

Supplementary Figure 4 Effects of insertion of a cranial window (cw) on glial reactivity in the absence of invasive injury. (**a, b**) Immunohistochemical labeling of GFAP shows that it is up-regulated only in astrocytes close to the pial surface, and not in deeper layers below the cw, in the non-lesioned somatosensory cortex of GLAST/eGFP mice 14 days after craniotomy (14 dpo) and implantation of the cw. (**c, d**) Astrocytes at all accessible depths within the cortex retained their normal round and bushy morphology, and did not polarize towards the cw. Scale bars: 100 μm (**a**, **b**), 50 μm (**c**, **d**)

Nature Neuroscience: doi:10.1038/nn.3371

Supplementary Figure 5

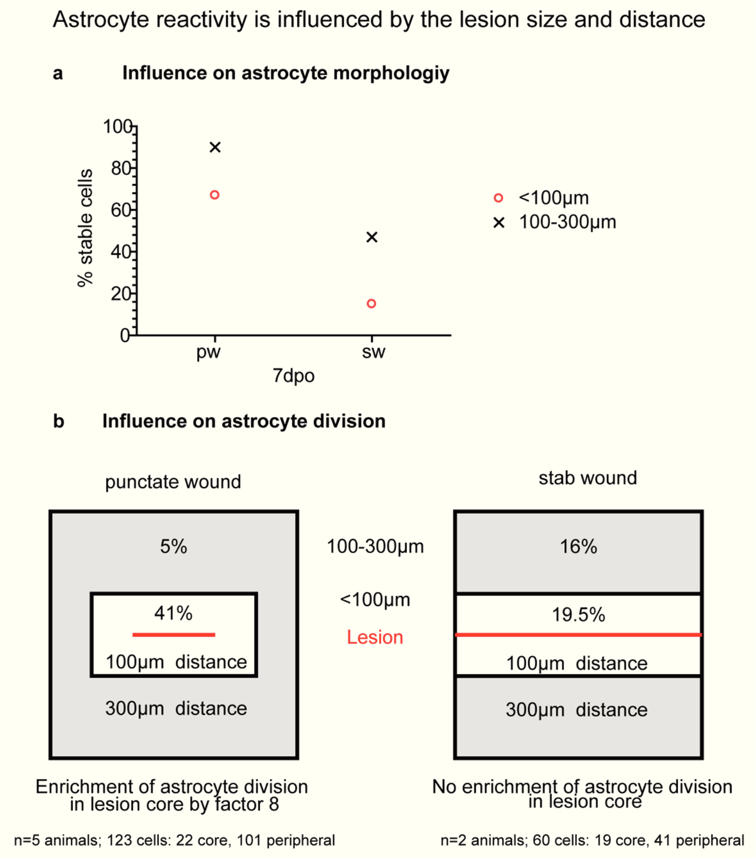

Supplementary Figure 5 The intensity of astrocyte reaction varies with the size and proximity of the lesion. (**a**) *In vivo* imaging of live astrocytes following acute lesion reveals increased reactivity of astrocytes in the vicinity to the lesion (< 100 µm away) and after more extensive (stab wound; sw) injury. (**b**) Astrocyte division was largely confined to 100 µm of a punctate wound (pw), but was found in a broader zone (up to 300 µm away) around a larger stab wound.

Nature Neuroscience: doi:10.1038/nn.3371

Supplementary Figure 6

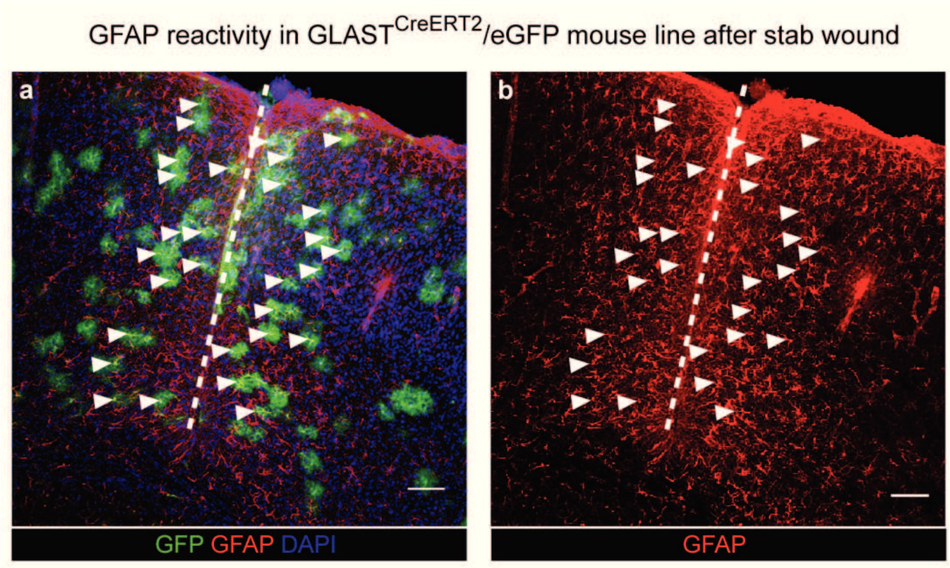

Supplementary Figure 6 GFAP reactivity in GLAST/eGFP mice after stab wounding. (**a, b**) Up-regulation of GFAP (red channel) after stab wounding (dashed line) in recombined, GFP+ (**a**; green channel) astrocytes (colocalization is indicated by white arrowheads) in GLAST/eGFP mice. GFAP immunoreactivity was detected in almost all GFP+ astrocytes located within 300 µm of the stab wound at 7dpo, confirming that such an invasive injury induces typical hallmarks of astrogliosis in the majority of live imaged GFP+ cells (Fig. 2) close to the injury site. Scale bar: 100 µm

Nature Neuroscience: doi:10.1038/nn.3371

Supplementary Figure 7

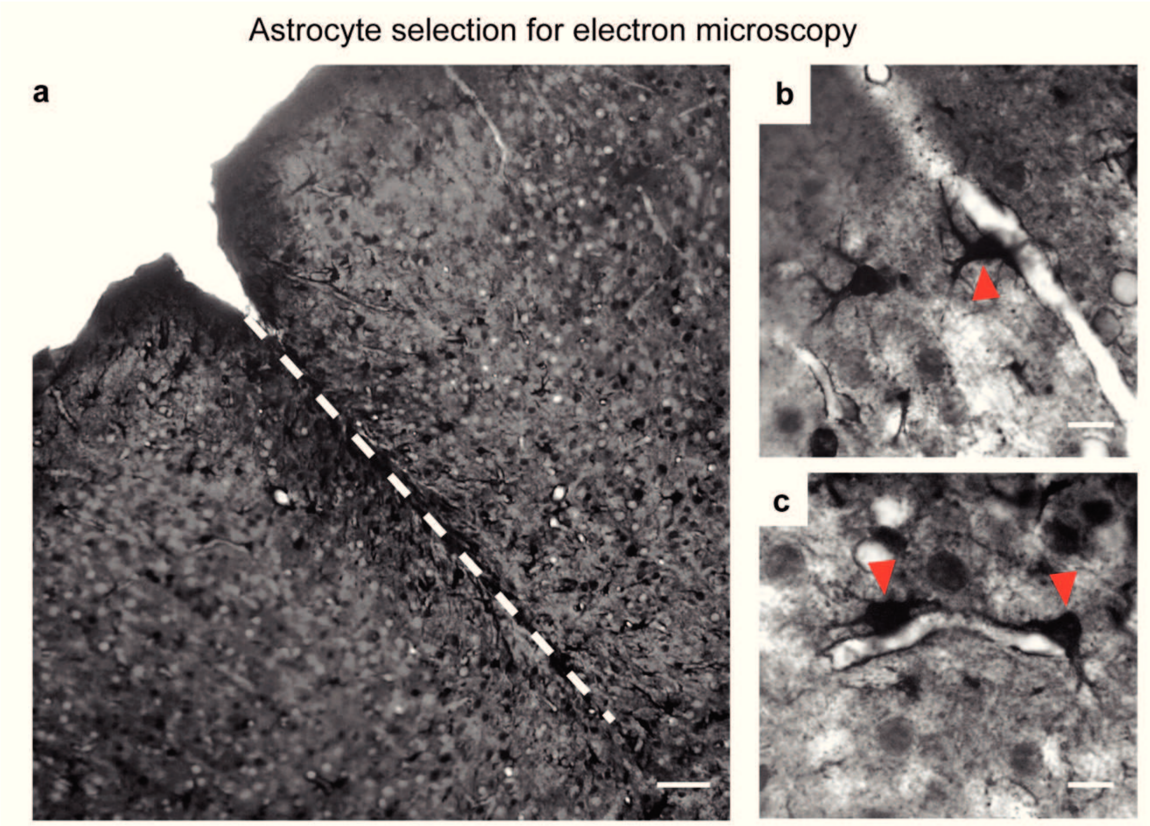

Supplementary Figure 7 Selection of candidate astrocytes for ultrastructural analysis by immunoelectron microscopy. (**a**) Labeled astrocytes in a 60 μm thick brain section of an Aldh1L1-eGFP mouse 7 days after stab wounding (dashed white line) visualized with anti-GFP/DAB reaction. (**b, c**) Candidate GFP+ astrocytes directly attached to a blood vessel (marked with red arrowheads) were selected for electron microscopic analysis. Scale bars: 100 μm (**a**), 20 μm (**b**, **c**)

Nature Neuroscience: doi:10.1038/nn.3371

Supplementary Figure 8

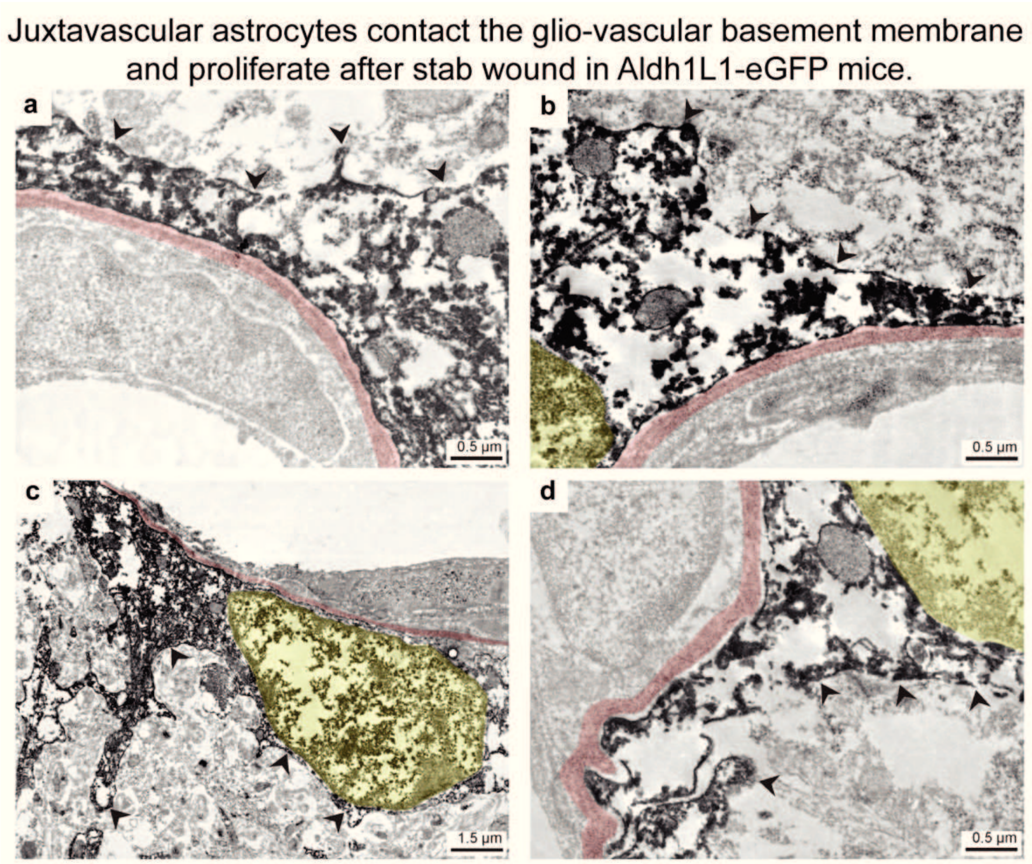

Supplementary Figure 8 Immunoelectron microscopy confirms the juxtavascular position of proliferating astrocytes after injury. (**a-d**) The electron micrographs show close-up views of proliferating (Ki67+ nuclei, color-coded in yellow) GFP+ astrocytes in stab-wounded brain sections from an Aldh1L1-eGFP mouse. The direct contact between cell somata (granular staining after antibody-DAB reaction) and the fused glio-vascular basement membrane (colored-coded in pink) of cerebral blood vessels, and the lack of an additional basement membrane on the parenchymal side of GFP+ astrocytes (marked with arrowheads), allow clear-cut determination of the juxtavascular position of proliferating astrocytes within the parenchyma.

Nature Neuroscience: doi:10.1038/nn.3371

Supplementary Figure 9

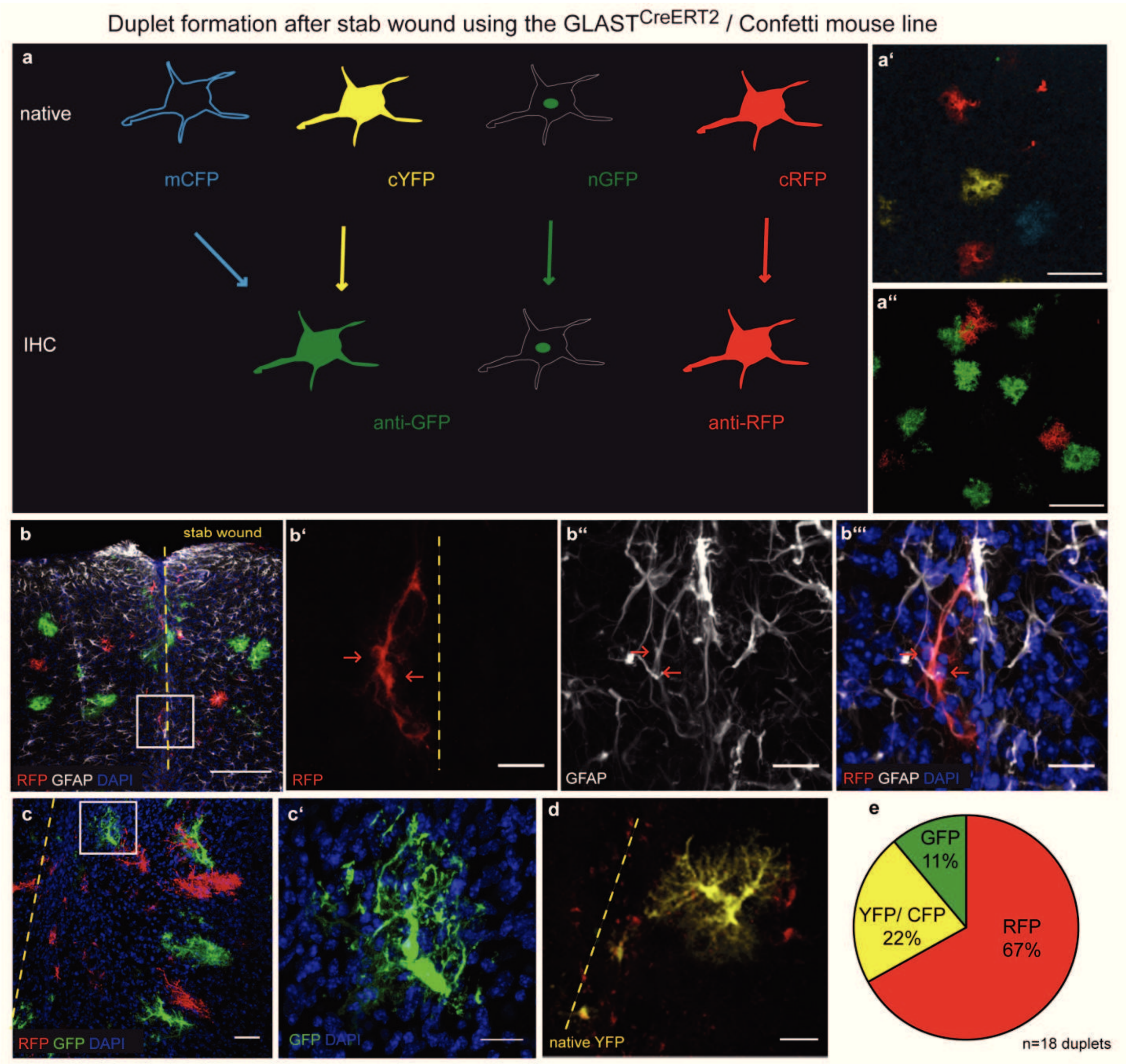

Supplementary Figure 9 The occurrence of unicolored astrocyte duplets in GLAST/Confetti mice after stab wounding indicates that they are the clonal products of cell division. (**a**) Stochastic recombination of tamoxifen-treated GLAST/Confetti mice enables one to identify clones of astrocytes expressing either membrane-bound (m) CFP, nuclear (n) GFP, or cytoplasmic (c) YFP or cRFP by fluorescence microscopy (native) and immunohistochemistry (IHC). (**a'**) Fluorescence image of mCFP-, nGFP-, cYFP- or cRFP-labeled astrocytes in a fixed brain section. (**a''**) Immunohistochemical staining with anti-GFP, labels GFP+ nuclei but also mCFP+ and cYFP+ astrocytes indiscriminately. (**b-e**) After stab wounding of mice in which recombination was induced with a low dose of tamoxifen, unicolored duplets were detected ipsilateral to the lesion at 7 dpo in all 3 color channels. (**b-b'''**) A RFP+ cell duplet, which also expresses GFAP (red arrows), near the site of the lesion (yellow dashed line) to which these cells extended elongated, polarized processes. (**c, c'**) Duplet which originated from either a YFP+ or CFP+ astrocyte, immunolabeled with anti-GFP. (**d**) YFP+ duplet close to the lesion site (yellow dashed line). (**e**) RFP+ astrocyte duplets account for the majority of the cell pairs detected (2 animals, >20 sections). Scale bars: 100 µm (**a'**, **a''**, **b**), 20 µm (**b'-d**)

Nature Neuroscience: doi:10.1038/nn.3371

Supplementary Figure 10

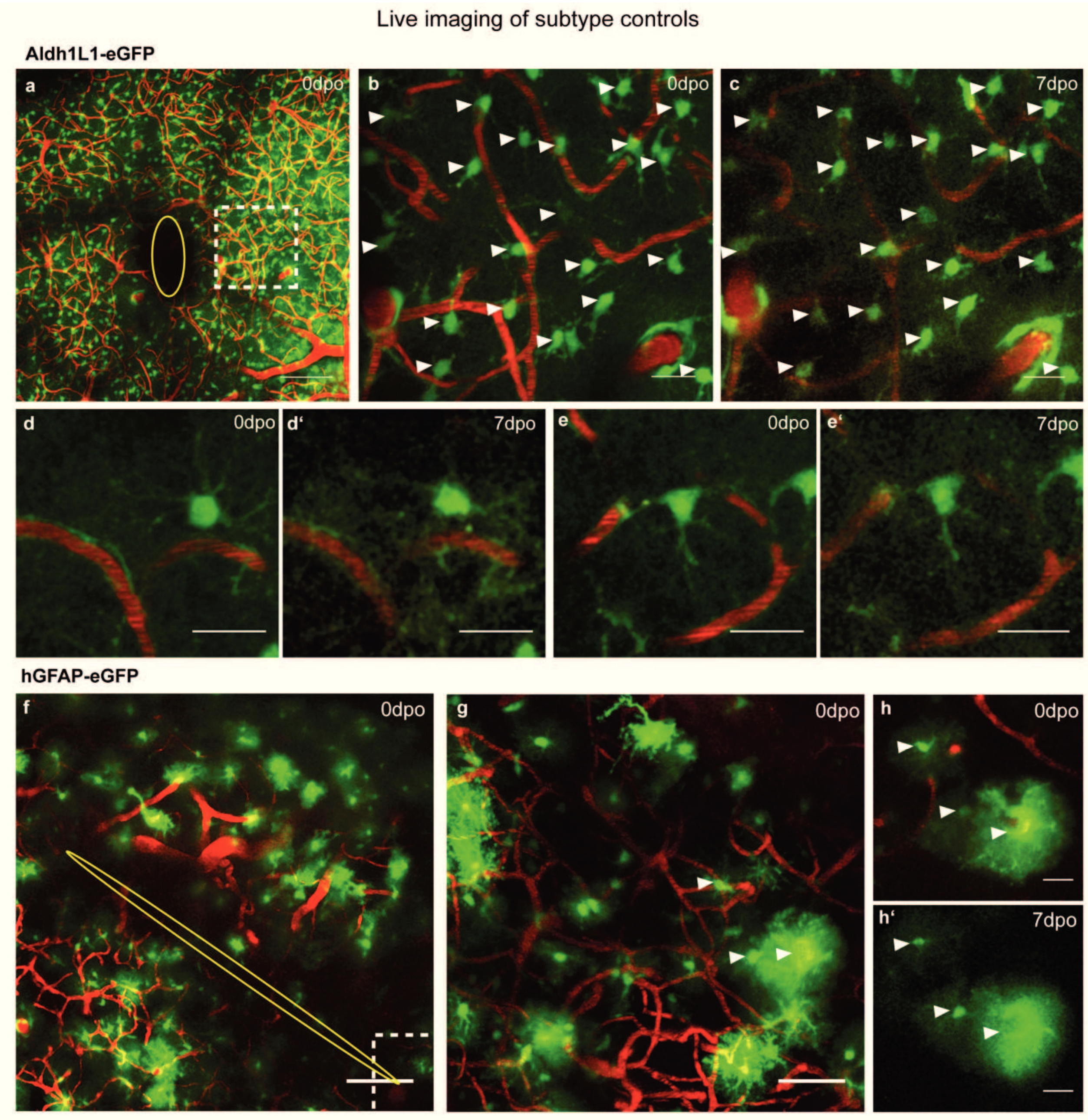

Supplementary Figure 10 Live imaging of GFP-labeled astrocytes after injury in different reporter mouse lines. (**a-e'**) In addition to GLAST/eGFP mice, Aldh1L1-eGFP mice[19,20], which allow labeling of all astrocytes (bright signal restricted to cell somata), were repeatedly imaged by *in vivo* 2pLSM to assess the behavior of GFP+ astrocytes (green channel) following infliction of a punctate wound. (**b, c**) GPF+ astrocytes retained stable positions (white arrowheads) at 0dpo and 7 days later (7dpo); (**d-e'**) Close-up of two GFP+ cells with stable position and morphology. (**f-h'**) A third line, namely hGFAP-eGFP mice[32] labeling a subset of astrocytes with highest GFAP expression, was imaged to assess responses of GFP+ astrocytes following stab wound. (**g, h**) Close-up of three cells (white arrowheads) in proximity the lesion at 0dpo, and (**h'**) in equidistant localization 7 days after injury (7dpo). Blood vessels labeled with TexasRed-dextran (red channel) served as positional landmarks and allowed for localization of the injury site marked by the yellow ellipse (**a**, **f**). Scale bars: 100µm (**a**, **f**), 50µm (**g**), 20µm (**b-e'**, **h, h'**)

Nature Neuroscience: doi:10.1038/nn.3371

SUPPLEMENTARY MOVIES

Movie 1: Live imaging of GFP+ astrocytes and TexasRed-dextran-labeled blood vessels in the cerebral cortex grey matter of a GLAST/eGFP mouse. The optical sections are 5 µm thick and total stack depth is 250 µm. Magnification: 20x zoom 2

Movie 2: Live imaging of a juxtavascular astrocyte contacting an injured blood vessel that was undergoing division upon injury on 0dpo (see Fig. 3a, b and Movie 3). The optical sections are 5 µm thick and total stack depth is 175 µm. Magnification: 20x zoom2

Movie 3: A juxtavascular astrocyte in contact to an injured blood vessel and forming a duplet, imaged 7 days after lesion (see Fig. 3c). The optical sections are 5 µm thick and total stack depth is 75 µm. Magnification: 20x zoom 2

Movie 4: Live imaging of astrocyte polarization 7 days after stab wound. The optical sections are 5 µm thick and total stack depth is 100 µm. Magnification: 20x zoom 5

Movie 5: Superimposition of 3D images after image registration reveals astrocytes that remain stationary after acute lesion. Overlay of GFP+ astrocytes (green: 0dpo; white: 7dpo) and blood vessels (red: 0dpo; blue: 7dpo) after image registration (see Suppl. Fig. 2 and Methods). The optical sections are 5 µm thick and total stack depth is 150 µm. Magnification: 20x zoom 2

Movie 6: Live imaging of GFP+ astrocytes and TexasRed-dextran-labeled blood vessels in the cerebral cortex grey matter of an Aldh1L1-eGFP mouse after stab wound (0dpo). The optical sections are 5 µm thick and total stack depth is 450 µm. Magnification: 20x

Nature Neuroscience: doi:10.1038/nn.3371

4 Discussion

4.1 Heterogeneity of reactive astrocytes after acute injury *in vivo*

This is the first long-term live imaging study tracing the behavior of GFP+ astrocytes in response to stab wound injury *in vivo* addressing morphological changes like polarization (elongated processes towards the lesion), division (newly formed cell duplets), hypertrophy (swelling of the cell soma), but also observing cells with unchanged morphology during the first week after injury. Depending on the injury size (small punctate wound or larger stab wound), hypertrophic swelling of cell somata (43% punctate wound vs. 86% stab wound) and lesion-directed polarization of astrocytes (10% punctate wound vs. 53% stab wound) was significantly higher in the larger lesion paradigm [264]. Notably, overall the proportion of proliferating astrocytes (14-16%) within 300µm distance to a punctate wound or stab wound was similar, whereas the spatial distribution of astrocyte duplets differed. In contrast to a small punctate wound, dividing astrocytes were not restricted to 100µm around the lesion core, but found more widespread (>300µm) after a larger stab wound. The influence of the lesion distance on astrocyte proliferation confirms what had been described by Barreto et al. after ischemia in Aldh1L1-eGFP mice, showing a small number of proliferating astrocytes (11% BrdU+ at day 7) that were preferentially located within 100µm distance to the lesion core [120].

As live imaging revealed some astrocytes that neither divided nor polarized, hypertrophy – a common hallmark of reactive astrocytes even in moderate lesion paradigms [139] – was assessed based on the swelling of astrocyte somata and main cellular processes [28]. Considering that GFAP labeling might underrepresent the astrocyte volume, dye-filling of single cells in fixed tissue labeling the cell membrane [28,265] and *in vivo* live imaging of endogenous GFP signals labeling the entire astrocyte (e.g. in GLAST^{CreERT2}/ CAG-eGFP mice) allow reliable analysis of cellular hypertrophy. Taking advantage of live imaging, hypertrophic changes of individual GFP+ astrocytes were traced and quantified as volume ratios of astrocytic somata (without their ramified processes). Within 7 days after stab wound the cell somata of hypertrophic astrocytes (86% of all GFP+ cells) were in average three times enlarged. Hypertrophic swelling after acute injury had been also live imaged in GFAP-eGFP transgenic mice or SR101 labeled astrocytes by others reporting recently transient swelling as early response after cortical contusion associated with edema and hypoperfusion in peri-concussive areas [266], or even persistent astrocyte swelling induced by spreading depolarization after ischemia [267]. However, even under physiological conditions astrocyte swelling could be linked to altering ion concentrations [268], or it might even imply phagocytic activity [33].

While mechanisms underlying astrocyte swelling have been described [269-272], the function of persistent hypertrophy observed by imaging even 7 days after stab wound remains poorly understood. However, astrocyte hypertrophy was linked to intermediate filament expression e.g. in GFAP-/-Vim-/- knock-out mice[153]. Furthermore, the correlation of hypertrophy after stab wound (live imaging) and GFAP up-regulation (immunohistochemical analysis) was assessed in this study. Based on data presented herein, the percentage of hypertrophic astrocytes (86%) overlaps with GFAP-labeling in the vast majority of GFP+ astrocytes in GLAST^{CreERT2}/ CAG-eGFP mice 7 days after stab wound (93.5% GFAP+/GFP+) [220]. Notably, after small punctuate wound almost all astrocytes up-regulated GFAP (89% GFAP+/ GFP+ in Aldh1L1-eGFP), less than 50% of the GFP+ astrocyte became hypertrophic, showing that hypertrophic swelling in contrast to GFAP up-regulation was influenced by the injury size {Bardehle, 2013 #442}. Thus, GFAP up-regulation is assumed as more sensitive reaction to a minimal insult, while after large stab wound GFAP expression accompanies with hypertrophy in almost all astrocytes close to the injury.

Additionally, live imaging revealed hypertrophic astrocytes with stable domains in accordance to non-overlapping territories reported by [28]. This was different for astrocytes with polarized morphology, also referred to as 'palisading astrocytes' in response to epileptic seizures [265]. Unlike in epileptic brains [265] or cryogenic TBI [115], where palisading astrocytes were found proximal to the lesion and spatially separated from GFAP+ astrocytes, after stab wound polarized astrocytes were GFAP+ and spatially intermingled as a subpopulation of all GFAP+ astrocytes (93.5% of all GFP+ cells) [220]{Bardehle, 2013 #442}.

However, the regulation and function of astrocyte polarization after injury is so far poorly understood, and requires further investigations, e.g. ultrastructural analysis of polarized protrusions.

Currently it remains hypothetical, whether the elongate shape of some reactive astrocytes – similar to radial glial precursors – might be indicative for de-differentiation of quiescent mature astrocytes into a more plastic state, i.e. with proliferative and migratory potential. Surprisingly, the herein presented live imaging data showed that astrocyte polarization was neither associated with proliferation (only ~10% overlap), nor with migration that was not observed after stab wound (see also part 4.2) {Bardehle, 2013 #442}.

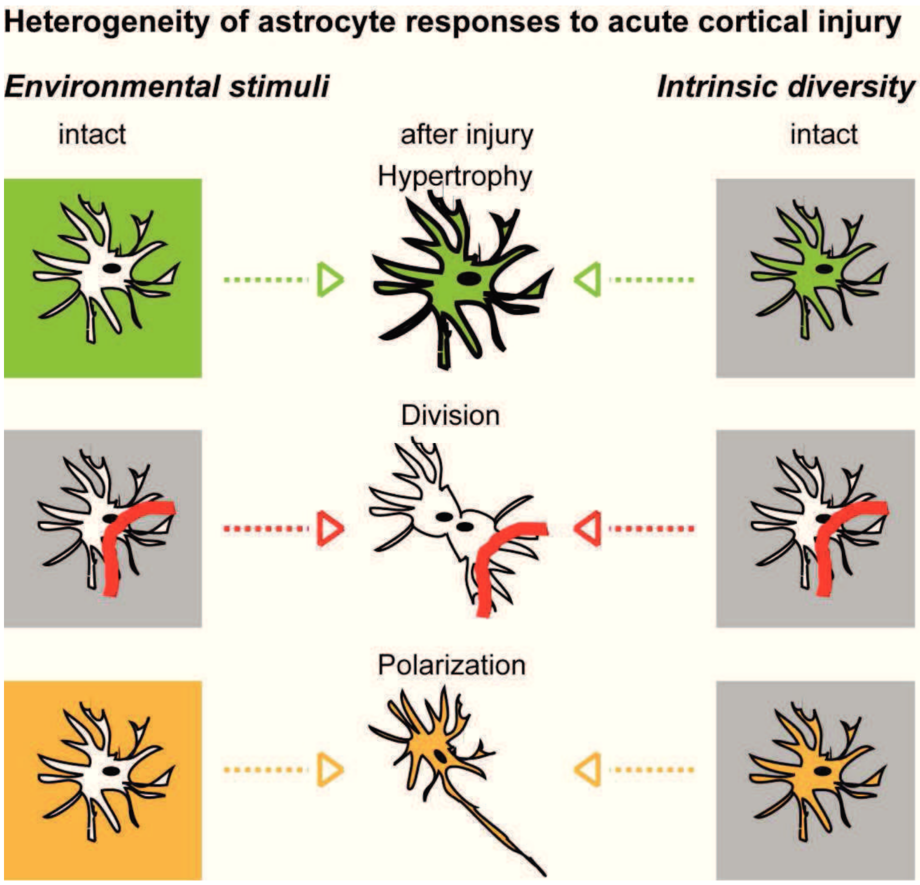

Figure 4.1 Working model for the heterogeneity of astrocyte behavior after acute cortical injury. *In vivo* live imaging revealed morphological changes of reactive astrocytes including hypertrophy, polarization and division (center column) that might be driven by different environmental stimuli (left column) or intrinsic diversity of astrocyte subsets (right column).

In summary, this *in vivo* live imaging study revealed novel insights into the heterogeneous behavior of astrocytes following acute cortical injury. Based on the presented findings, a working model (Figure 4.1) was proposed showing putative mechanisms underlying the heterogeneity of astrocyte responses: (1) intrinsic diversity of astrocyte populations and (2) the influence of extrinsic factors including cell-cell interactions. On the one hand intrinsic differences in the expression profile of reactive astrocytes have been also suggested from transcriptome data [161,162] and immunohistochemical analyses [32,115]. On the other hand environmental stimuli (e.g. lesion size, the distance to the lesion, vascular niche; part 4.3) and the interaction between different glial cells [45,274], pericytes [215], vasculature [121], blood derived factors [142,172] and the immune system [4] might influence the reaction of astrocytes and their function after injury.

4.2 Astrocyte recruitment to the injury site

The accumulation of astrocytes after injury has been previously shown *in situ* in various other studies [113,114,139]. Since there is no stably expressed antigen for labeling all astrocytes in different regions of the adult brain, alternatively the astrocyte population can be assessed *in vivo* using either a combination of astroglial markers like GLAST, GLT-1, S100ß or Aldh1L1 [33,37,55,161] for immunohistochemical analysis or fate mapping of GFP-labeled astrocytes in reporter mouse lines. Notably, GFAP immunoreactivity could lead easily to an overestimation of the increase in astrocyte numbers, due to the fact that in some brain regions, e.g. the intact cortical gray matter, most mature, quiescent astrocytes have undetectable levels of GFAP. Intermediate filaments are up-regulated in reactive astrocytes (and even other glial cells) upon injury leading to increased number of GFAP+ cells, which rather reflects changes in intrinsic expression profiles than an increase in cell numbers [116,161,275,276].
However, previous studies in our lab showed an increase in S100β+ or reporter+ astrocyte numbers of about 30-50% within one week after stab wound injury in wildtype mice or $GLAST^{CreERT2}$ driven, inducible reporter line [113,114]. Furthermore, those studies provided evidence that the increase in astrocyte number is due to astrocyte proliferation (30-50% of all BrdU+/S100β+ or BrdU+/reporter+ astrocytes) analyzed 7 days after injury.

Analysis of proliferating astrocytes in GLAST^{CreERT2}/ CAG-eGFP mice by live imaging revealed a lower number of astrocytes (14-16% of GFP+ astrocytes) that divided during the first week after injury [264]. Confirmed in fixed tissue acutely diving astrocytes labeled with Ki67 – a nuclear antigen expressed in mitotically active cells – only 14% of all astrocytes proliferated at day 7 after injury. Moreover, live imaging as well as clonal analysis in fixed tissue using GLAST^{CreERT2}/ Confetti mice revealed a limited number of astrocyte duplets restricted to two daughter cells, which remain closely together, and would account only for a moderate increase in astrocyte numbers {Bardehle, 2013 #442}. The extent of proliferation varies between different studies [113,114,264] using different labeling methods, different astrocyte markers (S100ß or inducible reporter) and eventually mouse strains of different background, the age of the animals, as well as surgical procedure inflicting a stab wound may vary individually.

Notably, these studies analyzing astrocyte proliferation used three different methods, i.e. (1) BrdU incorporation, (2) Ki67-labeling and (3) formation of astrocyte duplets followed by live imaging. BrdU is a thymidine analogue that incorporates in newly synthesized DNA strands during DNA replication (in S-phase of the cell cycle or repair). Thus, the mother cell and all progeny is BrdU+, and the label retains in further divisions (although will dilute). For tracing proliferating astrocytes after stab wound, BrdU was continuously administered (in the drinking water) from the day of injury until the day of perfusion (e.g. 7 days). Immunohistochemical analysis of BrdU+ nuclei revealed a high number of BrdU+ astrocytes (30-50%), which does not reflect the number of divisions – counted by live imaging – but includes additionally all progeny that arose within the time period analyzed (e.g. 7 days). In conclusion, both methods – BrdU-labeling and live imaging – monitor dividing cells over a period of time (e.g. day 0-7 after injury) with the difference that one cell division leads to labeling of two BrdU+ nuclei, but was counted as one event – visible as newly formed cell duplet – during live imaging. Assuming that astrocytes divide only once during the first week after injury (referred to the clonal analysis; Suppl. Figure 9 in [264]), which is in contrast to NG2+ glia [114], one would expect the double amount of BrdU+ astrocytes, compared to the number of cell divisions observed by *in vivo* live imaging. Considering these aspects, ~30% of BrdU+/reporter+ astrocytes (within 150µm distance to injury) reported earlier [113] are not contradicting to a small proportion of astrocytes that undergo a single division (~20% of GFP+ astrocytes within 100µm distance to injury, Suppl. Figure 5 in [264]) during live imaging over the same period of time (7 days after injury) and comparable distance to the stab wound. Furthermore, Ki67 labeling was used herein to quantify proliferating astrocytes at a certain time point after injury in fixed tissue. The nuclear antigen Ki67 is expressed in actively dividing cells (not expressed in G0 phase), thus labeling cells with active cell cycle at the time point of fixation (e.g. at day 7), but excluding those that divided earlier. In theory, adding up the numbers of Ki67+ astrocytes at several time points would resemble the number of live observed cell division over the same period of time, i.e. half of the number of BrdU+ cells (for a single round of division) neglecting cell death (not observed live *in vivo*). In this regard, the low number of astrocyte divisions visible by live imaging might be justified due to the fact that cell division was assessed based on morphological changes – a single GFP+ astrocyte (day 0) forming a cell duplet (observed earliest at day 5), which occurs during late mitotic phase (cytokinesis). In contrast, BrdU and Ki67 labels dividing cells in earlier cell cycle phases (S-phase), and Ki67 can be also up-regulated during S-phase without completing cytokinesis (seen as multi-nucleated cells), suggesting an overrepresentation of astrocyte proliferation in fixed tissue.

In conclusion, live imaging of astrocytes *in vivo* after TBI provides additional new insight into the time course of astrocyte proliferation (delayed, slow, single division), factors influencing astrocyte proliferation(e.g. vascular niche; see part 4.3) and fate mapping of the progeny (duplets remain closely together).

However, proliferation might not be the only mechanism recruiting astrocytes to the lesion site. As reactive astrocytes migrate *in vitro* [146,163,277,278], their migration from distant areas was also assumed after acute CNS lesion *in vivo* based on the polarized morphology of reactive astrocytes with lesion-directed orientation in fixed brain sections [141,155,200,220]. Therefore, live imaging was applied to study astrocyte migration *in vivo* after acute cortical injury in adult Glast^{CreERT2}/ CAG-eGFP reporter mice. But in contrast to the motility of astrocyte processes at synaptic terminals in acute brain slices [279], movement of astrocyte somata as reaction to acute cortical injury was not observed by 2pLSM in the here presented study. Thus, *in vivo* the correlation of astrocyte polarization and lesion-directed migration, that was reported by previous studies, not only for astrocytes *in vitro* [94,146], but also for transplanted astrocytes *in vivo* [280], was not verified by live imaging after cortical TBI in adult mice, rather suggesting migration-independent polarization of reactive cortical astrocytes with so far unknown functions.

Strikingly, the static position of reactive astrocytes – remaining for days and even weeks after injury – was in stark contrast to live imaging showing the motility of other glial cell types, such as microglia [108,224] or NG2+ cells, that have motile filopodia and migrate as early response to cortical injury [281] (von Streitberg, Straube, Dimou, unpublished data). Thus, technical concerns of the imaging procedure *per se*, e.g. laser induced artifacts, anesthesia, edema-related structural changes, which might impede motility could be ruled out.

Furthermore, the mouse model used for this live imaging study is taken into closer consideration. In GLAST^{CreERT2}/ CAG-eGFP mice recombination is driven by the GLAST promoter activity, which targets a specific astrocyte subpopulation, as not all astrocytes express the same levels of glutamate transporters, e.g. GLAST or GLT-1 [54]. In order to rule out, that recombined GFP+ astrocytes may react differently from other (non-labeled) astrocytes, control experiments were performed using other mouse lines: (1) Aldh1L1-eGFP mice with eGFP expression in all cortical astrocytes, and (2) hGFAP-eGFP mice labeling a subset of reactive astrocytes (see Table 1-2). Live imaging of GFP+ astrocytes in those mouse lines revealed similar behavior with low proliferation and stationary localization of GFP+ astrocytes after injury, proposing that the conclusion drawn from GFP+ astrocytes in GLAST^{CreERT2}/ CAG-eGFP mice are representative for the entire population of cortical astrocytes without neglecting a putative migratory subset of astrocyte amongst non-labeled cells.

In addition to recently published studies describing the local generation of astrocytes during development, their persistence within their developmental region [19] as well as a region-restricted astrocyte allocation after CNS injury [235] these finding suggest that astrocyte migration *in vivo* is restricted to postnatal development [19,282,283], young, transplanted cells [283-285], tumorigenic de-differentiation [286,287] or even to specific subsets in specific brain regions [280].

Taken together, the here presented data suggest only modest expansion of astrocytes in <300µm distance to acute injury by limited self-duplication (see below, part 4.3), but not by migration of reactive astrocytes.

Although fate mapping by live imaging of GFP+ astrocytes confirmed that astrocyte duplets originate from quiescent protoplasmic astrocytes, another source of cells – that would not be fluorescently labeled – giving rise to astroglia cannot be excluded. Crucially, even alternative mechanisms for astrocyte recruitment such as the trans-differentiation of glial precursor cells into astrocytes [288-290] or another origin of new glial cells as reported after spinal cord injury [291,292] are controversially debated [293].

4.3 Astrocyte proliferation in juxtavascular position

While the vascular system serves as an important scaffold for the migration of neuronal precursors in the developing and adult brain [294-296], it also promotes their proliferation in neurogenic niches [297,298]. However, the influence of a vascular niche on astrocyte proliferation after injury has not yet been described.

Volumetric analysis of the cerebrovascular system revealed 6-10µm as the mean distance of an astrocyte to the nearest blood vessels [98]. In comparison to the random spatial distribution of cells in the brain [299,300], astrocytes have been suggested to be in closer contact with the vasculature. Strikingly, some astrocyte somata were discovered to be even in direct contact with a blood vessel – at driving arteries, ascending veins or attached to capillaries – and those were referred as 'perivascular astrocytes' in the cortex [98], and also described earlier in the retina [301]. Noteworthy, while all astrocytes are supposed to contact the cerebral vasculature with astroglial endfeet (also see part 1.2.1) [2,27] , only a minor subset of all protoplasmic astrocytes in the postnatal and adult cortical gray matter (~30%) was found in this study with the cell soma directly apposed to a blood vessel. Moreover, the here presented live imaging study showed the formation of astrocyte duplets in direct contact with a blood vessel, indicating astrocyte proliferation in a specific vascular niche. Quantifications of proliferating astrocytes labeled with Ki67, in combination with an endothelial marker CD31 labeling all blood vessels in fixed tissue verified that the majority of proliferating astrocytes had direct cell soma-blood vessel contact. Ultrastructurally, the position of astrocyte somata at cerebral blood vessels was clearly defined as juxtavascular, rather than perivascular (in a perivascular Virchow-Robin space). By definition a cell is 'juxtavascular' when it is separated from the endothelial layer by a fused glio-vascular basement membrane, but not by an additional basement membrane from the brain parenchyma (see scheme Figure 1.4 C) [88]. Thus, previously termed ‘perivascular astrocytes’ [12,27,98] revealed anatomically proper juxtavascular position, and therefore are referred herein as ‘juxtavascular astrocytes’.

These novel findings of a juxtavascular proliferating astrocyte subset give rise to prospective studies on specific mechanisms and their functions after injury.

First, juxtavascular and non-juxtavascular astrocytes could be intrinsically diverse subpopulations (Figure 4.1), and/ or re-entry into the cell cycle could be promoted by different signaling cues in specific niches (see part 1.2.1). For further characterization, juxtavascular astrocytes could be isolated and subsequently screened for selective markers. In particular, since this small proportion of reactive astrocytes with proliferative capacity were recently shown to acquire stem cell potential including multipotency *in vitro* [32,172].

Second, juxtavascular proliferation of astrocytes might be specific for this type of TBI causing mechanical destruction of blood vessels. Thus, further investigations will also focus on other CNS pathologies (e.g. stroke, epilepsy) regarding the presence of proliferative astrocytes in juxtavascular positions. Preliminarily, also in ischemic brains the majority of proliferating astrocytes in the penumbra (zone with GFAP+ reactive astrocytes) bordering the ischemic core was found in direct contact with blood vessels (Frik, Bardehle, Götz unpublished data). Thus, juxtavascular proliferation of astrocytes seemingly appears not specifically after stab wound injury, but might be more generally associated with acute CNS injuries and disruption of the vasculature.

In conclusion, juxtavascular proliferating subset of astrocytes, that remain closely associated with their progeny, may be related to a specific role of juxtavascular astrocytes at the vascular-parenchymal interface, as reactive astrocyte have been suggested to be involved in restricting the infiltration of leukocytes after acute injury with leakage of the BBB [86,112] and vascular remodeling [116,165].

4.4 Revised concept of reactive astrogliosis and scar formation

This first *in vivo* imaging study of astrocyte responses to acute cortical injury in living mice provides novel insights into the heterogeneity of reactive astrocytes, and broadened our current understanding of astrogliosis involved in glial scar formation and regeneration potential [138,139,141,143,302]. The role of scar-forming astrocytes has been described as “two-edged sword” including beneficial and detrimental effects upon CNS injury [145,159,278,302,303]. While on the one hand secretion of ECM components (e.g. CSPGs) prevents axonal regeneration [304,305], on the other hand the control of leukocyte trafficking to restrict inflammation has neuroprotective functions [144,155,158,302,306]. However, the inter- and intracellular mechanisms through which reactive astrocytes communicate with other glial cells [281] and even non-glial cells such as pericytes [215,307], perivascular stromal cells [308] and monocytes [309] during scar formation, wound healing and regeneration remain poorly understood in the brain.

Here, live imaging was focused on morphological changes of a GFP+ subset of astrocytes after cortical injury, representative for most protoplasmic astrocytes in the cortical GM, and points out the following key findings: All astrocytes remained a stable position, but the local response was heterogeneous with a proliferative subset of astrocytes in juxtavascular position, a polarizing subset and a solely hypertrophic subset of astrocytes.

Most interestingly, these new imaging data disprove astrocyte migration after acute cortical injury, and revealed only a minor subset of proliferating astrocytes. Revising the current concept of glial scar formation {Silver, 2004 #96;Sofroniew, 2009 #98}, the assumptions of the here presented study do not verify a major contribution of astrocytes during scarring, but rather suggest different reactive astrocyte subsets with multifaceted functions. Especially, proliferative astrocytes with stem cell potential *in vitro* [172] might refer to a more plastic subset of astrocytes in juxtavascular positions.

While *in vivo* live 2pLSM is a well suited approach for visualizing cellular interactions and their contribution to scar formation {Davalos, 2012 #303;Hughes, 2013 #458;Nimmerjahn, 2005 #5;Steffens, 2012 #339}, intriguing new questions arose from those findings described here.

Which role does the large proportion of reactive astrocytes play that up-regulate GFAP and/ or become hypertrophic, but do not divide? Which niche factors or intrinsic signals guide the different astrocyte responses?

4.5 Influence of Cdc42 on astrocyte responses to injury *in vitro* and *in vivo*

The intrinsic role of the polarity protein and cell cycle regulator Cdc42 (see part 1.4) was investigated in regard to its function on astrocyte polarity, migration and proliferation following injury by conditional deletion in primary astrocyte cultures (part 3.1) [220] as well as in protoplasmic astrocytes of the adult mouse cortex (part 3.1) [220] and (part 3.2) [264].
The astrocyte behavior after *in vitro* scratch wound was monitored by time-lapse video microscopy. Under control conditions, astrocytes formed unipolar protrusions perpendicular to the scratch, migrated towards the leading edge of elongated protrusions and thereby filled the scratch wound within 5 days [220]. In contrast, *cc42-/-* astrocytes showed defects in MTOC re-orientation (see also part 1.3.1) associated with random, multi-directional protrusion formation and disoriented migration. Thus, perturbation of astrocyte polarity by loss of Cdc42 verified a crucial, cell-autonomous regulation of directional migration by Cdc42 *in vitro* as shown before [199], whereas its function seems compensable for the motility of other cell types [197]. Since Cdc42 regulates polarity cues that are important during migration and also mitosis [201,310], the proliferation rate of *cdc42*-deficient astrocytes was assessed live *in vitro* using video time-lapse microscopy.
Fate mapping of *cdc42-/-* astrocytes showed reduced proliferation after scratch wound (additional data in Figure 4.2), suggesting a mitotic defect that could be mechanistically related to an impaired G1/S phase transition and altered activity of JNK/ MAPK pathway as studied earlier in fibroblasts [310].

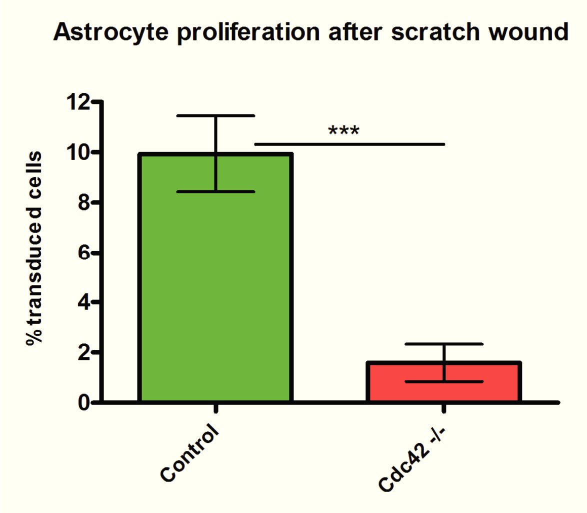

Figure 4.2 Proliferation defect of cdc42-/- astrocyte after scratch wound *in vitro.* Control (transduced with lentivirus (LV) LV-CMV-tdTomato) and cdc42-/- (transduced with LV-CMV-tdTomato-IRES-Cre) astrocyte cultures prepared from postnatal cdc42^{floxed} mice were monitored by time-lapse video microscopy for 5 days after scratch wound (as described by Robel, Bardehle et al. [220]). Astrocyte proliferation was assessed live, and significantly impaired in cdc42-/- astrocytes. Data shown as mean+/-SEM; n=13 wells from 3 independent experiments; student's t-test with ***p<0.001.

Like *in vitro*, the deletion of *cdc42* in astrocytes led to reduced astrocyte proliferation after stab wound [264] . Even though astrocytes did not migrate after acute cortical injury *in vivo* live imaging revealed an attenuated, heterogeneous response of cdc42-/- astrocytes shifted towards an increased proportion of cells with stable protoplasmic morphology, but less cells proliferated or polarized within 7 days after stab wound. To exclude that the impaired astrocyte response after loss of Cdc42 is linked to a delayed reaction of *cdc42-/-* astrocytes later time points after injury should also be considered. However, while the proliferation defect after conditional deletion of *cdc42* was confirmed in fixed sections [264], fate mapping of individual *cdc42-/-* GFP+ astrocytes and fixed analysis revealed contradictory effects on astrocyte polarization after stab wound [220]. Unlike to enhanced polarization in fixed, immunolabeled sections of the same mouse line, *cdc42-/-* astrocytes showed polarization defects with less unipolar cells oriented perpendicular to the injury by live imaging *in vitro* and *in vivo*. A reason for this discrepancy might be the different induction protocols (i.e. tamoxifen dose) for live imaging (low-dose) and histological analysis (high dose). High-dose induction results in high density of GFP+ astrocyte processes, therefore might lead to overestimation of polarization due to difficult separation of intermingled GFP+ protrusions from neighboring cells. Contrary, live imaging required a low induction protocol targeting only a small subset of astrocytes – supposedly with highest GLAST-promoter activity. Thus, GFP+ protrusions and their polarization could be theoretically underrepresented by detecting the live GFP signal using *in vivo* 2pLSM.

Importantly, the here presented data [220,264] provide evidence that (1) Cdc42 is not essential to induce protrusion formation *per se,* and (2) *in vivo* astrocyte polarity is regulated in a migration independent manner, unlike *in vitro* [220] and reported by others [200,280]. To which extent centrosome dynamics in reactive astrocytes is affected by *cdc42* deletion *in vivo*, can be so far only assumed from *in vitro* data [146,182,220], although compensatory signaling could explain reduced effects *in vivo.*

However, disruption of Cdc42 signaling interferes with astrocyte behavior supposedly by uncoupling upstream signals, e.g. integrin-mediated ECM contacts [94,311,312] and downstream targets, e.g. Par6/aPKC [184]. Thereby, the control of cytoskeletal stability, centrosome (MTOC) and Golgi orientation, which is important for cell migration [188,198,199], and polarity during mitosis [201,310] was impaired after loss of Cdc42.

Indeed, this study corroborated the role of Cdc42 in proliferation of reactive astrocytes after injury in the adult brain {Bardehle, 2013 #442}, and their recruitment to the lesion site [220]. Notably, although cdc42-/- astrocytes rarely proliferated after stab wound injury, few proliferative astrocytes were found preferentially in juxtavascular position (see also part 4.3). Supporting that even when proliferation is impaired, the proliferative capacity is restricted to a small subset of the juxtavascular astrocytes, and not adopted by other cells outside this niche.

Furthermore, this study provides evidence that cell-intrinsic regulation of polarity involving Cdc42 are essential for proper re-organization of subcellular compartments and filaments that underlie morphological changes and the behavior of reactive astrocytes. However, the attenuation of morphological changes, i.e. polarization and proliferation, observed live *in vivo* did not correlate with lower number of cells up-regulating GFAP (96% cdc42-/- vs. 94% of GFP+ cells; 7dpi) [220]. These findings suggest that astrogliosis is not generally affected by deletion of *cdc42*, but rather selective subsets and functional aspects.

Besides the cell-autonomous effects, a recent study showed impaired neuronal regeneration after spinal cord injury when Cdc42 was systemically blocked using a pharmacological inhibitor {Seo, 2013 #427}. Strikingly, even conditional deletion of *cdc42* in astrocytes led to increased number of Iba1+ microglia in close proximity to a stab wound [220], indicating that reduced astrocyte proliferation was accompanied by enhanced local inflammatory reaction mediated by activation of residing microglia (CD11b+, Iba1+, Cx3CR1+) and blood-derived macrophages (CD45+, CCR2+) [313-315]. Thus, a conditional, astrocyte-specific *cdc42* knock-out with impaired astrocytes proliferation serves as a useful model to further investigate the crosstalk of proliferating juxtavascular astrocytes with the immune system.

Moreover, these data suggest a regulatory role of Cdc42 in astrocyte polarity, proliferation (and migration) through different external stimuli (e.g. TGFβ, MMPs, cytokines), upstream signals (e.g. integrins, dystrophin) and downstream targets such as aPKC, PAR proteins and the JNK/MAPK pathway [95,182,196,199,311,316]. This would also explain why the effect of *cdc42* deletion in astrocytes *in vitro* – lacking crucial signaling components, cell-cell interactions, structural cell-ECM contacts and secreted factors – was more pronounced compared to the *in vivo* situation with putative activity of compensatory signaling cascades.

4.6 Comparison of astrocyte responses to injury *in vitro* and *in vivo*

The behavior of astrocytes after injury and factors involved in the recruitment of astrocytes at the lesion site were investigated in this study using two models: (1) scratch wound assay *in vitro* and (2) stab wound injury *in vivo*. While isolated astrocytes in primary cultures were suitable to study cell-autonomous properties, their response to injury – especially their migratory behavior – was found to be different *in vivo*. Although astrocytes *in vitro* and also *in vivo* may have proliferative capacity and elongate cellular processes towards the lesion site, subsequent lesion-directed migration was only observed by live imaging of scratch-wounded astrocyte cultures {Robel, 2011 #14}. Unlike *in vitro*, polarization was not associated with movement of cell somata in the direction of a stab wound *in vivo* [264]. Both mechanisms – cell division and migration – had been suggested to increase astrocyte numbers at the lesion site [113,114] based on astrocyte migration observed *in vitro* [146,163] and assumed after spinal cord injury [155,200]. However, so far migration of astrocytes towards acute cortical injury had not been shown using *in vivo* imaging. These live imaging experiments clearly corroborate heterogeneity of reactive astrocytes *in vitro*

as well as *in vivo*, unraveling different subsets of astrocytes that polarize or proliferate – with only small proportion of overlap – but do not migrate after acute cortical injury.
In comparison, limitations and benefits of both models used herein are based on differences in (1) cell differentiation, (2) cell morphology, (3) cellular contacts and signaling in distinct (3) lesion models *in vitro* and *in vivo* will be discussed below.

(1) ***Differentiation:*** Astrocytes develop in the postnatal brain and expand their population by proliferation and migration [19,282,283]. When isolated from postnatal cortices of 5-7 days old mice, immature astrocytes express GFAP and proliferate even after several weeks *in vitro*. This suggests that under these culture conditions astrocytes never acquire a fully differentiated, quiescent state, as they do in the adult brain. Mature protoplasmic astrocytes in the GM of the adult mouse cerebral cortex have – in contrast to some other brain regions – immunohistochemically undetectable levels of GFAP (see part 1.1). Unlike *in vivo*, astrocytes in culture divide repeatedly with an increased proliferation rate after scratch wound (~10%; peak at day 2-3). While in the healthy adult brain astrocytes are postmitotic and only a limited subset can re-enter the cell cycle after stab wound injury (~15%, peak at day 5-7) giving rise to two daughter cells that remain in close vicinity. Depending on the severity of the lesion, the time point, the labeling methods and mouse strain used, the proliferation rate of astrocytes can vary (discussed in part 4.2.) [113,114,264].

    Moreover, gene expression profiling identified profound differences between cultured astrocytes and astrocytes from different developmental stages *in vivo* [33]. These differences might imply higher reactivity and plasticity of *in vitro* differentiated astrocytes after scratch wound. Nevertheless, this *in vitro* assay is well-suited to study cell-autonomous mechanisms guiding reactive astrocyte behavior e.g. by loss-of-function experiments using pharmacological inhibitors or genetic deletion of signaling factors (see part 4.5) {Cau, 2005 #444;Etienne-Manneville, 2006 #13;Holtje, 2005 #4;Robel, 2011 #14}.

(2) *Morphology:* The morphological maturation of astrocytes including the organization of spatially separate domains and the branching of processes occurs within the first postnatal weeks in mice [18]. Postnatally isolated astrocytes growing in a monolayer with flat, amoeboid morphology (e.g. Figure 3 in [220]) can form cell-cell contacts, e.g. connexin-mediated gap junctions [44,317] and cadherin-mediated adherens junctions [318]. *In vivo*, protoplasmic astrocytes in the cortical GM have a bushy morphology with fine ramified processes (see Figure 1.2)[2,16,319] and establish a complex structural and functional network of cell-cell contacts to either other glial cells, e.g. NG2+ glia [45], or synapses and the vasculature [14]. Considering the complex cell architecture and connectivity of astrocytes (see part 1.2), active cell movement would require a disruption of cell-cell contacts and vascular endfeets, the retraction of cellular processes and re-integration at a new location. These aspects might explain why astrocytes do not migrate *in vivo* – in contrast to cultured postnatal astrocytes. On the contrary, other glial cells with ramified morphology – NG2+ glia – show motility of processes and even migrate after acute cortical injury [281], suggesting different signaling cues that influence glial motility and chemotactic attraction to the lesion site, as shown for microglia reaction [108,224].

(3) *Cell-cell contacts and signaling:* The reaction of astrocytes in a monoculture (~90% purity) is primarily driven through autocrine signaling, which can be influenced by mechanical, pharmacological or genetic manipulation. The lack of crucial cell-cell interactions, e.g. with other glial cell types, neurons and vascular endothelial cells, and certain paracrine signaling factors might explain differences in the reaction of astrocytes *in vitro* and *in vivo.* After injury, astrocytes in the brain parenchyma are exposed to inflammatory mediators released by activated microglia and infiltrating macrophages (e.g. TNFα, INFγ, leukotrienes, interleukins), secreted factors from endothelial cells (e.g. VEGF, endothelin 1, nitric oxide), accumulation of reactive oxygen species, ATP, glutamate and ions released from apoptotic neurons as well as circulating blood factors such as fibrinogen that influence astrocyte response to injury [32,139,141,142,162,320]. Furthermore, neurovascular coupling implies cell-matrix interactions (i.e. laminin-

integrin/dystroglycan) with essential roles for BBB integrity [321,322] and related to astrogliosis [94,96]. Injury-induced secretion of ECM proteins (e.g. CSPGs, tenascins, neurocan) and enzymatic activity of matrix metalloproteinases (MMPs) affect neuronal regeneration [111,138,145,309,322] and inflammation [108], but to which extent ECM/BM/BBB dynamics influence, or even prohibit, astrocyte migration in the brain remains speculative.

(4) *Lesion model*: Mechanical injury was performed *in vitro* as scratch wound and *in vivo* as stab wound to mimic an acute brain injury (part 1.3.3). Scratching a confluent astrocyte monolayer causes a cell-free cleft sensed by adjacent cells as loss of contact inhibition. Contact inhibition is a mechanism for controlling cell growth and division in cell-density dependent manner *in vitro* [323] and after brain injury [324]. Moreover, contact inhibition was suggested to regulate locomotion of cells through transmembrane proteins (cadherin, ephrin, delta) and the activation of Notch pathway and RhoGTPase signaling during health and disease [325]. *In vitro* scratch-induced migration of astrocytes is a sequential processes of (1) elongation of lesion-directed protrusions, (2) translocation of nucleus and cell soma towards the leading edge that (3) leads to wound closure (e.g. Movie 1 in [220]). In contrast, a cortical stab wound did not induce migration of reactive astrocytes – even though they polarized. This might be related to the fact, that mechanical tissue damage associated with neuronal loss [220] is followed by edema formation and infiltration of blood-derived cells [158,266,326]. Apart from rapid astrocytic swelling after acute TBI [270], live imaging revealed delayed astrocyte polarization and proliferation (3-7 days after stab wound) in comparison to other glial cells , e.g. NG2+ cells react strongly 1-3 days after stab wound (von Streitberg, Straube, Dimou, unpublished data), indicating that signals from other activated cells – rather than loss of contact inhibition – might trigger astrocyte responses *in vivo*. This would be consistent with varying extent of astrogliosis and its heterogeneity after acute TBI, epilepsy or in neurodegenerative models [28,172,264,265]. Moreover, gene expression profiles of reactive astrocytes *in vitro* [162] and from different CNS lesions, e.g. ischemia, neuroinflammation [161] or TBI (Sirko, Götz, unpublished data), corroborated a heterogeneous outcome of

astrogliosis. Whether morphological and transcriptional diversity can be related to different astrocyte subsets, and whether this would imply subset-specific functions in different chronic or acute CNS lesions [74] and other CNS regions like the spinal cord [155,200] requires further investigations.

In summary, these considerations clearly show that the *in vitro* scratch wound assay is well-suited for manipulation of intrinsic pathways in order to study cell-autonomous effects in astrocytes (e.g. by targeted gene deletion or pharmacological inhibition) [146,147,163,196,220]. Moreover, *in vivo* imaging techniques are advantageous for fate mapping of astrocytes in their natural environment within the healthy brain and in a reactive state after injury. These findings help to understand the multifaceted aspects of astrogliosis after TBI, with the major goal being to unravel underlying mechanisms of astrocyte heterogeneity. Prospective investigations on the cellular 'interactome' of glia, neurons, the vasculature as well as cells penetrating the brain parenchyma upon injury are important for improving the clinical outcome after CNS trauma by novel diagnostic and therapeutic approaches [270,327,328].

References

1 Somjen, G. G. Nervenkitt: notes on the history of the concept of neuroglia. *Glia* **1**, 2-9 (1988).
2 Kettenmann, H. & Ransom, B. *Neuroglia*. Vol. 3rd Edition (Oxford University Press, USA, 2012).
3 Verkhratsky A., a. B. A. *Introduction to Glia, in Glial Neurobiology: A Textbook*. (John Wiley & Sons, Ltd, 2007).
4 Prinz, M., Priller, J., Sisodia, S. S. & Ransohoff, R. M. Heterogeneity of CNS myeloid cells and their roles in neurodegeneration. *Nat Neurosci* **14**, 1227-1235 (2011).
5 Ransohoff, R. M. & Cardona, A. E. The myeloid cells of the central nervous system parenchyma. *Nature* **468**, 253-262 (2010).
6 Kettenmann, H., Hanisch, U. K., Noda, M. & Verkhratsky, A. Physiology of microglia. *Physiol Rev* **91**, 461-553 (2011).
7 Del Rio-Hortega, P. *Microglia. In: Cytology and Cellular Pathology of the Nervous System*. (Hoeber, 1932).
8 Chan, W. Y., Kohsaka, S. & Rezaie, P. The origin and cell lineage of microglia: new concepts. *Brain Res Rev* **53**, 344-354 (2007).
9 Trotter, J., Karram, K. & Nishiyama, A. NG2 cells: Properties, progeny and origin. *Brain Res Rev* **63**, 72-82 (2010).
10 Nishiyama, A., Komitova, M., Suzuki, R. & Zhu, X. Polydendrocytes (NG2 cells): multifunctional cells with lineage plasticity. *Nat Rev Neurosci* **10**, 9-22 (2009).
11 Dimou, L., Simon, C., Kirchhoff, F., Takebayashi, H. & Götz, M. Progeny of Olig2-expressing progenitors in the gray and white matter of the adult mouse cerebral cortex. *J Neurosci* **28**, 10434-10442 (2008).
12 Reichenbach, A. & Wolburg, H. *Astrocytes and ependymal glia, in Neuroglia.* 3 edn, (Oxford University Press, 2012).
13 Distler, C., Dreher, Z. & Stone, J. Contact spacing among astrocytes in the central nervous system: an hypothesis of their structural role. *Glia* **4**, 484-494 (1991).
14 Nedergaard, M., Ransom, B. & Goldman, S. A. New roles for astrocytes: redefining the functional architecture of the brain. *Trends Neurosci* **26**, 523-530 (2003).
15 Azevedo, F. A. *et al.* Equal numbers of neuronal and nonneuronal cells make the human brain an isometrically scaled-up primate brain. *J Comp Neurol* **513**, 532-541 (2009).
16 Oberheim, N. A. *et al.* Uniquely hominid features of adult human astrocytes. *J Neurosci* **29**, 3276-3287 (2009).
17 Kriegstein, A. & Alvarez-Buylla, A. The glial nature of embryonic and adult neural stem cells. *Annu Rev Neurosci* **32**, 149-184 (2009).
18 Bushong, E. A., Martone, M. E. & Ellisman, M. H. Maturation of astrocyte morphology and the establishment of astrocyte domains during postnatal hippocampal development. *Int J Dev Neurosci* **22**, 73-86 (2004).
19 Ge, W. P., Miyawaki, A., Gage, F. H., Jan, Y. N. & Jan, L. Y. Local generation of glia is a major astrocyte source in postnatal cortex. *Nature* **484**, 376-380 (2012).
20 Rowitch, D. H. & Kriegstein, A. R. Developmental genetics of vertebrate glial-cell specification. *Nature* **468**, 214-222 (2010).
21 Zerlin, M., Levison, S. W. & Goldman, J. E. Early patterns of migration, morphogenesis, and intermediate filament expression of subventricular zone cells in the postnatal rat forebrain. *J Neurosci* **15**, 7238-7249 (1995).

22 Freeman, M. R. Specification and morphogenesis of astrocytes. *Science* **330**, 774-778 (2010).
23 Miller, R. H. & Raff, M. C. Fibrous and protoplasmic astrocytes are biochemically and developmentally distinct. *J Neurosci* **4**, 585-592 (1984).
24 Hochstim, C., Deneen, B., Lukaszewicz, A., Zhou, Q. & Anderson, D. J. Identification of positionally distinct astrocyte subtypes whose identities are specified by a homeodomain code. *Cell* **133**, 510-522 (2008).
25 Doetsch, F., Caille, I., Lim, D. A., Garcia-Verdugo, J. M. & Alvarez-Buylla, A. Subventricular zone astrocytes are neural stem cells in the adult mammalian brain. *Cell* **97**, 703-716 (1999).
26 Roelofs, R. F. *et al.* Adult human subventricular, subgranular, and subpial zones contain astrocytes with a specialized intermediate filament cytoskeleton. *Glia* **52**, 289-300 (2005).
27 Mathiisen, T. M., Lehre, K. P., Danbolt, N. C. & Ottersen, O. P. The perivascular astroglial sheath provides a complete covering of the brain microvessels: an electron microscopic 3D reconstruction. *Glia* **58**, 1094-1103 (2010).
28 Wilhelmsson, U. *et al.* Redefining the concept of reactive astrocytes as cells that remain within their unique domains upon reaction to injury. *Proc Natl Acad Sci U S A* **103**, 17513-17518 (2006).
29 Beckervordersandforth, R. *et al.* In vivo fate mapping and expression analysis reveals molecular hallmarks of prospectively isolated adult neural stem cells. *Cell Stem Cell* **7**, 744-758 (2010).
30 Wu, X. *et al.* Cdc42 controls progenitor cell differentiation and beta-catenin turnover in skin. *Genes Dev* **20**, 571-585 (2006).
31 Doetsch, F., Garcia-Verdugo, J. M. & Alvarez-Buylla, A. Cellular composition and three-dimensional organization of the subventricular germinal zone in the adult mammalian brain. *J Neurosci* **17**, 5046-5061 (1997).
32 Robel, S., Berninger, B. & Götz, M. The stem cell potential of glia: lessons from reactive gliosis. *Nat Rev Neurosci* **12**, 88-104 (2011).
33 Cahoy, J. D. *et al.* A transcriptome database for astrocytes, neurons, and oligodendrocytes: a new resource for understanding brain development and function. *J Neurosci* **28**, 264-278 (2008).
34 Doyle, J. P. *et al.* Application of a translational profiling approach for the comparative analysis of CNS cell types. *Cell* **135**, 749-762 (2008).
35 Lovatt, D. *et al.* The transcriptome and metabolic gene signature of protoplasmic astrocytes in the adult murine cortex. *J Neurosci* **27**, 12255-12266 (2007).
36 Heintz, N. Gene expression nervous system atlas (GENSAT). *Nat Neurosci* **7**, 483 (2004).
37 Yang, Y. *et al.* Molecular comparison of GLT1+ and ALDH1L1+ astrocytes in vivo in astroglial reporter mice. *Glia* **59**, 200-207 (2011).
38 Rash, J. E., Yasumura, T., Hudson, C. S., Agre, P. & Nielsen, S. Direct immunogold labeling of aquaporin-4 in square arrays of astrocyte and ependymocyte plasma membranes in rat brain and spinal cord. *Proc Natl Acad Sci U S A* **95**, 11981-11986 (1998).
39 Feng, L., Hatten, M. E. & Heintz, N. Brain lipid-binding protein (BLBP): a novel signaling system in the developing mammalian CNS. *Neuron* **12**, 895-908 (1994).
40 Hartfuss, E., Galli, R., Heins, N. & Götz, M. Characterization of CNS precursor subtypes and radial glia. *Dev Biol* **229**, 15-30 (2001).
41 Barry, D. & McDermott, K. Differentiation of radial glia from radial precursor cells and transformation into astrocytes in the developing rat spinal cord. *Glia* **50**, 187-197 (2005).
42 Fitch, M. T. & Silver, J. Glial cell extracellular matrix: boundaries for axon growth in development and regeneration. *Cell Tissue Res* **290**, 379-384 (1997).
43 Smith, G. M. & Strunz, C. Growth factor and cytokine regulation of chondroitin sulfate proteoglycans by astrocytes. *Glia* **52**, 209-218 (2005).

44 Kunzelmann, P. *et al.* Late onset and increasing expression of the gap junction protein connexin30 in adult murine brain and long-term cultured astrocytes. *Glia* **25**, 111-119 (1999).

45 Nagy, J. I., Ionescu, A. V., Lynn, B. D. & Rash, J. E. Coupling of astrocyte connexins Cx26, Cx30, Cx43 to oligodendrocyte Cx29, Cx32, Cx47: Implications from normal and connexin32 knockout mice. *Glia* **44**, 205-218 (2003).

46 Dermietzel, R. & Spray, D. C. From neuro-glue ('Nervenkitt') to glia: a prologue. *Glia* **24**, 1-7 (1998).

47 Pekny, M. *et al.* Mice lacking glial fibrillary acidic protein display astrocytes devoid of intermediate filaments but develop and reproduce normally. *Embo J* **14**, 1590-1598 (1995).

48 Kamphuis, W. *et al.* GFAP Isoforms in Adult Mouse Brain with a Focus on Neurogenic Astrocytes and Reactive Astrogliosis in Mouse Models of Alzheimer Disease. *PLoS One* **7**, e42823 (2012).

49 Levitt, P. & Rakic, P. Immunoperoxidase localization of glial fibrillary acidic protein in radial glial cells and astrocytes of the developing rhesus monkey brain. *J Comp Neurol* **193**, 815-840 (1980).

50 Nolte, C. *et al.* GFAP promoter-controlled EGFP-expressing transgenic mice: a tool to visualize astrocytes and astrogliosis in living brain tissue. *Glia* **33**, 72-86 (2001).

51 Doetsch, F., Petreanu, L., Caille, I., Garcia-Verdugo, J. M. & Alvarez-Buylla, A. EGF converts transit-amplifying neurogenic precursors in the adult brain into multipotent stem cells. *Neuron* **36**, 1021-1034 (2002).

52 Shibata, T. *et al.* Glutamate transporter GLAST is expressed in the radial glia-astrocyte lineage of developing mouse spinal cord. *J Neurosci* **17**, 9212-9219 (1997).

53 Ullensvang, K., Lehre, K. P., Storm-Mathisen, J. & Danbolt, N. C. Differential developmental expression of the two rat brain glutamate transporter proteins GLAST and GLT. *Eur J Neurosci* **9**, 1646-1655 (1997).

54 Regan, M. R. *et al.* Variations in promoter activity reveal a differential expression and physiology of glutamate transporters by glia in the developing and mature CNS. *J Neurosci* **27**, 6607-6619 (2007).

55 Mori, T. *et al.* Inducible gene deletion in astroglia and radial glia--a valuable tool for functional and lineage analysis. *Glia* **54**, 21-34 (2006).

56 Lehre, K. P., Davanger, S. & Danbolt, N. C. Localization of the glutamate transporter protein GLAST in rat retina. *Brain Res* **744**, 129-137 (1997).

57 Jungblut, M. *et al.* Isolation and characterization of living primary astroglial cells using the new GLAST-specific monoclonal antibody ACSA-1. *Glia* **60**, 894-907 (2012).

58 de Vivo, L., Melone, M., Rothstein, J. D. & Conti, F. GLT-1 Promoter Activity in Astrocytes and Neurons of Mouse Hippocampus and Somatic Sensory Cortex. *Front Neuroanat* **3**, 31 (2009).

59 Martinez-Hernandez, A., Bell, K. P. & Norenberg, M. D. Glutamine synthetase: glial localization in brain. *Science* **195**, 1356-1358 (1977).

60 Derouiche, A. & Rauen, T. Coincidence of L-glutamate/L-aspartate transporter (GLAST) and glutamine synthetase (GS) immunoreactions in retinal glia: evidence for coupling of GLAST and GS in transmitter clearance. *J Neurosci Res* **42**, 131-143 (1995).

61 Norenberg, M. D. & Martinez-Hernandez, A. Fine structural localization of glutamine synthetase in astrocytes of rat brain. *Brain Res* **161**, 303-310 (1979).

62 Misson, J. P., Edwards, M. A., Yamamoto, M. & Caviness, V. S., Jr. Identification of radial glial cells within the developing murine central nervous system: studies based upon a new immunohistochemical marker. *Brain Res Dev Brain Res* **44**, 95-108 (1988).

63 Cocchia, D. Immunocytochemical localization of S-100 protein in the brain of adult rat. An ultrastructural study. *Cell Tissue Res* **214**, 529-540 (1981).

64 Kondo, H., Takahashi, H. & Takahashi, Y. Immunohistochemical study of S-100 protein in the postnatal development of Muller cells and astrocytes in the rat retina. *Cell Tissue Res* **238**, 503-508 (1984).
65 Horner, P. J. *et al.* Proliferation and differentiation of progenitor cells throughout the intact adult rat spinal cord. *J Neurosci* **20**, 2218-2228 (2000).
66 Coskun, V. *et al.* CD133+ neural stem cells in the ependyma of mammalian postnatal forebrain. *Proc Natl Acad Sci U S A* **105**, 1026-1031 (2008).
67 Suzuki, A. *et al.* Astrocyte-neuron lactate transport is required for long-term memory formation. *Cell* **144**, 810-823 (2011).
68 Brown, A. M. & Ransom, B. R. Astrocyte glycogen and brain energy metabolism. *Glia* **55**, 1263-1271 (2007).
69 Kimelberg, H. K. Functions of mature mammalian astrocytes: a current view. *Neuroscientist* **16**, 79-106 (2010).
70 Ullian, E. M., Sapperstein, S. K., Christopherson, K. S. & Barres, B. A. Control of synapse number by glia. *Science* **291**, 657-661 (2001).
71 Bergles, D. E. & Jahr, C. E. Synaptic activation of glutamate transporters in hippocampal astrocytes. *Neuron* **19**, 1297-1308 (1997).
72 Pfrieger, F. W. & Barres, B. A. Synaptic efficacy enhanced by glial cells in vitro. *Science* **277**, 1684-1687 (1997).
73 Haydon, P. G. & Carmignoto, G. Astrocyte control of synaptic transmission and neurovascular coupling. *Physiol Rev* **86**, 1009-1031 (2006).
74 Sofroniew, M. V. & Vinters, H. V. Astrocytes: biology and pathology. *Acta Neuropathol* **119**, 7-35 (2010).
75 Parpura, V. *et al.* Glial cells in (patho)physiology. *J Neurochem* **121**, 4-27 (2012).
76 Reichenbach, A., Derouiche, A. & Kirchhoff, F. Morphology and dynamics of perisynaptic glia. *Brain Res Rev* **63**, 11-25 (2010).
77 Halassa, M. M., Fellin, T. & Haydon, P. G. The tripartite synapse: roles for gliotransmission in health and disease. *Trends Mol Med* **13**, 54-63 (2007).
78 Rothstein, J. D. *et al.* Knockout of glutamate transporters reveals a major role for astroglial transport in excitotoxicity and clearance of glutamate. *Neuron* **16**, 675-686 (1996).
79 Perego, C. *et al.* The GLT-1 and GLAST glutamate transporters are expressed on morphologically distinct astrocytes and regulated by neuronal activity in primary hippocampal cocultures. *J Neurochem* **75**, 1076-1084 (2000).
80 Sontheimer, H., Fernandez-Marques, E., Ullrich, N., Pappas, C. A. & Waxman, S. G. Astrocyte Na+ channels are required for maintenance of Na+/K(+)-ATPase activity. *J Neurosci* **14**, 2464-2475 (1994).
81 Verkhratsky, A. & Parpura, V. Recent advances in (patho)physiology of astroglia. *Acta Pharmacol Sin* **31**, 1044-1054 (2010).
82 Di Castro, M. A. *et al.* Local Ca2+ detection and modulation of synaptic release by astrocytes. *Nat Neurosci* **14**, 1276-1284 (2011).
83 David, Y. *et al.* Astrocytic dysfunction in epileptogenesis: consequence of altered potassium and glutamate homeostasis? *J Neurosci* **29**, 10588-10599 (2009).
84 Seifert, G., Carmignoto, G. & Steinhauser, C. Astrocyte dysfunction in epilepsy. *Brain Res Rev* **63**, 212-221 (2010).
85 Prodinger, C. *et al.* CD11c-expressing cells reside in the juxtavascular parenchyma and extend processes into the glia limitans of the mouse nervous system. *Acta Neuropathol* **121**, 445-458 (2011).

86 Ballabh, P., Braun, A. & Nedergaard, M. The blood-brain barrier: an overview: structure, regulation, and clinical implications. *Neurobiol Dis* **16**, 1-13 (2004).

87 Abbott, N. J., Ronnback, L. & Hansson, E. Astrocyte-endothelial interactions at the blood-brain barrier. *Nat Rev Neurosci* **7**, 41-53 (2006).

88 Krüger, M. & Bechmann, I. CNS pericytes: concepts, misconceptions, and a way out. *Glia* **58**, 1-10 (2010).

89 Rubin, L. L. & Staddon, J. M. The cell biology of the blood-brain barrier. *Annu Rev Neurosci* **22**, 11-28 (1999).

90 Risau, W. & Wolburg, H. Development of the blood-brain barrier. *Trends Neurosci* **13**, 174-178 (1990).

91 Steiner, E. *et al.* Loss of astrocyte polarization upon transient focal brain ischemia as a possible mechanism to counteract early edema formation. *Glia* **60**, 1646-1659 (2012).

92 Sixt, M. *et al.* Endothelial cell laminin isoforms, laminins 8 and 10, play decisive roles in T cell recruitment across the blood-brain barrier in experimental autoimmune encephalomyelitis. *J Cell Biol* **153**, 933-946 (2001).

93 McCarty, J. H. Cell adhesion and signaling networks in brain neurovascular units. *Curr Opin Hematol* **16**, 209-214 (2009).

94 Robel, S. *et al.* Conditional deletion of beta1-integrin in astroglia causes partial reactive gliosis. *Glia* **57**, 1630-1647 (2009).

95 Peng, H., Ong, Y. M., Shah, W. A., Holland, P. C. & Carbonetto, S. Integrins regulate centrosome integrity and astrocyte polarization following a wound. *Dev Neurobiol* (2012).

96 Peng, H., Shah, W., Holland, P. & Carbonetto, S. Integrins and dystroglycan regulate astrocyte wound healing: the integrin beta1 subunit is necessary for process extension and orienting the microtubular network. *Dev Neurobiol* **68**, 559-574 (2008).

97 Bechmann, I. *et al.* Turnover of rat brain perivascular cells. *Exp Neurol* **168**, 242-249 (2001).

98 McCaslin, A. F., Chen, B. R., Radosevich, A. J., Cauli, B. & Hillman, E. M. In vivo 3D morphology of astrocyte-vasculature interactions in the somatosensory cortex: implications for neurovascular coupling. *J Cereb Blood Flow Metab* **31**, 795-806 (2011).

99 Iliff, J. J. *et al.* A paravascular pathway facilitates CSF flow through the brain parenchyma and the clearance of interstitial solutes, including amyloid beta. *Sci Transl Med* **4**, 147ra111 (2012).

100 Haj-Yasein, N. N. *et al.* Glial-conditional deletion of aquaporin-4 (Aqp4) reduces blood-brain water uptake and confers barrier function on perivascular astrocyte endfeet. *Proc Natl Acad Sci U S A* **108**, 17815-17820 (2011).

101 Wang, X., Takano, T. & Nedergaard, M. Astrocytic calcium signaling: mechanism and implications for functional brain imaging. *Methods Mol Biol* **489**, 93-109 (2009).

102 Attwell, D. *et al.* Glial and neuronal control of brain blood flow. *Nature* **468**, 232-243 (2010).

103 Gordon, G. R., Mulligan, S. J. & MacVicar, B. A. Astrocyte control of the cerebrovasculature. *Glia* **55**, 1214-1221 (2007).

104 Iadecola, C. & Nedergaard, M. Glial regulation of the cerebral microvasculature. *Nat Neurosci* **10**, 1369-1376 (2007).

105 Daneman, R., Zhou, L., Kebede, A. A. & Barres, B. A. Pericytes are required for blood-brain barrier integrity during embryogenesis. *Nature* **468**, 562-566 (2010).

106 Liebner, S., Czupalla, C. J. & Wolburg, H. Current concepts of blood-brain barrier development. *Int J Dev Biol* **55**, 467-476 (2011).

107 van Vliet, E. A. *et al.* Blood-brain barrier leakage may lead to progression of temporal lobe epilepsy. *Brain* **130**, 521-534 (2007).

108 Davalos, D. *et al.* Fibrinogen-induced perivascular microglial clustering is required for the development of axonal damage in neuroinflammation. *Nat Commun* **3**, 1227 (2012).
109 Carvey, P. M., Hendey, B. & Monahan, A. J. The blood-brain barrier in neurodegenerative disease: a rhetorical perspective. *J Neurochem* **111**, 291-314 (2009).
110 Hamm, S. *et al.* Astrocyte mediated modulation of blood-brain barrier permeability does not correlate with a loss of tight junction proteins from the cellular contacts. *Cell Tissue Res* **315**, 157-166 (2004).
111 Wolburg, H., Noell, S., Fallier-Becker, P., Mack, A. F. & Wolburg-Buchholz, K. The disturbed blood-brain barrier in human glioblastoma. *Mol Aspects Med* **33**, 579-589 (2012).
112 Krüger, M., Hartig, W., Reichenbach, A., Bechmann, I. & Michalski, D. Blood-Brain Barrier Breakdown after Embolic Stroke in Rats Occurs without Ultrastructural Evidence for Disrupting Tight Junctions. *PLoS One* **8**, e56419 (2013).
113 Buffo, A. *et al.* Origin and progeny of reactive gliosis: A source of multipotent cells in the injured brain. *Proc Natl Acad Sci U S A* **105**, 3581-3586 (2008).
114 Simon, C., Götz, M. & Dimou, L. Progenitors in the adult cerebral cortex: cell cycle properties and regulation by physiological stimuli and injury. *Glia* **59**, 869-881 (2011).
115 Kim, W. R. *et al.* Regional difference of reactive astrogliosis following traumatic brain injury revealed by hGFAP-GFP transgenic mice. *Neurosci Lett* **513**, 155-159 (2012).
116 Bye, N. *et al.* Neurogenesis and glial proliferation are stimulated following diffuse traumatic brain injury in adult rats. *J Neurosci Res* **89**, 986-1000 (2011).
117 Miyake, T., Hattori, T., Fukuda, M., Kitamura, T. & Fujita, S. Quantitative studies on proliferative changes of reactive astrocytes in mouse cerebral cortex. *Brain Res* **451**, 133-138 (1988).
118 Myer, D. J., Gurkoff, G. G., Lee, S. M., Hovda, D. A. & Sofroniew, M. V. Essential protective roles of reactive astrocytes in traumatic brain injury. *Brain* **129**, 2761-2772 (2006).
119 Rite, I., Machado, A., Cano, J. & Venero, J. L. Intracerebral VEGF injection highly upregulates AQP4 mRNA and protein in the perivascular space and glia limitans externa. *Neurochem Int* **52**, 897-903 (2008).
120 Barreto, G. E., Sun, X., Xu, L. & Giffard, R. G. Astrocyte proliferation following stroke in the mouse depends on distance from the infarct. *PLoS One* **6**, e27881 (2011).
121 Friedman, B. *et al.* Acute vascular disruption and aquaporin 4 loss after stroke. *Stroke* **40**, 2182-2190 (2009).
122 Sontheimer, H. Malignant gliomas: perverting glutamate and ion homeostasis for selective advantage. *Trends Neurosci* **26**, 543-549 (2003).
123 Buckingham, S. C. *et al.* Glutamate release by primary brain tumors induces epileptic activity. *Nat Med* **17**, 1269-1274 (2011).
124 Furnari, F. B. *et al.* Malignant astrocytic glioma: genetics, biology, and paths to treatment. *Genes Dev* **21**, 2683-2710 (2007).
125 Tian, G. F. *et al.* An astrocytic basis of epilepsy. *Nat Med* **11**, 973-981 (2005).
126 Lee, S. H., Magge, S., Spencer, D. D., Sontheimer, H. & Cornell-Bell, A. H. Human epileptic astrocytes exhibit increased gap junction coupling. *Glia* **15**, 195-202 (1995).
127 Steinhauser, C., Seifert, G. & Bedner, P. Astrocyte dysfunction in temporal lobe epilepsy: K+ channels and gap junction coupling. *Glia* **60**, 1192-1202 (2012).
128 Aronica, E. *et al.* Upregulation of metabotropic glutamate receptor subtype mGluR3 and mGluR5 in reactive astrocytes in a rat model of mesial temporal lobe epilepsy. *Eur J Neurosci* **12**, 2333-2344 (2000).
129 Hupp, S. *et al.* Astrocytic tissue remodeling by the meningitis neurotoxin pneumolysin facilitates pathogen tissue penetration and produces interstitial brain edema. *Glia* **60**, 137-146 (2012).

130 Henderson, L. J., Sharma, A., Monaco, M. C., Major, E. O. & Al-Harthi, L. Human Immunodeficiency Virus Type 1 (HIV-1) Transactivator of Transcription through Its Intact Core and Cysteine-Rich Domains Inhibits Wnt/beta-Catenin Signaling in Astrocytes: Relevance to HIV Neuropathogenesis. *J Neurosci* **32**, 16306-16313 (2012).
131 Schachtele, S. J., Hu, S. & Lokensgard, J. R. Modulation of experimental herpes encephalitis-associated neurotoxicity through sulforaphane treatment. *PLoS One* **7**, e36216 (2012).
132 Kraft, A. W. *et al.* Attenuating astrocyte activation accelerates plaque pathogenesis in APP/PS1 mice. *Faseb J* (2012).
133 Weggen, S., Diehlmann, A., Buslei, R., Beyreuther, K. & Bayer, T. A. Prominent expression of presenilin-1 in senile plaques and reactive astrocytes in Alzheimer's disease brain. *Neuroreport* **9**, 3279-3283 (1998).
134 Wyss-Coray, T. *et al.* Adult mouse astrocytes degrade amyloid-beta in vitro and in situ. *Nat Med* **9**, 453-457 (2003).
135 Saijo, K. *et al.* A Nurr1/CoREST pathway in microglia and astrocytes protects dopaminergic neurons from inflammation-induced death. *Cell* **137**, 47-59 (2009).
136 Hall, E. D., Oostveen, J. A. & Gurney, M. E. Relationship of microglial and astrocytic activation to disease onset and progression in a transgenic model of familial ALS. *Glia* **23**, 249-256 (1998).
137 Rothstein, J. D. *et al.* Beta-lactam antibiotics offer neuroprotection by increasing glutamate transporter expression. *Nature* **433**, 73-77 (2005).
138 Fitch, M. T. & Silver, J. CNS injury, glial scars, and inflammation: Inhibitory extracellular matrices and regeneration failure. *Exp Neurol* **209**, 294-301 (2008).
139 Sofroniew, M. V. Molecular dissection of reactive astrogliosis and glial scar formation. *Trends Neurosci* **32**, 638-647 (2009).
140 Habgood, M. D. *et al.* Changes in blood-brain barrier permeability to large and small molecules following traumatic brain injury in mice. *Eur J Neurosci* **25**, 231-238 (2007).
141 Buffo, A., Rolando, C. & Ceruti, S. Astrocytes in the damaged brain: molecular and cellular insights into their reactive response and healing potential. *Biochem Pharmacol* **79**, 77-89 (2010).
142 Schachtrup, C. *et al.* Fibrinogen triggers astrocyte scar formation by promoting the availability of active TGF-beta after vascular damage. *J Neurosci* **30**, 5843-5854 (2010).
143 Silver, J. & Miller, J. H. Regeneration beyond the glial scar. *Nat Rev Neurosci* **5**, 146-156 (2004).
144 Sofroniew, M. V. Reactive astrocytes in neural repair and protection. *Neuroscientist* **11**, 400-407 (2005).
145 McKeon, R. J., Schreiber, R. C., Rudge, J. S. & Silver, J. Reduction of neurite outgrowth in a model of glial scarring following CNS injury is correlated with the expression of inhibitory molecules on reactive astrocytes. *J Neurosci* **11**, 3398-3411 (1991).
146 Etienne-Manneville, S. In vitro assay of primary astrocyte migration as a tool to study Rho GTPase function in cell polarization. *Methods Enzymol* **406**, 565-578 (2006).
147 Holtje, M. *et al.* Role of Rho GTPase in astrocyte morphology and migratory response during in vitro wound healing. *J Neurochem* **95**, 1237-1248 (2005).
148 Deller, T. *et al.* Up-regulation of astrocyte-derived tenascin-C correlates with neurite outgrowth in the rat dentate gyrus after unilateral entorhinal cortex lesion. *Neuroscience* **81**, 829-846 (1997).
149 Ridet, J. L., Malhotra, S. K., Privat, A. & Gage, F. H. Reactive astrocytes: cellular and molecular cues to biological function. *Trends Neurosci* **20**, 570-577 (1997).
150 Pekny, M. & Pekna, M. Astrocyte intermediate filaments in CNS pathologies and regeneration. *J Pathol* **204**, 428-437 (2004).

151 Brenner, M. *et al.* Mutations in GFAP, encoding glial fibrillary acidic protein, are associated with Alexander disease. *Nat Genet* **27**, 117-120 (2001).
152 Pekny, M., Stanness, K. A., Eliasson, C., Betsholtz, C. & Janigro, D. Impaired induction of blood-brain barrier properties in aortic endothelial cells by astrocytes from GFAP-deficient mice. *Glia* **22**, 390-400 (1998).
153 Wilhelmsson, U. *et al.* Absence of glial fibrillary acidic protein and vimentin prevents hypertrophy of astrocytic processes and improves post-traumatic regeneration. *J Neurosci* **24**, 5016-5021 (2004).
154 Jarlestedt, K. *et al.* Attenuation of reactive gliosis does not affect infarct volume in neonatal hypoxic-ischemic brain injury in mice. *PLoS One* **5**, e10397 (2010).
155 Okada, S. *et al.* Conditional ablation of Stat3 or Socs3 discloses a dual role for reactive astrocytes after spinal cord injury. *Nat Med* **12**, 829-834 (2006).
156 Herrmann, J. E. *et al.* STAT3 is a critical regulator of astrogliosis and scar formation after spinal cord injury. *J Neurosci* **28**, 7231-7243 (2008).
157 Khurgel, M., Koo, A. C. & Ivy, G. O. Selective ablation of astrocytes by intracerebral injections of alpha-aminoadipate. *Glia* **16**, 351-358 (1996).
158 Bush, T. G. *et al.* Leukocyte infiltration, neuronal degeneration, and neurite outgrowth after ablation of scar-forming, reactive astrocytes in adult transgenic mice. *Neuron* **23**, 297-308 (1999).
159 Faulkner, J. R. *et al.* in *J Neurosci* Vol. 24 2143-2155 (2004).
160 Brambilla, R. *et al.* Transgenic inhibition of astroglial NF-kappa B leads to increased axonal sparing and sprouting following spinal cord injury. *J Neurochem* **110**, 765-778 (2009).
161 Zamanian, J. L. *et al.* Genomic analysis of reactive astrogliosis. *J Neurosci* **32**, 6391-6410 (2012).
162 Hamby, M. E. *et al.* Inflammatory mediators alter the astrocyte transcriptome and calcium signaling elicited by multiple G-protein-coupled receptors. *J Neurosci* **32**, 14489-14510 (2012).
163 Lim, J. H. *et al.* Extracellular signal-regulated kinase involvement in human astrocyte migration. *Brain Res* **1164**, 1-13 (2007).
164 Zheng, C. *et al.* VEGF reduces astrogliosis and preserves neuromuscular junctions in ALS transgenic mice. *Biochem Biophys Res Commun* **363**, 989-993 (2007).
165 Krum, J. M., Mani, N. & Rosenstein, J. M. Roles of the endogenous VEGF receptors flt-1 and flk-1 in astroglial and vascular remodeling after brain injury. *Exp Neurol* **212**, 108-117 (2008).
166 Endoh, M., Maiese, K. & Wagner, J. Expression of the inducible form of nitric oxide synthase by reactive astrocytes after transient global ischemia. *Brain Res* **651**, 92-100 (1994).
167 Buskila, Y., Farkash, S., Hershfinkel, M. & Amitai, Y. Rapid and reactive nitric oxide production by astrocytes in mouse neocortical slices. *Glia* **52**, 169-176 (2005).
168 Cherian, L., Hlatky, R. & Robertson, C. S. Nitric oxide in traumatic brain injury. *Brain Pathol* **14**, 195-201 (2004).
169 Bishop, A. & Anderson, J. E. NO signaling in the CNS: from the physiological to the pathological. *Toxicology* **208**, 193-205 (2005).
170 Alvarez, J. I. *et al.* The Hedgehog pathway promotes blood-brain barrier integrity and CNS immune quiescence. *Science* **334**, 1727-1731 (2011).
171 Ohlig, S. *et al.* An emerging role of Sonic hedgehog shedding as a modulator of heparan sulfate interactions. *J Biol Chem* (2012).
172 Sirko, S. *et al.* Reactive glia in the injured brain acquire stem cell properties in response to Sonic hedgehog. *Cell Stem Cell* (2013).
173 Kang, W. & Hebert, J. M. Signaling pathways in reactive astrocytes, a genetic perspective. *Mol Neurobiol* **43**, 147-154 (2011).

174 Sarafian, T. A. *et al.* Disruption of astrocyte STAT3 signaling decreases mitochondrial function and increases oxidative stress in vitro. *PLoS One* **5**, e9532 (2010).

175 Beck, K. & Schachtrup, C. Vascular damage in the central nervous system: a multifaceted role for vascular-derived TGF-beta. *Cell Tissue Res* **347**, 187-201 (2012).

176 Buckwalter, M. *et al.* Molecular and functional dissection of TGF-beta1-induced cerebrovascular abnormalities in transgenic mice. *Ann N Y Acad Sci* **977**, 87-95 (2002).

177 Fraser, M. M. *et al.* Pten loss causes hypertrophy and increased proliferation of astrocytes in vivo. *Cancer Res* **64**, 7773-7779 (2004).

178 Codeluppi, S. *et al.* The Rheb-mTOR pathway is upregulated in reactive astrocytes of the injured spinal cord. *J Neurosci* **29**, 1093-1104 (2009).

179 Wilhelmsson, U. *et al.* Astrocytes negatively regulate neurogenesis through the Jagged1-mediated notch pathway. *Stem Cells* **30**, 2320-2329 (2012).

180 Goldshmit, Y. & Bourne, J. Upregulation of EphA4 on astrocytes potentially mediates astrocytic gliosis after cortical lesion in the marmoset monkey. *J Neurotrauma* **27**, 1321-1332 (2010).

181 Garvalov, B. K. *et al.* Cdc42 regulates cofilin during the establishment of neuronal polarity. *J Neurosci* **27**, 13117-13129 (2007).

182 Robel, S. *Diverse Functions of Astroglial Cells: The Role of Molecular Pathways Regulating Polarity.*, LMU, (2010).

183 Etienne-Manneville, S. Polarity proteins in glial cell functions. *Curr Opin Neurobiol* **18**, 488-494 (2008).

184 Cau, J. & Hall, A. Cdc42 controls the polarity of the actin and microtubule cytoskeletons through two distinct signal transduction pathways. *J Cell Sci* **118**, 2579-2587 (2005).

185 Fuchs, S. *et al.* Stage-specific control of neural crest stem cell proliferation by the small rho GTPases Cdc42 and Rac1. *Cell Stem Cell* **4**, 236-247 (2009).

186 Wang, J. B., Sonn, R., Tekletsadik, Y. K., Samorodnitsky, D. & Osman, M. A. IQGAP1 regulates cell proliferation through a novel CDC42-mTOR pathway. *J Cell Sci* **122**, 2024-2033 (2009).

187 Warner, S. J., Yashiro, H. & Longmore, G. D. The Cdc42/Par6/aPKC polarity complex regulates apoptosis-induced compensatory proliferation in epithelia. *Curr Biol* **20**, 677-686 (2010).

188 Raftopoulou, M. & Hall, A. Cell migration: Rho GTPases lead the way. *Dev Biol* **265**, 23-32 (2004).

189 Allen, W. E., Zicha, D., Ridley, A. J. & Jones, G. E. A role for Cdc42 in macrophage chemotaxis. *J Cell Biol* **141**, 1147-1157 (1998).

190 Palazzo, A. F. *et al.* Cdc42, dynein, and dynactin regulate MTOC reorientation independent of Rho-regulated microtubule stabilization. *Curr Biol* **11**, 1536-1541 (2001).

191 Luckashenak, N., Wahe, A., Breit, K., Brakebusch, C. & Brocker, T. Rho-family GTPase Cdc42 controls migration of Langerhans cells in vivo. *J Immunol* **190**, 27-35 (2013).

192 Nobes, C. D. & Hall, A. Rho, rac, and cdc42 GTPases regulate the assembly of multimolecular focal complexes associated with actin stress fibers, lamellipodia, and filopodia. *Cell* **81**, 53-62 (1995).

193 Hall, A. Rho GTPases and the actin cytoskeleton. *Science* **279**, 509-514 (1998).

194 Harris, K. P. & Tepass, U. Cdc42 and vesicle trafficking in polarized cells. *Traffic* **11**, 1272-1279 (2010).

195 Hall, A. Rho GTPases and the control of cell behaviour. *Biochem Soc Trans* **33**, 891-895 (2005).

196 Osmani, N., Vitale, N., Borg, J. P. & Etienne-Manneville, S. Scrib controls Cdc42 localization and activity to promote cell polarization during astrocyte migration. *Curr Biol* **16**, 2395-2405 (2006).

197 Czuchra, A. *et al.* Cdc42 is not essential for filopodium formation, directed migration, cell polarization, and mitosis in fibroblastoid cells. *Mol Biol Cell* **16**, 4473-4484 (2005).

198 Nobes, C. D. & Hall, A. Rho GTPases control polarity, protrusion, and adhesion during cell movement. *J Cell Biol* **144**, 1235-1244 (1999).
199 Etienne-Manneville, S. & Hall, A. Integrin-mediated activation of Cdc42 controls cell polarity in migrating astrocytes through PKCzeta. *Cell* **106**, 489-498 (2001).
200 Seo, T. B., Chang, I. A., Lee, J. H. & Namgung, U. Beneficial function of Cdc2 activity in astrocytes on axonal regeneration after spinal cord injury. *J Neurotrauma* (2013).
201 Cappello, S. *et al.* The Rho-GTPase cdc42 regulates neural progenitor fate at the apical surface. *Nat Neurosci* **9**, 1099-1107 (2006).
202 Blum, R. *et al.* Neuronal network formation from reprogrammed early postnatal rat cortical glial cells. *Cereb Cortex* **21**, 413-424 (2011).
203 Heinrich, C. *et al.* Directing astroglia from the cerebral cortex into subtype specific functional neurons. *PLoS Biol* **8**, e1000373 (2010).
204 Heinrich, C., Götz, M. & Berninger, B. Reprogramming of postnatal astroglia of the mouse neocortex into functional, synapse-forming neurons. *Methods Mol Biol* **814**, 485-498 (2012).
205 Heinrich, C. *et al.* Generation of subtype-specific neurons from postnatal astroglia of the mouse cerebral cortex. *Nat Protoc* **6**, 214-228 (2011).
206 Corti, S. *et al.* Direct reprogramming of human astrocytes into neural stem cells and neurons. *Exp Cell Res* **318**, 1528-1541 (2012).
207 Götz, M. & Huttner, W. B. The cell biology of neurogenesis. *Nat Rev Mol Cell Biol* **6**, 777-788 (2005).
208 Morrens, J., Van Den Broeck, W. & Kempermann, G. Glial cells in adult neurogenesis. *Glia* **60**, 159-174 (2012).
209 Gage, F. H. Neurogenesis in the adult brain. *J Neurosci* **22**, 612-613 (2002).
210 Ninkovic, J. & Götz, M. Signaling in adult neurogenesis: from stem cell niche to neuronal networks. *Curr Opin Neurobiol* **17**, 338-344 (2007).
211 Souza-Offtermatt, G., Udolph, A., Staubach, K.-H. & Sterk, P. *Intensivkurs Chirurgie*. 1 edn, (Elsevier,Urban&FischerVerlag, 2004).
212 Bullock, R., Maxwell, W. L., Graham, D. I., Teasdale, G. M. & Adams, J. H. Glial swelling following human cerebral contusion: an ultrastructural study. *J Neurol Neurosurg Psychiatry* **54**, 427-434 (1991).
213 Ylera, B. *et al.* Chronically CNS-injured adult sensory neurons gain regenerative competence upon a lesion of their peripheral axon. *Curr Biol* **19**, 930-936 (2009).
214 Bittigau, P. *et al.* Modeling pediatric head trauma: mechanisms of degeneration and potential strategies for neuroprotection. *Restor Neurol Neurosci* **13**, 11-23 (1998).
215 Göritz, C. *et al.* A pericyte origin of spinal cord scar tissue. *Science* **333**, 238-242 (2011).
216 Karow, M. *et al.* Reprogramming of pericyte-derived cells of the adult human brain into induced neuronal cells. *Cell Stem Cell* **11**, 471-476 (2012).
217 Correa-Cerro, L. S. & Mandell, J. W. Molecular mechanisms of astrogliosis: new approaches with mouse genetics. *J Neuropathol Exp Neurol* **66**, 169-176 (2007).
218 Nakamura, T., Colbert, M. C. & Robbins, J. Neural crest cells retain multipotential characteristics in the developing valves and label the cardiac conduction system. *Circ Res* **98**, 1547-1554 (2006).
219 Snippert, H. J. *et al.* Intestinal crypt homeostasis results from neutral competition between symmetrically dividing Lgr5 stem cells. *Cell* **143**, 134-144 (2010).
220 Robel, S., Bardehle, S., Lepier, A., Brakebusch, C. & Götz, M. Genetic deletion of cdc42 reveals a crucial role for astrocyte recruitment to the injury site in vitro and in vivo. *J Neurosci* **31**, 12471-12482 (2011).

221 Hirrlinger, P. G. *et al.* Expression of reef coral fluorescent proteins in the central nervous system of transgenic mice. *Mol Cell Neurosci* **30**, 291-303 (2005).
222 Denk, W. *et al.* Anatomical and functional imaging of neurons using 2-photon laser scanning microscopy. *J Neurosci Methods* **54**, 151-162 (1994).
223 Holtmaat, A. *et al.* Long-term, high-resolution imaging in the mouse neocortex through a chronic cranial window. *Nat Protoc* **4**, 1128-1144 (2009).
224 Nimmerjahn, A., Kirchhoff, F. & Helmchen, F. Resting microglial cells are highly dynamic surveillants of brain parenchyma in vivo. *Science* **308**, 1314-1318 (2005).
225 Steffens, H., Nadrigny, F. & Kirchhoff, F. In vivo two-photon imaging of neurons and glia in the mouse spinal cord. *Cold Spring Harb Protoc* **2012** (2012).
226 Dibaj, P. *et al.* In vivo imaging reveals rapid morphological reactions of astrocytes towards focal lesions in an ALS mouse model. *Neurosci Lett* **497**, 148-151 (2011).
227 Ericson, M. B. *et al.* Two-photon laser-scanning fluorescence microscopy applied for studies of human skin. *J Biophotonics* **1**, 320-330 (2008).
228 Rompolas, P. *et al.* Live imaging of stem cell and progeny behaviour in physiological hair-follicle regeneration. *Nature* **487**, 496-499 (2012).
229 Schiessl, I. M., Bardehle, S. & Castrop, H. Superficial nephrons in BALB/c and C57BL/6 mice facilitate in vivo multiphoton microscopy of the kidney. *PLoS One* **8**, e52499 (2013).
230 Helmchen, F., Fee, M. S., Tank, D. W. & Denk, W. A miniature head-mounted two-photon microscope. high-resolution brain imaging in freely moving animals. *Neuron* **31**, 903-912 (2001).
231 Helmchen, F. & Denk, W. Deep tissue two-photon microscopy. *Nat Methods* **2**, 932-940 (2005).
232 Denk, W., Strickler, J. H. & Webb, W. W. Two-photon laser scanning fluorescence microscopy. *Science* **248**, 73-76 (1990).
233 Meyer-Luehmann, M. *et al.* Rapid appearance and local toxicity of amyloid-beta plaques in a mouse model of Alzheimer's disease. *Nature* **451**, 720-724 (2008).
234 Nimmerjahn, A., Kirchhoff, F., Kerr, J. N. & Helmchen, F. Sulforhodamine 101 as a specific marker of astroglia in the neocortex in vivo. *Nat Methods* **1**, 31-37 (2004).
235 Tsai, H. H. *et al.* Regional astrocyte allocation regulates CNS synaptogenesis and repair. *Science* **337**, 358-362 (2012).
236 Hofer, S. B., Mrsic-Flogel, T. D., Bonhoeffer, T. & Hubener, M. Experience leaves a lasting structural trace in cortical circuits. *Nature* **457**, 313-317 (2009).
237 Trachtenberg, J. T. *et al.* Long-term in vivo imaging of experience-dependent synaptic plasticity in adult cortex. *Nature* **420**, 788-794 (2002).
238 Kelly, E. A. & Majewska, A. K. Chronic imaging of mouse visual cortex using a thinned-skull preparation. *J Vis Exp* (2010).
239 Shih, A. Y., Mateo, C., Drew, P. J., Tsai, P. S. & Kleinfeld, D. A polished and reinforced thinned-skull window for long-term imaging of the mouse brain. *J Vis Exp* (2012).
240 Yoder, E. J. & Kleinfeld, D. Cortical imaging through the intact mouse skull using two-photon excitation laser scanning microscopy. *Microsc Res Tech* **56**, 304-305 (2002).
241 Yang, G., Pan, F., Parkhurst, C. N., Grutzendler, J. & Gan, W. B. Thinned-skull cranial window technique for long-term imaging of the cortex in live mice. *Nat Protoc* **5**, 201-208 (2010).
242 Xu, H. T., Pan, F., Yang, G. & Gan, W. B. Choice of cranial window type for in vivo imaging affects dendritic spine turnover in the cortex. *Nat Neurosci* **10**, 549-551 (2007).
243 Goldman, R. D. *Live Cell Imaging: A Laboratory Manual*. Pap/Dvdr edn, (Cold Spring Harbor Laboratory Press; Pap/Dvdr edition (October 1, 2004), 2004).
244 Keck, T. *et al.* Massive restructuring of neuronal circuits during functional reorganization of adult visual cortex. *Nat Neurosci* **11**, 1162-1167 (2008).

245 Stosiek, C., Garaschuk, O., Holthoff, K. & Konnerth, A. In vivo two-photon calcium imaging of neuronal networks. *Proc Natl Acad Sci U S A* **100**, 7319-7324 (2003).
246 Tian, G. F. *et al.* Imaging of cortical astrocytes using 2-photon laser scanning microscopy in the intact mouse brain. *Adv Drug Deliv Rev* **58**, 773-787 (2006).
247 Takano, T. *et al.* Astrocyte-mediated control of cerebral blood flow. *Nat Neurosci* **9**, 260-267 (2006).
248 Schaffer, C. B. *et al.* Two-photon imaging of cortical surface microvessels reveals a robust redistribution in blood flow after vascular occlusion. *PLoS Biol* **4**, e22 (2006).
249 Blinder, P., Shih, A. Y., Rafie, C. & Kleinfeld, D. Topological basis for the robust distribution of blood to rodent neocortex. *Proc Natl Acad Sci U S A* **107**, 12670-12675 (2010).
250 Misgeld, T. & Kerschensteiner, M. In vivo imaging of the diseased nervous system. *Nat Rev Neurosci* **7**, 449-463 (2006).
251 Winkler, F. *et al.* Imaging glioma cell invasion in vivo reveals mechanisms of dissemination and peritumoral angiogenesis. *Glia* **57**, 1306-1315 (2009).
252 Kienast, Y. *et al.* Real-time imaging reveals the single steps of brain metastasis formation. *Nat Med* **16**, 116-122 (2010).
253 Hasenbach, K. *et al.* Monitoring the glioma tropism of bone marrow-derived progenitor cells by 2-photon laser scanning microscopy and positron emission tomography. *Neuro Oncol* **14**, 471-481 (2012).
254 Takano, T., Han, X., Deane, R., Zlokovic, B. & Nedergaard, M. Two-photon imaging of astrocytic Ca2+ signaling and the microvasculature in experimental mice models of Alzheimer's disease. *Ann N Y Acad Sci* **1097**, 40-50 (2007).
255 Sigler, A. & Murphy, T. H. In vivo 2-photon imaging of fine structure in the rodent brain: before, during, and after stroke. *Stroke* **41**, S117-123 (2010).
256 Kirchhoff, F., Debarbieux, F., Kronland-Martinet, C., Cojocaru, G. R. & Popa-Wagner, A. Combined two-photon laser-scanning microscopy and spectral microCT X-ray imaging to characterize the cellular signature and evolution of microstroke foci. *Rom J Morphol Embryol* **53**, 671-675 (2012).
257 Yanev, P. & Dijkhuizen, R. M. In vivo imaging of neurovascular remodeling after stroke. *Stroke* **43**, 3436-3441 (2012).
258 Rosidi, N. L. *et al.* Cortical microhemorrhages cause local inflammation but do not trigger widespread dendrite degeneration. *PLoS One* **6**, e26612 (2011).
259 Nikic, I. *et al.* A reversible form of axon damage in experimental autoimmune encephalomyelitis and multiple sclerosis. *Nat Med* **17**, 495-499 (2011).
260 Nimmerjahn, A. Two-photon imaging of microglia in the mouse cortex in vivo. *Cold Spring Harb Protoc* **2012** (2012).
261 Fuhrmann, M. *et al.* Microglial Cx3cr1 knockout prevents neuron loss in a mouse model of Alzheimer's disease. *Nat Neurosci* **13**, 411-413 (2010).
262 Koenigsknecht-Talboo, J. *et al.* Rapid microglial response around amyloid pathology after systemic anti-Abeta antibody administration in PDAPP mice. *J Neurosci* **28**, 14156-14164 (2008).
263 Nimmerjahn, A. & Helmchen, F. In vivo labeling of cortical astrocytes with sulforhodamine 101 (SR101). *Cold Spring Harb Protoc* **2012**, 326-334 (2012).
264 Bardehle, S. *et al.* Live imaging of astrocyte responses to acute injury reveals selective juxtavascular proliferation. *Nat Neurosci* (2013).
265 Oberheim, N. A. *et al.* Loss of astrocytic domain organization in the epileptic brain. *J Neurosci* **28**, 3264-3276 (2008).
266 Sword, J., Masuda, T., Croom, D. & Kirov, S. A. Evolution of neuronal and astroglial disruption in the peri-contusional cortex of mice revealed by in vivo two-photon imaging. *Brain* (2013).

References

267 Risher, W. C., Croom, D. & Kirov, S. A. Persistent astroglial swelling accompanies rapid reversible dendritic injury during stroke-induced spreading depolarizations. *Glia* **60**, 1709-1720 (2012).
268 Florence, C. M., Baillie, L. D. & Mulligan, S. J. Dynamic volume changes in astrocytes are an intrinsic phenomenon mediated by bicarbonate ion flux. *PLoS One* **7**, e51124 (2012).
269 Thrane, A. S. *et al.* Critical role of aquaporin-4 (AQP4) in astrocytic Ca2+ signaling events elicited by cerebral edema. *Proc Natl Acad Sci U S A* **108**, 846-851 (2011).
270 Kimelberg, H. K. Astrocytic swelling in cerebral ischemia as a possible cause of injury and target for therapy. *Glia* **50**, 389-397 (2005).
271 Schell, M. J., Molliver, M. E. & Snyder, S. H. D-serine, an endogenous synaptic modulator: localization to astrocytes and glutamate-stimulated release. *Proc Natl Acad Sci U S A* **92**, 3948-3952 (1995).
272 Mongin, A. A. & Kimelberg, H. K. ATP regulates anion channel-mediated organic osmolyte release from cultured rat astrocytes via multiple Ca2+-sensitive mechanisms. *Am J Physiol Cell Physiol* **288**, C204-213 (2005).
273 Enger, R. *et al.* Molecular scaffolds underpinning macroglial polarization: An analysis of retinal Muller cells and brain astrocytes in mouse. *Glia* (2012).
274 Alonso, G. NG2 proteoglycan-expressing cells of the adult rat brain: possible involvement in the formation of glial scar astrocytes following stab wound. *Glia* **49**, 318-338 (2005).
275 Takamiya, Y., Kohsaka, S., Toya, S., Otani, M. & Tsukada, Y. Immunohistochemical studies on the proliferation of reactive astrocytes and the expression of cytoskeletal proteins following brain injury in rats. *Brain Res* **466**, 201-210 (1988).
276 Miyake, T., Okada, M. & Kitamura, T. Reactive proliferation of astrocytes studied by immunohistochemistry for proliferating cell nuclear antigen. *Brain Res* **590**, 300-302 (1992).
277 Renault-Mihara, F. *et al.* Spinal cord injury: emerging beneficial role of reactive astrocytes' migration. *Int J Biochem Cell Biol* **40**, 1649-1653 (2008).
278 Fitch, M. T., Doller, C., Combs, C. K., Landreth, G. E. & Silver, J. Cellular and molecular mechanisms of glial scarring and progressive cavitation: in vivo and in vitro analysis of inflammation-induced secondary injury after CNS trauma. *J Neurosci* **19**, 8182-8198 (1999).
279 Hirrlinger, J., Hulsmann, S. & Kirchhoff, F. Astroglial processes show spontaneous motility at active synaptic terminals in situ. *Eur J Neurosci* **20**, 2235-2239 (2004).
280 Auguste, K. I. *et al.* Greatly impaired migration of implanted aquaporin-4-deficient astroglial cells in mouse brain toward a site of injury. *Faseb J* **21**, 108-116 (2007).
281 Hughes, E. G., Kang, S. H., Fukaya, M. & Bergles, D. E. Oligodendrocyte progenitors balance growth with self-repulsion to achieve homeostasis in the adult brain. *Nat Neurosci*, doi:10.1038/nn.3390 (2013).
282 Jacobsen, C. T. & Miller, R. H. Control of astrocyte migration in the developing cerebral cortex. *Dev Neurosci* **25**, 207-216 (2003).
283 Cayre, M., Canoll, P. & Goldman, J. E. Cell migration in the normal and pathological postnatal mammalian brain. *Prog Neurobiol* **88**, 41-63 (2009).
284 Zhou, H. F. & Lund, R. D. Neonatal host astrocyte migration into xenogeneic cerebral cortical grafts. *Brain Res Dev Brain Res* **65**, 127-131 (1992).
285 Goldberg, W. J. & Bernstein, J. J. Fetal cortical astrocytes migrate from cortical homografts throughout the host brain and over the glia limitans. *J Neurosci Res* **20**, 38-45 (1988).
286 Ritch, P. A., Carroll, S. L. & Sontheimer, H. Neuregulin-1 enhances motility and migration of human astrocytic glioma cells. *J Biol Chem* **278**, 20971-20978 (2003).
287 Fortin, S. P. *et al.* Cdc42 and the guanine nucleotide exchange factors Ect2 and trio mediate Fn14-induced migration and invasion of glioblastoma cells. *Mol Cancer Res* **10**, 958-968 (2012).

288 Zhao, J. W., Raha-Chowdhury, R., Fawcett, J. W. & Watts, C. Astrocytes and oligodendrocytes can be generated from NG2+ progenitors after acute brain injury: intracellular localization of oligodendrocyte transcription factor 2 is associated with their fate choice. *Eur J Neurosci* **29**, 1853-1869 (2009).
289 Magnus, T. *et al.* Evidence that nucleocytoplasmic Olig2 translocation mediates brain-injury-induced differentiation of glial precursors to astrocytes. *J Neurosci Res* **85**, 2126-2137 (2007).
290 Tatsumi, K. *et al.* Genetic fate mapping of Olig2 progenitors in the injured adult cerebral cortex reveals preferential differentiation into astrocytes. *J Neurosci Res* **86**, 3494-3502 (2008).
291 Meletis, K. *et al.* Spinal cord injury reveals multilineage differentiation of ependymal cells. *PLoS Biol* **6**, e182 (2008).
292 Barnabe-Heider, F. *et al.* Origin of new glial cells in intact and injured adult spinal cord. *Cell Stem Cell* **7**, 470-482 (2010).
293 Guo, F. *et al.* Macroglial plasticity and the origins of reactive astroglia in experimental autoimmune encephalomyelitis. *J Neurosci* **31**, 11914-11928 (2011).
294 Le Magueresse, C. *et al.* Subventricular zone-derived neuroblasts use vasculature as a scaffold to migrate radially to the cortex in neonatal mice. *Cereb Cortex* **22**, 2285-2296 (2012).
295 Bozoyan, L., Khlghatyan, J. & Saghatelyan, A. Astrocytes control the development of the migration-promoting vasculature scaffold in the postnatal brain via VEGF signaling. *J Neurosci* **32**, 1687-1704 (2012).
296 Snapyan, M. *et al.* Vasculature guides migrating neuronal precursors in the adult mammalian forebrain via brain-derived neurotrophic factor signaling. *J Neurosci* **29**, 4172-4188 (2009).
297 Shen, Q. *et al.* Endothelial cells stimulate self-renewal and expand neurogenesis of neural stem cells. *Science* **304**, 1338-1340 (2004).
298 Goldman, S. A. & Chen, Z. Perivascular instruction of cell genesis and fate in the adult brain. *Nat Neurosci* **14**, 1382-1389 (2011).
299 Zhang, S. & Murphy, T. H. Imaging the impact of cortical microcirculation on synaptic structure and sensory-evoked hemodynamic responses in vivo. *PLoS Biol* **5**, e119 (2007).
300 Tsai, P. S. *et al.* Correlations of neuronal and microvascular densities in murine cortex revealed by direct counting and colocalization of nuclei and vessels. *J Neurosci* **29**, 14553-14570 (2009).
301 Reichenbach, A. & Wolburg, H. *Astrocytes and ependymal glia.* . 2. Edition edn, 19-35 (Oxford University Press, Oxford, 2005).
302 Rolls, A., Shechter, R. & Schwartz, M. The bright side of the glial scar in CNS repair. *Nat Rev Neurosci* **10**, 235-241 (2009).
303 Karimi-Abdolrezaee, S. & Billakanti, R. Reactive astrogliosis after spinal cord injury-beneficial and detrimental effects. *Mol Neurobiol* **46**, 251-264 (2012).
304 McKeon, R. J., Hoke, A. & Silver, J. Injury-induced proteoglycans inhibit the potential for laminin-mediated axon growth on astrocytic scars. *Exp Neurol* **136**, 32-43 (1995).
305 Galtrey, C. M. & Fawcett, J. W. The role of chondroitin sulfate proteoglycans in regeneration and plasticity in the central nervous system. *Brain Res Rev* **54**, 1-18 (2007).
306 Escartin, C. & Bonvento, G. Targeted activation of astrocytes: a potential neuroprotective strategy. *Mol Neurobiol* **38**, 231-241 (2008).
307 Winkler, E. A., Bell, R. D. & Zlokovic, B. V. Central nervous system pericytes in health and disease. *Nat Neurosci* **14**, 1398-1405 (2011).
308 Fernandez-Klett, F. *et al.* Early loss of pericytes and perivascular stromal cell-induced scar formation after stroke. *J Cereb Blood Flow Metab* **33**, 428-439 (2013).
309 Shechter, R., Raposo, C., London, A., Sagi, I. & Schwartz, M. The glial scar-monocyte interplay: a pivotal resolution phase in spinal cord repair. *PLoS One* **6**, e27969 (2011).

310 Yang, L., Wang, L. & Zheng, Y. Gene targeting of Cdc42 and Cdc42GAP affirms the critical involvement of Cdc42 in filopodia induction, directed migration, and proliferation in primary mouse embryonic fibroblasts. *Mol Biol Cell* **17**, 4675-4685 (2006).
311 Schwartz, M. A. & Shattil, S. J. Signaling networks linking integrins and rho family GTPases. *Trends Biochem Sci* **25**, 388-391 (2000).
312 Camand, E., Peglion, F., Osmani, N., Sanson, M. & Etienne-Manneville, S. N-cadherin expression level modulates integrin-mediated polarity and strongly impacts on the speed and directionality of glial cell migration. *J Cell Sci* **125**, 844-857 (2012).
313 Saederup, N. *et al.* Selective chemokine receptor usage by central nervous system myeloid cells in CCR2-red fluorescent protein knock-in mice. *PLoS One* **5**, e13693 (2010).
314 Varvel, N. H. *et al.* Microglial repopulation model reveals a robust homeostatic process for replacing CNS myeloid cells. *Proc Natl Acad Sci U S A* **109**, 18150-18155 (2012).
315 Hanisch, U. K. & Kettenmann, H. Microglia: active sensor and versatile effector cells in the normal and pathologic brain. *Nat Neurosci* **10**, 1387-1394 (2007).
316 Schmidt, A., Durgan, J., Magalhaes, A. & Hall, A. Rho GTPases regulate PRK2/PKN2 to control entry into mitosis and exit from cytokinesis. *Embo J* **26**, 1624-1636 (2007).
317 Nagy, J. I. & Rash, J. E. Connexins and gap junctions of astrocytes and oligodendrocytes in the CNS. *Brain Res Brain Res Rev* **32**, 29-44 (2000).
318 Tran, M. D., Wanner, I. B. & Neary, J. T. Purinergic receptor signaling regulates N-cadherin expression in primary astrocyte cultures. *J Neurochem* **105**, 272-286 (2008).
319 Ransom, B. R. R. u. C. B. *Astrocytes: Multitalented Stars of the Central Nervous System*. Vol. 814 (SpringerLink, 2012).
320 Davalos, D. & Akassoglou, K. Fibrinogen as a key regulator of inflammation in disease. *Semin Immunopathol* **34**, 43-62 (2012).
321 McCarty, J. H. Integrin-mediated regulation of neurovascular development, physiology and disease. *Cell Adh Migr* **3**, 211-215 (2009).
322 Baeten, K. M. & Akassoglou, K. Extracellular matrix and matrix receptors in blood-brain barrier formation and stroke. *Dev Neurobiol* **71**, 1018-1039 (2011).
323 Nakatsuji, Y. & Miller, R. H. Homotypic cell contact-dependent inhibition of astrocyte proliferation. *Glia* **22**, 379-389 (1998).
324 Ota, M. & Sasaki, H. Mammalian Tead proteins regulate cell proliferation and contact inhibition as transcriptional mediators of Hippo signaling. *Development* **135**, 4059-4069 (2008).
325 Mayor, R. & Carmona-Fontaine, C. Keeping in touch with contact inhibition of locomotion. *Trends Cell Biol* **20**, 319-328 (2010).
326 Shechter, R. *et al.* Infiltrating blood-derived macrophages are vital cells playing an anti-inflammatory role in recovery from spinal cord injury in mice. *PLoS Med* **6**, e1000113 (2009).
327 Stabenfeldt, S. E., Irons, H. R. & Laplaca, M. C. Stem cells and bioactive scaffolds as a treatment for traumatic brain injury. *Curr Stem Cell Res Ther* **6**, 208-220 (2011).
328 Saatman, K. E. *et al.* Classification of traumatic brain injury for targeted therapies. *J Neurotrauma* **25**, 719-738 (2008).

Acknowledgements

I would like to express my sincere gratitude to

Magdalena Götz for the excellent supervision, inspiring ideas and great support throughout my PhD, and foremost for giving me the chance to work on this exciting project and to develop my scientific career.

Leda Dimou for suggestions and discussions on my work, experimental training and especially for our collaboration in setting the 2pLSM up.

Melanie Meyer-Lühmann, who supported this work from the beginning until the end by sharing her imaging expertise, providing excess to the 2pLSM as well as helpful discussions as thesis committee member.

Frank Bradke for providing supportive advises on the RhoGTPase study as contribution in my thesis committee.

ALL current and former lab colleagues at the ISF and LMU for their enormous cooperativeness.

Steffi for helping me initially with the project and techniques.

Detlef, Carmen, Tatjana, Gabi, Moni and the team at the animal facility, as well as the "Werkstatt" team for supporting this work with excellent technical assistance.

Martin and Felix, who crucially strengthened this work with their expert knowledge, ambition and enthusiasm leading to our very successful collaboration.

Christiane, Francesca, Sarah, Judith, Gregor, Julia, Corinna, Christoph, Sofia and Jesica for making my lab days brighter and for spending entertaining and relaxing leisure-times together.

Regina, Katja, Joanna K., Lena, Teresa, Joanna M. and **Ina**, who accompanied me as great friends throughout all phases of my PhD.

my **family** – especially my parents, grandparents and my sister – for inspiring my scientific fascination, as well as for encouraging and supporting my decisions and career.

My achievements are based on all your boundless support and cooperation!

THANK YOU VERY MUCH!

Appendix

I. Abbreviations

2pLSM	Two-photon laser scanning microscopy
Aldh1L1	Aldehyde dehydrogenase 1 family, member L1
ALS	Amyotrophic lateral sclerosis
AQP4	Aquaporin 4
BBB	Blood–brain barrier
BM	Basement membrane
CAG	Chicken β-actin promoter
CAT	Chloramphenicol acetyltransferase
Cdc42	Cell division cycle 42
CFP	Cyan fluorescent protein
CSF	Cerebrospinal fluid
CSPG	Chondroitin sulfate proteoglycans
CNS	Central nervous system
EAE	Experimental autoimmune encephalomyelitis
eGFP	Enhanced green fluorescent protein
ECM	Extracellular matrix
EGF	Epithelial grow factor
EM	Electron microscopy
FGF	Fibroblast growth factor
dpo	Days post operation
GFAP	Glial fibrillary acidic protein
GLAST	Glutamate-aspartate transporter
GM	Gray matter
GS	Glutamine synthetase
hGFAP	Human glial fibrillary acidic protein
i.p.	Intraperitoneal
i.v.	Intravenous
MMP	Matrix metalloproteinase
MTOC	Microtuble organizing center
NA	Numerical aperture
NPC	Neural precursor cell
NO	Nitric oxide

OPC	Oligodendrocyte precursor cell
RFP	Red fluorescent protein
ROS	Reactive oxygen species
SCI	Spinal cord injury
SHH	Sonic hedgehog
SR101	Sulforhodamine 101
SVZ	Subventricular zone
TGF	Tumor growth factor
TBI	Traumatic brain injury
VEGF	Vascular endothelial growth factor
VZ	Ventricular zone
WM	White matter
YFP	Yellow fluorescent protein

II. List of Figures

III. List of Tables